Mercury in Historical Silver Refining Wastes
in Guanajuato, Mexico

by

Ainsleigh Loria

A thesis submitted to the Faculty of Graduate Studies
of the University of Manitoba
in partial fulfillment of the requirements of the degree of

Master of Science

Department of Environment and Geography
University of Manitoba
Winnipeg

ABSTRACT

Silver (Ag) production in the Americas between the 16th and 19th century is thought to be one of the largest sources of anthropogenic mercury (Hg) emissions in history. A closer look at the chemistry of the *patio* process involved in silver refining during that time suggests that the production of calomel (Hg_2Cl_2), a solid by-product in which Hg is present as Hg(I), has been overlooked, resulting in an overestimation of Hg emissions into the atmosphere. However, calomel has yet to be reported in the environmental wastes from such processes. This thesis examines whether there is evidence of calomel in wastes generated from the *patio* process in Guanajuato, Mexico, using a combination of in-situ gaseous elemental mercury (Hg(0) or GEM) analysis, total Hg, qualitative Hg(I) analysis, scanning and transmission electron microscopy (SEM and TEM), and a calomel photodegradation experiment. The results showed widespread, elevated GEM concentrations in the ground-level air (range: 8 to 454 ng m^{-3}) and in the interstitial air of reprocessed mineral wastes, sediments, and soils (maximum: 44,700 ng m^{-3}) in Guanajuato. The qualitative Hg(I) analysis indicated the presence of Hg(I) in all analyzed samples, which is diagnostic of the presence of calomel. This is further supported by the results of the calomel photodegradation experiment, in which the GEM pattern agreed with our field observations when mineral wastes were exposed to the sunlight. The microscopy analyses of a waste-containing soil sample suggested that Hg was present in all valence states, with HgS being the dominant species. Overall, our results are consistent with calomel degradation via disproportionation, forming GEM and Hg(II). GEM is held in the interstitial air of wastes until released to the ground-level air upon disturbance, while Hg(II) is likely fixed in the environment as HgS. The findings of this work stress the need for further investigation of the fate of Hg used in the historical *patio* process, especially the environmental stability of the calomel by-product. The work should also provide grounds for the implementation of long-term mercury monitoring in Guanajuato and in other historical silver mining regions to assess the health and safety risk.

ACKNOWLEDGEMENTS

I would first like to thank my supervisor, Dr. Feiyue Wang, for proposing this project that was seemingly tailored specifically for me and my interests. Thank you for your support and guidance throughout my graduate studies. I am forever grateful to have been a part of this work and I hope that this is just the beginning of many collaborations with our wonderful colleagues in Mexico in the years to come.

A very special thanks goes to all of our collaborators down in Guanajuato and San Luis Potosí, Mexico: Drs. Yann René Ramos-Arroyo, Diana Rocha, Gustavo Cruz-Jiménez, Israel Razo Soto, and Ma. Catalina Alfaro de la Torre. Without all of you, we would have never been able to achieve such success during our field campaign. Thank you for your hospitality, for your collaboration, and interest towards this project. I would also like to acknowledge your students: Diego, Jose-Carlos, Adolfo, Fatima, Yaneli, Daniel, and Xebastian, for volunteering their time and enthusiasm in the field.

I would also like to express my gratitude to Dr. Saúl Guerrero for his insight and guidance that he so graciously offered me throughout the course of my MSc study. Your counsels have been invaluable to this project and to you, I owe a lot of my success. I am honoured to build on the incredible work that you have done.

Acknowledgements also go to Dr. Michael Schindler, Ravi Sidhu, and Mark Cooper for spending countless hours coaching me through the microscopy work. I had a lot of fun learning these techniques and I am thankful for your guidance and collaboration during the process.

Thanks also goes to my committee members, Drs. Peter Outridge and Mostafa Fayek, for offering their expertise and taking the time to comment on and improve my work.

Thanks to Dr. Gary Stern, my undergraduate supervisor, for the continued support and belief in my capabilities. Thank for you the extra push to finish up my undergraduate work, which ultimately helped me earn my first ever scientific publication in 2020.

Thank you to the Wang lab mom, Debbie Armstrong, for the advice throughout my years at CEOS. I appreciate all of time and effort you put forth in helping me, especially with the Hg(I) analysis.

Thanks to all of my CEOS colleagues, fellow graduate students, and personnel alike, for sharing laughs, coffee breaks, and treats over the years.

Thanks also goes to my support system: Emilio, my family, and my friends for the love and encouragement, now and always. I am grateful for your support during the difficult times and for your help in celebrating my successes.

Lastly, thank you to the Natural Sciences and Engineering Council of Canada (NSERC, F.W.) and the University of Manitoba for the fellowship for the financial support for this research.

To my grandma, Luz Sarmiento. I know that you would be so proud.
July 23, 1932 – January 2, 2014

TABLE OF CONTENTS

LIST OF TABLES

LIST OF FIGURES

ABBREVIATIONS

Chemical symbols

Bismuth	Bi
Chloride	Cl
Copper	Cu
Gallium	Ga
Iron	Fe
Lead	Pb
Mercury	Hg
Oxygen	O
Silver	Ag
Sodium	Na
Sulphur	S
Tin	Sn

Chemical species and compounds

2-mercaptoethanol	2-ME
Acanthite, silver sulfide	Ag_2S
Argentiferous galena, lead sulfide	PbS
Atacamite	$Cu_2Cl(OH)_3$
Bismuth	Bi
Calomel, mercurous chloride	Hg_2Cl_2
Chlorargyrite, silver chloride	AgCl
Cinnabar	HgS
Dimethylmercury	DMHg
Gallium	Ga
Gaseous elemental mercury	GEM, Hg(0)
Mercurous	Hg(I)
Mercuric chloride	$HgCl_2$
Mercuric	Hg(II)
Mercury nitrate	$HgNO_3$
Metallic mercury	Hg(0)
Methylmercury	MeHg
Monomethyl mercury	MMHg
Sodium chloride	NaCl
Schuetteite	$Hg_3O_2SO_4$
Paratacamite	$Cu_2(OH)_3Cl$
Particulate mercury	PHg
Polyethersulfone	PES
Reactive gaseous mercury	RGM
Total mercury	THg

Acronyms

Auger electrons	AE
Backscattered electrons	BSE
Certified Reference Material	CRM
Direct mercury analysis	DMA

Energy-dispersive x-ray spectroscopy	EDS
Focused ion beam	FIB
Guanajuato Mining District	GMD
High performance liquid chromatography	HPLC
Ion chromatography	IC
Inductively coupled plasma-mass spectrometry	ICP-MS
Powder x-ray diffraction	PXRD
Scanning electron microscopy	SEM
Scanning transmission electron microscopy	STEM
Secondary electrons	SE
Selected area electron diffraction	SAED
Transmission electron microscopy	TEM

Units

Cubic metre	m^3
Electron volts	eV
Gram	g
Hour	h
Kilogram	kg
Kilotonne (1 kt = 10^6 kg)	kt
Litre	L
Metre	m
Microgram	µg
Micrometre	µm
Milligram	mg
Millilitre	mL
Nanogram	ng
Microgram per gram (1 µg g^{-1} = 1 mg kg^{-1})	µg g^{-1}
Microgram per litre	µg L^{-1}
Milligram per kilogram	mg kg^{-1}
Nanogram per cubic metre	ng m^{-3}
Nanogram per gram	ng g^{-1}
Parts per billion (1,000 ppb = 1 ppm)	ppb
Parts per million (1 ppm = µg g^{-1})	ppm

Other

Atomic number	Z

CONTRIBUTION OF AUTHORS

The manuscript in Chapter 2 entitled "Widespread, Elevated Concentrations of Gaseous Elemental Mercury in Guanajuato, Mexico, Centuries After Historical Silver Refining by Mercury Amalgamation" is currently under review by the journal *Environmental Science and Technology*. It was first-authored by me with contributions from all co-authors. Drs. Yann Rene Ramos-Arroyo, Diana Rocha, Gustavo Cruz-Jiménez, Israel Razo Soto, Ma. Catalina Alfaro de la Torre, and Feiyue Wang were all involved in the field campaign that took place in Guanajuato, Mexico in July 2019. Dr. Saúl Guerrero offered his invaluable insight during planning phase of the field campaign and on the written manuscript. Debbie Armstrong was fundamental in developing the method for the Hg(I) analysis in our laboratory. I wrote the first draft of the manuscript, which was finalized by Dr. Feiyue Wang and I with input from all the co-authors.

The data presented in Chapter 3 entitled "Onwards – Additional Analyses" were collected by me (all analyses), with significant contributions from Debbie Armstrong (Hg(I) method development), Ravi Sidhu (scanning electron microscopy), Dr. Michael Schindler (scanning electron microscopy, transmission electron microscopy), and Dr. Feiyue Wang (overall experimental design and input on data interpretation). Debbie and Dr. Schindler both processed a great amount of the data.

CHAPTER ONE: INTRODUCTION AND BACKGROUND

1.1. Rationale and Context

Silver (Ag) production in the Americas between the 16th and 19th century is considered one of the largest sources of anthropogenic mercury (Hg) emissions in history (Streets et al., 2011, 2017, 2019). Revisiting the chemistry involved in historical Ag refining by amalgamation in Hispanic America (Guerrero, 2012, 2015, 2016), otherwise known as the *patio* process, suggested that Hg emissions from Ag refining processes may have been overestimated in the global Hg budget. This is because calomel (Hg_2Cl_2), a solid by-product that forms during the *patio* process, had been previously unaccounted for in Hg emission estimates from historical Ag refining processes (Outridge et al., 2018).

In past literature, it was widely assumed that the chemistry involved in both gold (Au) and Ag amalgamation was similar and that much of the Hg lost during refinement could be attributed to volatilization to the atmosphere. Under this premise, it was estimated that 60 to 85% of the Hg used in historical Ag refining processes was emitted to the atmosphere via volatilization (Nriagu, 1993; Camargo, 2002; Hagan et al., 2011; Streets et at., 2011; Robins et al., 2012).

However, Guerrero's work (2012) revealed that the long-standing assumption about the similarities between Au and Ag amalgamation chemistry were incorrect. His work focused on the *patio* process and used stoichiometry along with historical importation records to evaluate the amount of mercury consumed by chemical transformation to calomel. He estimated that calomel formation accounted for 66 to 93% of the Hg used during the *patio* process, while physical losses, such as spills and emissions to the atmosphere, would account for only 7 to 34% of the Hg used. Some Hg emission estimates for Ag refining processes have since been adjusted to account for the formation of calomel (Zhang et al., 2014; Outridge et al., 2018; Streets et al., 2019).

While there is support for both high (Amos et al., 2013) and low (Zhang et al., 2014) Hg emission estimate scenarios from historical Ag refining processes, a comprehensive review of the global Hg budget found that most of the evidence is in line with a low emission scenario (Outridge et al., 2018). The low Hg emission scenario is substantiated by the formation of calomel (Guerrero, 2012), upper oceanic total Hg concentrations and evasion rate estimates (Amos et al., 2014), as well as Hg deposition profiles in a number of natural archives, such as lake sediments (Engstrom et al., 2014; Zhang et al., 2014), peat bogs (Roos-Barraclough et al., 2003, 2006; Shotyk et al., 2005; Enrico et al., 2017), and glacier cores (Beal et al., 2015; Zheng et al., 2015; Kang et al., 2016; Outridge et al., 2018). To date, no studies have investigated the presence of calomel in the environment in historical Ag refining regions. Evidence of calomel, or lack thereof, in historical Ag amalgamation wastes would be valuable to further constrain the Hg emission factor and resolve the uncertainty regarding Hg emission estimates from historical Ag refining by amalgamation.

1.2. Thesis Objective

The main objective of this MSc thesis was to investigate whether there is evidence of calomel in historical Ag amalgamation waste. To explore this research question, a field investigation was conducted in the historical Ag mining region of Guanajuato (Mexico) to identify sites containing high incidences of Hg using gaseous elemental mercury (GEM) measurements as a probe. At selected sites, samples of mineral waste/soil/sediment were collected, and subsequent analyses including total Hg, microscopy, and Hg(I) analysis were conducted to examine Hg speciation in the samples. A laboratory study investigated GEM production during calomel photodegradation was also performed.

1.3. Mercury

Mercury is a naturally occurring element usually present in low environmental concentrations. It is also a globally distributed contaminant that has raised human and environmental health concerns due to its persistence and toxicity. Mercury is naturally released into the environment through geologic processes, such as weathering of cinnabar (HgS), forest fires, geothermal emissions, and volcanic eruptions. It may also enter the atmosphere by the volatilization from oceanic or terrestrial environments. However, it is the high output from anthropogenic sources, including coal combustion, mining activities, as well as metal and cement production, that have increased Hg concentrations in the atmospheric, oceanic, and terrestrial environments considerably above background levels (e.g. AMAP/UNEP, 2018).

Mercury exists in three oxidation states: metallic mercury, Hg(0); mercurous mercury, Hg(I), and mercuric mercury, Hg(II). The monovalent form, Hg(I), is uncommon due to its relative instability, stemming from its electronic configuration comprised of a half-full valence shell (s orbital) (Greenwood & Earnshaw, 1997). Hg(I) compounds tend to stabilize by forming metallic bonds with other Hg(I) atoms, generating a Hg dimer (Hg-Hg or Hg_2^{2+}). Mercury dimers are susceptible to degradation through a process called disproportionation, in which Hg_2^{2+} is simultaneously oxidized and reduced to generate Hg(0) and Hg(II) (Ullrich et al., 2001), as shown in equation 1.

$$Hg_2Cl_2 \rightleftharpoons Hg + HgCl_2 \qquad (1)$$

Its chemical form and the environmental conditions dictate its biogeochemical cycle through in the environment. Atmospheric deposition, photochemical reactions, and microbial methylation are all examples of important processes in the biogeochemical of Hg, as they facilitate transport from one environmental compartment to another (e.g., Liu et al., 2012).

In the atmosphere, Hg manifests primarily as GEM; a stable form which can be transported extensive distances before undergoing conversion to more reactive forms and depositing onto land or into the ocean (AMAP/UNEP, 2018). Anthropogenic sources may emit other Hg species, including reactive gaseous mercury (RGM), which are water-soluble Hg compounds in flue gases, and particulate Hg (PHg), which comprise of Hg bound or adsorbed to particulate matter in the atmosphere (Streets et al., 2005; Pacyna et al., 2006). In the terrestrial environment, Hg ores are dominant as Hg(II) in the form of sulfides, as cinnabar or metacinnabar (HgS; Greenwood & Earnshaw, 1997). In aquatic media, Hg is typically present as Hg(0) and Hg(II), including both inorganic and organic species in the latter valence state. In its organic form, Hg is present as methylmercury (MeHg), either monomethylmercury (MMHg) and dimethylmercury (DMHg).

Methylmercury is a potent neurotoxin that exhibits bioaccumulation and biomagnification within the food web (e.g. AMAP/UNEP, 2018). Acute Hg toxicity to humans may present as damage to the central nervous system and result in symptoms, such as tremors, ataxia, blurred vision, slurred speech, blindness, deafness, sensory issues, paresthesia, and death (USEPA, 1997). Chronic Hg exposure to MeHg occurs primarily through the consumption of contaminated aquatic organisms. Monitoring dietary intake of contaminated fish and large predatory aquatic organisms is especially important for pregnant women since MeHg can cross the placenta and blood-brain barrier (USEPA, 1997). This may disrupt the development of the central nervous system of prenatal babies and later manifest as neurological issues such as IQ deficiencies and abnormalities in motor function and muscle tone.

To protect human health and the environment from the adverse effects of Hg, the Minamata Convention on Mercury entered into force in 2017 to reduce anthropogenic emissions of Hg on a global scale (AMAP/UNEP, 2018).

1.4. Mercury Emissions Estimates from Historical Silver Refining Processes

One of the major challenges in evaluating the effectiveness of the Minamata Convention is the uncertainties associated with Hg released from historical anthropogenic activities. This is especially true for Ag refining processes in the Americas from the 16th to late 19th centuries (Outridge et al., 2018).

Nriagu (1993) was the first to recognize the global significance of Hg releases from Ag mining in the Americas under Spanish reign and estimated that a total of 196 kilotonnes (kt, 1 kt = 10^6 kg) of Hg was released to the environment from 1570 to 1900, which would account for ~13% of global anthropogenic releases of Hg over the entire human history (Streets et al., 2017). Still, uncertainties exist regarding the fate and effects of these large quantities of Hg released from Ag mining processes in the Americas. With the assumption that Hg emission processes in Ag refining are similar to those involved in artisanal Au mining, earlier studies have suggested that as much as 60 to 85% of the Hg was emitted to the atmosphere, with only a small fraction lost to local land and water bodies (Nriagu, 1993; Camargo, 2002; Hagan et al., 2012; Amos et al., 2014). Applying this high emission factor (or even if we use the conservative estimate of 40 to 52% from Streets et al., 2011 and 2017), global Hg budget models show that Ag mining in Spanish America would have contributed significantly to the present-day, global atmospheric and oceanic Hg levels and inventories (Outridge et al., 2018).

Revisiting the fundamental chemistry behind Ag amalgamation has suggested that historical Hg emissions from Ag mining in Spanish America could be much less than previously thought (Guerrero, 2012, 2015, 2016, 2018). The chemistry behind the Ag extraction process known as amalgamation or the *patio* process had been widely assumed to be similar to Au amalgamation, but they were shown by Guerrero (2012, 2015) to be two fundamentally different processes. Gold amalgamation was a one-to-one process, utilizing 1 unit of Hg to extract 1 unit of Au. In Au amalgamation, the added elemental Hg directly forms amalgam with elemental Au present in the ore. In contrast, the ratio in Ag amalgamation was two units of Hg to extract one unit of Ag; this ratio was referred to as *la correspondencia* (Guerrero, 2012). During the *patio* process, the added elemental Hg is involved in a redox reaction, reducing Ag(I) in the ore to Ag(0), which could then undergo amalgamation with excess elemental Hg, and oxidizing to Hg(I) to form calomel (Hg_2Cl_2). The stoichiometry suggests that a significant portion (estimated to be between 66 to 94% of the Hg used (Guerrero, 2012)) would be lost as calomel. Thus, a minor fraction would have been lost through spills and volatilization, resulting in a gross over-estimation of volatile Hg emissions from historical Ag refining by amalgamation (Guerrero, 2012). The formation of calomel as a by-product has been supported by historical importation statistics and consumption records (Guerrero, 2012, 2015, 2016), a laboratory experiment simulating the *patio* process (Johnson and Whittle, 1999), and Hg emission estimates from Ag mining in the present-day global Hg budget (Outridge et al., 2018). Thus, investigating the presence or absence, as well as the role of calomel in historical amalgamation waste is an important task to further understand the fate of Hg from historical Ag refining processes, the implications for public health, and for refining emission estimates for the global Hg budget.

1.5. The History of Silver Refining by Amalgamation in the New World

Subduction tectonic processes resulted in the formation of the metal-rich Cordilleran and Andean mountain ranges across the Americas (Sillitoe, 1972). The Ag deposits within the New Spain (present-day Mexico) are comprised mostly of argentiferous galena (lead sulfide, PbS) and acanthite (silver sulfide, Ag_2S, *negros* or *negrillos*). Weathering of acanthite ores gives rise to chlorargyrite (silver chloride, AgCl, *colorados*, or *pacos*) in the oxidation zone and native elemental Ag (*tacana* or *machacado*) is also present to some extent (Brading and Cross, 1972). In contrast, Ag deposits in the Andes are part of tin (Sn) systems (Guerrero, 2015).

Spanish miners were unfamiliar with the AgS ores found in the Americas, as they were different from the typical galena ores seen in Europe. This meant that refining processes would need to be modified for better extraction efficiency. Until the mid-16th century, all Ag refining practices in the New World (presently the Americas) were limited to smelting (Brading and Cross, 1972). The breakthrough of Ag amalgamation with Hg, which has been disputably credited to Pachuca Bartolomé de Medina (Brading and Cross, 1972; Guerrero, 2015), allowed Ag production to occur on an industrial scale, particularly in the Vice-Royalty of Peru (present-day Peru and Bolivia) and New Spain (Figure 1-1). Typically, Ag was obtained from galena as a by-product during the extraction of Pb by smelting. It was eventually found that

Ag was effectively extracted from AgCl ores through the process of amalgamation (otherwise known as the *patio* process) with Hg and that any AgS present would first need to be converted to AgCl. Historical records indicate that the Almadén Hg mine in Spain was the primary source of liquid elemental Hg imported into New Spain for Ag refining during the Colonial period (Guerrero, 2016). Almadén bore an abundance of cinnabar, which supplied New Spain with approximately 58,000 tons of Hg throughout the Colonial period. It is estimated that smelting accounted for 36% of the silver produced in New Spain, while amalgamation accounted for the remaining 64% (Guerrero, 2016).

Figure 1-1. Map of Spanish America with some Ag-refining centres over present-day international boarders at the height of the Spanish Empire circa 1800. World and Imperio Español (1714-1800) maps modified from Canuckguy (2006) and Ostiudo (2014), Wikimedia Commons.

The constituents of the amalgamation process include salt, water, elemental Hg, and the ground Ag ore. When extracting Ag from a AgCl ore, the amalgam (Ag_2Hg_n) is formed by adding liquid elemental Hg, which reduces Ag(I) in AgCl to Ag(0) which can amalgamate with Hg(0), simultaneously oxidizing Hg(0) to Hg(II) forming calomel as a by-product. The amalgam is then heated to recover the liquid Hg and extract the native Ag. When AgS is present, an oxidative leaching process is used to convert AgS to AgCl by oxidizing sulfur (S) from S^{2-} to elemental S by adding a soluble copper (Cu) salt known as *magistral*, salt (NaCl), and water. Each step of the refining process can be summarized in chemical equations 2 to 4 (Johnson and Whittle, 1999).

$$Ag_2S\ (s) + 2\ Cu^{2+}\ (aq) + 8\ Cl^{-}\ (aq) \rightleftharpoons 2\ AgCl_{\ (s)} + 2\ [CuCl_3]^{2-}_{\ (aq)} + S\ (s) \quad (2)$$

$$(n+2)\ Hg\ (l) + 2\ AgCl\ (s) \rightleftharpoons Ag_2Hg_n\ (l) + Hg_2Cl_2\ (s) \quad (3)$$

$$Ag_2Hg_n\ (l) + heat \rightleftharpoons n\ Hg\ (l) + 2\ Ag\ (s) \quad (4)$$

Reaction 2 describes the oxidative leaching step to convert AgS to AgCl. The reduction of AgCl by Hg to elemental Ag, as well as the formation of the amalgam with excess Hg and the generation of Hg_2Cl_2 are condensed into Reaction 3. Reaction 4 represents the heating of the amalgam to recover the Hg and obtain the Ag product.

A variety of side reactions may occur during this process, inevitably forming other by-products that are not outlined in these reactions. In a laboratory study, Johnson and Whittle (1999) observed the formation of paratacamite ($Cu_2(OH)_3Cl$) and small amounts of atacamite after Reaction 2, as well as the formation of cinnabar which may occur with the Hg formed during Reaction 2 and the S produced from Reaction 2. Another study examining mining waste from Au amalgamation and calcine waste (Kim et al., 2004) characterized cinnabar and schuetteite ($Hg_3O_2SO_4$) in their samples, which they hypothesized to have formed during long-term Hg(0) burial in reducing high-sulfide sediments. Mercury in the form of schuetteite was also found in adobe bricks made from mud and mine tailings in Guanajuato, Mexico (Puy-Alquiza et al., 2019). A characterization study of Hg in amalgamation waste tailings from Cedral in San Luis Potosí, Mexico by Bayer (2013) found that cinnabar was the dominant (90%) Hg species, with very minor amounts (<10%) of Hg chlorides (indiscernible between $HgCl_2$ and Hg_2Cl_2).

An optional addition to the amalgamation recipe was iron (Fe). Historical records from the Vice-Royalty of New Spain indicate that Fe fillings were sometimes added to reduce the amount of Hg lost, although this did not affect the amount of Ag being produced (Guerrero, 2012). The reason that the amount of Ag produced would be unaffected was that Fe competes with Hg to reduce Ag, which would only affect the amount of calomel produced.

1.6. Calomel

Calomel or mercurous chloride, is an odorless, inorganic Hg(I) salt. It is white or yellow-white in colour but may also have hues of grey or brown when exposed to light or when found as a mineral in Hg deposits (Mindat, no date). The name calomel is said to be derived from calos signifying good and melas meaning black (Risse, 1973; Davis, 2000). Calomel is sparingly soluble in water ($K_{sp} = 1.43 \times 10^{-18}$ at 25°C; Rumble, 2020). It is fairly stable in air due to its low vapour pressure, although as a Hg(I) compound, calomel is susceptible to degradation via disproportionation. In the form of calomel, Hg(I) is present as a Hg dimer (Hg-Hg or Hg_2^{2+}), which simultaneously oxidizes and reduces itself, forming both Hg(0) and Hg(II) over time and in various conditions, including UV light, heat, in the human body, and when exposed to certain chemicals (e.g., ammonia, hydrogen sulfide, alkali sulphides, other salts) (Roseveare, 1930; Booer, 1944; Sastri and Kalidas, 1955; Awitor et al., 2000; Schlüter K., 2000; Clarkson and Magos, 2006; Copan et al., 2015). However, the kinetics of calomel disproportionation and the environmental conditions under which disproportionation may be induced are not well-defined.

In the present day, calomel is commonly used in electrochemistry as a reference electrode, though it is also occasionally used in cosmetics and agriculture. In 19th century medicine, it was used extensively as a purgative/laxative for the treatment of infectious diseases, such as syphilis, smallpox, measles, dipheria, hydrocephalus, pneumonia, malaria, yellow fever, and many others (Risse, 1973; Davis, 2000). The widespread use of calomel in medicine ceased when the toxic effects were recognized during the mid-20th century when children were being treated with calomel for teething pain and constipation. Some of the long-term effects include neurological symptoms, such as tremors, ataxia and erethism (Risse, 1973). Exposure routes include inhalation, dermal contact absorption and ingestion. The associated acute, short-term effects include a cough and sore throat for inhalation, redness and irritation for dermal contact and for ingestion, excessive salivation, ashy-coloured of the mouth and throat, inflammation of the gums, ulcerations in the mouth, loose and lost teeth, gastrointestinal irritation, diarrhea, vomiting and metallic taste (Risse, 1973; Davis, 2000).

Although calomel has been historically notorious in the field of medicine, its environmental impacts are not well-known. Because of its susceptibility to disproportionate, there is the possibility of re-emissions of GEM stemming from calomel disproportionation under undefined environmental conditions (Amos et al., 2014; Outridge et al., 2018; Streets et al., 2019).

1.7. Mercury in Historical Silver Mining Regions in the Americas

To date, studies regarding Hg contamination sourced from historical Ag amalgamation from the Colonial era are mainly limited to a few areas: Potosí (Bolivia), Cedral (Mexico), near Puno (Peru), Fresnillo (Mexico), and Guanajuato (Mexico) (Figure 1-1). This is despite the fact that Ag amalgamation was used extensively throughout Spanish America.

Potosí, Bolivia, is a historically renowned Ag mining area that has produced over 56,000 tons of Ag (Rice et al., 2005). From the late 16th until the mid-19th century, the *patio* process was used extensively in Potosí to extract Ag from ore. Higueras et al. (2012) conducted GEM surveys around the Cerro Rico mine in Potosí, which showed low GEM concentrations (mean: 5.5 ng m^{-3}; maximum: 31 ng m^{-3}) in the refining areas (called *ingenios*) and in the town. Excavation of the topsoil in the *ingenios*, however, gave rise to instantaneous GEM releases that forced GEM concentrations as high as 3,000 ng m^{-3}. Higueras et al. (2012) proposed that low ambient concentrations were due to transformations of metallic Hg into more stable mineral phases, such as cinnabar (HgS, red), metacinnabar (HgS, black) and/or schuetteite ($Hg_3(SO_4)O_2$). Total Hg concentrations in soil were also reported, which were low (ranging from 13.6 to 101.2 mg kg^{-1}) in comparison to contaminated regions, such as the Almadén Hg mine in Spain (6 to 9,000 mg kg^{-1} in soils; Higueras et al., 2003).

Hagan et al. (2011) estimated Hg emissions from Ag smelting during the Colonial era in Potosí using historical records of mercury use and the modelling program, AERMOD. They also reported total Hg concentrations in soils in proximity to smelters, which ranged from 0.105 to 155 mg kg^{-1}, and used sequential extractions to predict the speciation of Hg in soil. Their results showed that the most prevalent Hg species were in the form of cinnabar, metacinnabar, and elemental Hg. Similarly, Robins et al. (2012) used historical records and AERMOD to estimate Hg emissions from the Huancavelica cinnabar mine in Peru. The Hg produced from Huancavelica would have been used in Potosí for Ag amalgamation.

Downstream from Potosí and the Cerro Rico mine, Hudson-Edwards et al. (2001) investigated alluvial wastes in the Pilcomayo river in Bolivia. This river collected the historical wastes from the Ag refining. The alluvial wastes deposited in the Pilcomayo were determined to be enriched in various metals, including both Ag and Hg, which are functioning as an important metal source to the river in the present-day and imply that vast amounts of Hg from Ag amalgamation were lost to the terrestrial environment.

Kennedy and Kelloway (2020) recently identified a historical Ag refinery (Trapiche) that employed the *patio* process near Puno, Peru, near the Bolivian border. They found traces of remnant Hg >10 mg kg^{-1} in over 50% of their samples that were analyzed using portable x-ray fluorescence spectroscopy. The spatial distribution patterns of the elements were determined to be consistent with the *patio* process, with the highest concentrations of Hg (> 500 mg kg^{-1}) detected near the patio in proximity to the metallurgical ovens, where the amalgams were heated.

Silver amalgamation also occurred broadly throughout New Spain (present-day Mexico) from the mid-16th century until the 19th century (Guerrero, 2012). Few studies thus far have addressed Hg pollution from amalgamation sites, referred to as *haciendas* in Mexico rather than *ingenios* as in South America.

Ogura et al. (2003) analyzed amalgamation waste tailings/soils that were reprocessed for remnant Ag downstream of a site in Zacatecas, Mexico to determine extraction efficiency of Hg during reprocessing activities. They found that 121 mg kg^{-1} of Hg was extracted from the extractable (acid leached) fraction (168 mg kg^{-1}). They concluded that a proportion of the remaining, unextracted Hg in the soil was metallic (Hg(0)), as only half evaporated during the course of 18 months.

Leura Vicencio et al. (2017) found that 80% of their soil samples in the vicinity of *haciendas* in Cedral, Mexico exceeded the Mexican maximum permissible limit of Hg for residential soils (23 mg kg^{-1}), with total Hg concentrations in soil samples and mining waste ranging from 1 to 116 mg kg^{-1} and 8 to 548 mg kg^{-1}, respectively. They determined the soluble fraction of Hg in tailings and soils to be significantly lower than the total concentration (only up to 0.54% of the total concentration), which suggests the prevalence of an insoluble Hg mineral species, such as cinnabar (Bayer, 2013; Leura Vicencio et al., 2017). Bayer (2013) examined Hg speciation in amalgamation tailings from both Cedral (San Luis Potosí, Mexico) and Fresnillo (Zacatecas, Mexico) using x-ray methods. Their results showed that the vast majority of the Hg (up to 90%) in the tailings was cinnabar or metacinnabar. They also determined a small fraction (less than 10%) to be in the form of calomel or mercuric chloride ($HgCl_2$), although the analytical method could not distinguish between the two species.

Another study based in Cedral evaluated the impact of Hg usage for Ag extraction on the environment, as well as the population living in the area (Morton-Bermea et al., 2015). They determined the mean and maximum total Hg concentrations in soils to be 9.7 and 55.7 mg kg^{-1}. In wastes, the mean and maximum total Hg concentrations were 24.4 and 59.4 mg kg^{-1}, respectively. Using the sequential extraction technique, they determined that 85 to 97% of the Hg in their samples was in a stable/insoluble chemical form, corresponding to either HgO and/or HgS. Lastly, they measured Hg in the blood of children living in the area and found that 16 of the 20 children had total mercury concentrations exceeding the recommended guideline (5.8 μg L^{-1}). This finding contradicted their sequential extraction results which indicated that most of the Hg in the tailings and soils were not bioavailable. Thus, a follow up study was conducted by Morton-Bermea et al. (2021) to assess the human exposure component that resulted in the moderately elevated total Hg concentrations observed in children's blood samples. An additional 80 blood samples from children residing in the region were taken for this study. Only 6 of the 80 exceeded the recommended guideline, but mean and median values were higher than studies with sample populations that were not exposed to Hg. Their study deemed inhalation as the most significant exposure route of Hg to the human population. Furthermore, they suggested that GEM and PHg (associated with particles less than 2.5 μm in size ($PM_{2.5}$)) generated from the tailings were the sources of Hg exposure.

Lastly, a case study in Guanajuato, Mexico characterized adobe mud bricks used to build the walls of *haciendas* made from mud and mine tailings produced from smelting and amalgamation (Puy-Alquiza et al., 2019). Their mineralogical analysis by x-ray diffraction showed evidence of Hg in the form of schuetteite.

1.8. Guanajuato Mining District (GMD)

The GMD (Figure 1-2) is located in central Mexico between the Central Mexican Plateau and the Trans-Mexican Volcanic Belt. It is in a temperate sub-humid climate which becomes semi-warm further south (Woitrin-Bibot et al., 2015). The mean annual air temperature is 18.7°C (range: 5–35°C) (Ramos-Arroyo et al., 2004). This region is subjected to intense, convective, and orographic rainfalls, especially during the summer months. The GMD is a part of the Lerma River basin hydrological system, with the Guanajuato River flowing through, and limited by the Purísima dam as the exit point of the basin. The city of Guanajuato was named a UNESCO World Heritage Site in 1988 due to its importance in history as an economic centre, its rich culture and its picturesque, colonial architecture. The city of Guanajuato is home to approximately 184,000 citizens (Instituto Nacional de Estadística Geografía e Informática México, 2015) and visited by hundreds of thousands of tourists each year.

Figure 1-2. Map of Mexico (modified from Google Maps (2020)) outlining the general geographical location of the Guanajuato Mining District (GMD) within the state of Guanajuato.

To date, there is limited literature regarding Hg pollution from Ag mining processes in the Guanajuato area, which is regarded as one of the most important historical Ag producing centres in the world during the Spanish Colonial era from 1554 up until the Independence movement which began in 1810 (Woitrin-Bibot et al., 2015). The Ag ores in the GMD are hosted in three vein systems, including La Luz, Veta Madre, and La Sierra (Ramos-Arroyo and Siebe-Grabach, 2006). Four different extraction processes have historically been used in the region: smelting and amalgamation from 1554 onwards, then cyanidation to reprocess residual Ag from the amalgamation and smelting wastes at the turn of the 20th century, and flotation after 1940 (Ramos-Arroyo et al., 2004). The mining processes generated a considerable amount of waste, which was discarded into the river where it accumulated (Guerrero, 2016). Though various efforts were put forth by the municipal government to clean the river during the 17th century, the disposal of mining waste only became regulated in 1930. Of particular interest to this study is the waste material from the amalgamation process, as large quantities of liquid elemental Hg were used. However, the original amalgamation waste materials have since been re-processed by either cyanidation or flotation (Ramos-Arroyo et al., 2004). The waste products from the subsequent processes have been discarded in the form of deposits in and around the GMD.

1.9. Thesis Structure

This thesis comprises of four chapters. This first chapter is the introduction which defines the research rationale, the thesis objective, the structure of the thesis, and presents background information that will help to understand the work undertaken. The second chapter was written in the form of a manuscript submitted to the journal *Environmental Science & Technology*. It reports widespread GEM in the ground-level air and interstitial air of reprocessed mineral wastes, sediments, and soils in the Guanajuato Mining District (GMD) and attributes these observations to calomel disproportionation, which is supported by subsequent laboratory analyses of Hg(I) and calomel photodegradation. The data included in this chapter are: GEM data from the ground-level and interstitial air of reprocessed mineral wastes, sediments, and soils, a calomel photodisproportionation experiment in ultraviolet-visible (UV-vis) light, and a qualitative Hg(I) analysis. The third chapter presents data from subsequent microscopy analyses conducted on the solid samples (reprocessed mineral wastes, soils, and sediments) from the GMD that were not included in the manuscript. Moreover, commentary and observations during the Hg(I) method development process and quantitative analysis attempt are included in this chapter. These comments were not included in the manuscript (Chapter 2), but should be useful for the continuation of this work. The fourth and final chapter is a research summary and draws conclusions based on the research outlined in this thesis. Recommendations for future work are also discussed in this chapter.

REFERENCES

AMAP/UN Environment. (2019). Technical Background Report for the Global Mercury Assessment 2018. Retrieved from Arctic Monitoring and Assessment Programme, Oslo, Norway / UN Environment Programme, Chemicals and Health Branch, Geneva, Switzerland.

Amos, H. M., Jacob, D. J., Streets, D. G., & Sunderland, E. M. (2013). Legacy impacts of all time anthropogenic emissions on the global mercury cycle. *Global Biogeochemical Cycles*, *27*(2), 410-421. https://doi.org/10.1002/gbc.20040

Awitor, K. O., Bernard, L., Coupat, B., Fournier, J. P., & Verdier, P. (2000). Measurement of mercurous chloride vapor pressure. *New Journal of Chemistry*, *24*, 399–401. https://doi.org/10.1039/b000238k

Bayer, F. M. (2013). *Quecksilberspeziation von Bergbaurückständen aus Fresnillo und Cedral, Mexiko Erklärung*. Karlsruhe Institute of Technology, (in German).

Beal, S. A., Osterberg, E. C., Zdanowicz, C. M., & Fisher, D. A. (2015). Ice core perspective on mercury pollution during the past 600 years. *Environmental Science and Technology*, *49*, 7641–7647. https://doi.org/10.1021/acs.est.5b01033

Booer, J. R. (1944). The behaviour of mercury compounds in soil. *Annals of Applied Biology*, *31*(4), 340–359. https://doi.org/10.1111/j.1744-7348.1944.tb06747.x

Brading, D. A., & Cross, H. E. (1972). Colonial Silver Mining: Mexico and Peru. *The Hispanic American Historical Review*, *52*(4), 545–579. https://doi.org/10.1215/00182168-52.4.545

Camargo, J. A. (2002). Contribution of Spanish-American silver mines (1570-1820) to the present high mercury concentrations in the global environment: a review. *Chemosphere*, *48*, 51–57. https://doi.org/10.1016/S0045-6535(02)00047-4

Canuckguy (2006). Blank Map World. Wikimedia Commons, public domain. Retrieved from https://commons.wikimedia.org/wiki/File:BlankMap-World.svg

Clarkson, T. W., & Magos, L. (2006). The toxicology of mercury and its chemical compounds. *Critical Reviews in Toxicology*, *36*(8), 609–662. https://doi.org/10.1080/10408440600845619

Copan, L., Fowles, J., Barreau, T., & McGee, N. (2015). Mercury toxicity and contamination of households from the use of skin creams adulterated with mercurous chloride (calomel). *International Journal of Environmental Research and Public Health*, *12*(9), 10943–10954. https://doi.org/10.3390/ijerph120910943

Davis, L. E. (2000). Unregulated potions still cause mercury poisoning. *The Western Journal of Medicine*, *173*(1), 19. Retrieved from http://www.ncbi.nlm.nih.gov/pubmed/10903282

Engstrom, D. R., Fitzgerald, W. F., Cooke, C. A., Lamborg, C. H., Drevnick, P. E., Swain, E. B., Balogh, S. J., & Balcom, P. H. (2014). Atmospheric Hg emissions from preindustrial gold and silver extraction in the Americas: A reevaluation from lake-sediment archives. *Environmental Science & Technology*, *48*(12), 6533–6543. https://doi.org/10.1021/es405558e

Enrico, M., Roux, L., Heimbu, L.-E., Van Beek, P., Souhaut, M., Chmeleff, R., & Sonke, J. E. (2017). Holocene atmospheric mercury levels reconstructed from peat bog mercury stable isotopes. *Environmental Science & Technology*, *51*, 5899–5906. https://doi.org/10.1021/acs.est.6b05804

Greenwood, N. N. & Earnshaw, A. (1997). *Chemistry of the elements* (2nd ed.). Oxford, UK: Butterworth-Heinemann.

Guerrero, S. (2012). Chemistry as a tool for historical research: Identifying paths of historical mercury pollution in the Hispanic New World. *Bulletin of Historic Chemistry*, *37*(2), 61–70. https://doi.org/10.1080/07341512.2016.1191864

Guerrero, S. (2015). *The Environmental History of Silver Refining in New Spain and Mexico, 16c to 19c: A Shift of Paradigm*. McGill University.

Guerrero, S. (2016). The history of silver refining in New Spain, 16c to 18c: back to the basics. *History and Technology*, *32*(1), 2–32. https://doi.org/10.1080/07341512.2016.1191864

Guerrero, S. (2018). The environmental history of silver production, and its impact on the United Nations Minamata Convention on mercury. In *Session on Global Production and Distribution of Silver, World Economic History Congress*. Boston, USA. Retrieved from http://wehc2018.org/wp-content/uploads/2018/04/WEHCguerreroMinamata-2.pdf

Hagan, N., Robins, N., Hsu-Kim, H., Halabi, S., Morris, M., Woodall, G., Zhang, T., Bacon, A., Richter, D. d. B., & Vandenberg, J. (2011). Estimating historical atmospheric mercury concentrations from silver mining and their legacies in present-day surface soil in Potosí, Bolivia. *Atmospheric Environment*, *45*(40), 7619–7626. https://doi.org/10.1016/j.atmosenv.2010.10.009

Higueras, P., Llanos, W., García, M. E., Millán, R., & Serrano, C. (2012). Mercury vapor emissions from the Ingenios in Potosí (Bolivia). *Journal of Geochemical Exploration*, *116*, 1–7. https://doi.org/10.1016/j.gexplo.2011.05.004

Higueras, P., Oyarzun, R., Biester, H., Lillo, J., & Lorenzo, S. (2003). A first insight into mercury distribution and speciation in soils from the Almadén mining district, Spain. *Journal of Geochemical Exploration*, *8*, 95–104. https://doi.org/10.1016/S0375-6742(03)00185-7

Hudson-Edwards, K. A., Macklin, M. G., Miller, J. R., & Lechler, P. J. (2001). Sources, distribution and storage of heavy metals in the Río Pilcomayo, Bolivia. *Journal of Geochemical Exploration*, *72*(3), 229–250. https://doi.org/10.1016/S0375-6742(01)00164-9

Instituto Nacional de Estadística Geografía e Informática, México. (2015) Municipalidad Guanajuato Census 2015. Retrieved from http://www.citypopulation.de/php/mexico-admin.php?adm2id=11015

Johnson, D. A. & Whittle, K. (1999). The chemistry of the Hispanic-American amalgamation process. *Journal of the Chemical Society, Dalton Transactions*, 23, 4239–4243. https://doi.org/10.1039/a905612b

Kang, S., Huang, J., Wang, F., Zhang, Q., Zhang, Y., Li, C., Wang, L., Chen, P., Sharma, C. M., Li, Q., Sillanpää, M., Hou, J., Xu, B., & Guo, J. (2016). Atmospheric mercury depositional chronology reconstructed from lake sediments and ice core in the Himalayas and Tibetan Plateau. *Environmental Science and Technology*, *50*, 5859–2869. https://doi.org/10.1021/acs.est.5b04172

Kennedy, S. A., & Kelloway, S. J. (2020). Identifying metallurgical practices at a colonial silver refinery in Puno, Peru, using portable X-Ray fluorescence spectroscopy (pXRF). *Journal of Archaeological Science: Reports*, *33*. https://doi.org/10.1016/j.jasrep.2020.102568

Kim, C. S., Rytuba, J. J., & Brown, G. E. (2004). Geological and anthropogenic factors influencing mercury speciation in mine wastes: An EXAFS spectroscopy study. *Applied Geochemistry*, *19*(3), 379–393. https://doi.org/10.1016/S0883-2927(03)00147-1

Leura Vicencio, A. K., Carrizales Yañez, L., & Razo Soto, I. (2017). Mercury pollution assessment of mining wastes and soils from former silver amalgamation area in North-Central Mexico. *Revista Internacional de Contaminacion Ambiental*, *33*(4), 655–669. https://doi.org/10.20937/RICA.2017.33.04.09

Liu, G., Cai, Y., & O'Driscoll, N. (2012). *Environmental Chemistry and Toxicology of Mercury*. (G. Liu, Y. Cai, & N. O'Driscoll, Eds.). Hoboken, NJ, USA: John Wiley & Sons, Inc. https://doi.org/10.1002/9781118146644

Calomel (n.d.). Mindat. Retrieved from https://www.mindat.org/min-869.html

Morton Bermea, O., Castro-Larragoitia, J., Arellano Álvarez, Á. A., Pérez-Rodríguez, R. J., Leura-Vicencio, A., Schiavo, B., Salgado-Martínez, E., Razo Soto, I., & Hernández Álvarez, E. (2021). Mercury in Blood of Children Exposed to Historical Residues from Metallurgical Activity. *Exposure and Health*. https://doi.org/10.1007/s12403-021-00382-z

Morton-Bermea, O., Jiménez-Galicia, R. G., Castro-Larragoitia, J., Hernández-Álvarez, E., Pérez-Rodríguez, R., García-Arreola, M. E., García-Gavillán, I., & Segovia, N. (2015). Anthropogenic impact of the use of Hg in mining activities in Cedral S.L.P. Mexico. *Environmental Earth Sciences*, *74*(2), 1161–1168. https://doi.org/10.1007/s12665-015-4102-7

Nriagu, J. (1993). Legacy of mercury pollution. *Nature, 363,* 589.

Ogura, T., Ramírez-Ortiz, J., Arroyo-Villaseñor, Z. M., Hernández-Martínez, S., Palafox-Hernández, J. P., García de Alba, L. H., & Fernando, Q. (2003). Zacatecas (Mexico) companies extract Hg from surface soil contaminated by ancient mining industries. *Water, Air, & Soil Pollution, 148,* 167–177.

Ostiudo (2014). Imperio Español (1714-1800). Wikimedia Commons, CC BY-SA 3.0. Retrieved from https://commons.wikimedia.org/w/index.php?curid=31694331#/media/File:Imperio_Espa%C3%B1ol_(1714-1800).png

Outridge, P. M., Mason, R. P., Wang, F., Guerrero, S., & Heimburger-Boavida, L.-E. (2018). Updated Global and Oceanic Mercury Budgets for the United Nations Global Mercury Assessment 2018. *Environmental Science and Technology*, *52*, 11466–11477. https://doi.org/10.1021/acs.est.8b01246

Pacyna, E. G., Pacyna, J. M., Fudala, J., Strzelecka-Jastrzab, E., Hlawiczka, S., & Panasiuk, D. (2006). Mercury emissions to the atmosphere from anthropogenic sources in Europe in 2000 and their scenarios until 2020. *Science of the Total Environment*, *370*, 147–156. https://doi.org/10.1016/j.scitotenv.2006.06.023

Puy-Alquiza, M. J., Miranda-Avilés, R., Ordaz Zubia, V. Y., Moncada, C. D., Zanor, G. A., Salazar-Hernández, M. D. C., Li, Y., & Loza-Aguirre, I. (2019). The mine tailings as construction material in the viceregal period: Case study in Guanajuato City, Mexico. *Boletin de La Sociedad Geologica Mexicana*, *71*(2), 543–564. https://doi.org/10.18268/BSGM2019v71n2a18

Ramos-Arroyo, Y. R., Prol-Ledesma, R. M., & Siebe-Grabach, C. (2004). Características geológicas y mineralógicas e historia de extracción del Distrito de Guanajuato, México. *Revista Mexicana de Ciencias Geologicas*, *21*(2), 268–284, (in Spanish with English abstract).

Ramos-Arroyo, Y. R. & Siebe-Grabach, C. (2006). Estrategia para identificar jales con potencial de riesgo ambiental en un distrito minero: estudio de caso en el Distrito de Guanajuato, Mexico. *Revista Mexicana de Ciencias Geológicas*, 23(1), 54-74 (in Spanish with English abstract).

Rice, C. M., Steele, G. B., Barfod, D. N., Boyce, A. J., & Pringle, M. S. (2005). Duration of magmatic, hydrothermal, and supergene activity at Cerro Rico de Potosi, Bolivia. Econ. Geol., *100*(8), 1647–1656. https://doi.org/10.2113/gsecongeo.100.8.1647

Risse, G. B. (1973). Calomel and the American Medical Sects during the Nineteenth Century. History of Patienthood View project Historical Ecology of Diseases View project. *Mayo Clinic Proceedings*, *48*, 57–64. Retrieved from https://www.researchgate.net/publication/18819864

Robins, N. A., Hagan, N., Halabi, S., Hsu-Kim, H., Dario, R., Espinoza Gonzales, R. D., Morris, M., Woodall, G., Richter, D. d. B., Heine, P., Zhang, T., Bacon, A., & Vandenberg, J. (2012). Estimations of historical atmospheric mercury concentrations from mercury refining and present-day soil concentrations of total mercury in Huancavelica, Peru. *Science of the Total Environment*, 426, 146–154. https://doi.org/10.1016/j.scitotenv.2012.03.082

Roos-Barraclough, F., & Shotyk, W. (2003). Millennial-scale records of atmospheric mercury deposition obtained from ombrotrophic and minerotrophic peatlands in the Swiss Jura mountains. *Environmental Science & Technology*, *37*(2), 235–244. https://doi.org/10.1021/es0201496

Roos-Barraclough, F., Givelet, N., Cheburkin, A. K., Shotyk, W., & Norton, S. A. (2006). Use of Br and Se in peat to reconstruct the natural and anthropogenic fluxes of atmospheric Hg: A 10000-year record from Caribou Bog, Maine. *Environmental Science & Technology*, *40*(10), 3188–3194. https://doi.org/10.1021/es051945p

Roseveare, W. E. (1930). The x-ray photochemical reaction between potassium oxalate and mercuric chloride. *Journal of the American Chemical Society*, *52*(7), 2612–2619. https://doi.org/10.1021/ja01370a005

Rumble, J. R. "Solubility Product Constants of Inorganic Salts," in CRC Handbook of Chemistry and Physics (Electronic ed. 2020, 100th ed.). Boca Raton, FL: CRC Press/Taylor & Francis.

Sastri, M. N. & Kalidas, C. (1955). Photochemical estimation of mercuric chloride by Eder's reaction with ceric ion as sensitizer. *Fresenius' Zeitschrift Für Anal. Chem.*, *148*, 3–6. https://doi.org/10.1007/BF00444794

Schlüter, K. (2000). Review: Evaporation of mercury from soils. An integration and synthesis of current knowledge. *Environmental Geology*, *39*(3–4), 249–271. https://doi.org/10.1007/s002540050005

Sillitoe, R. (1972). Relation of metal provinces in western America to subduction of oceanic lithosphere. *Geological Society of America Bulletin*, 83(3), 813–817. https://doi.org/10.1130/0016-7606(1972)83[813:ROMPIW]2.0.CO;2

Shotyk, W., Goodsite, M. E., Roos-Barraclough, F., Givelet, N., Le Roux, G., Weiss, D., Cheburkin, A. K., Knudsen, K., Heinemeier, J., Van Der Knaap, W. O., Norton, S. A., & Lohse, C. (2005). Accumulation rates and predominant atmospheric sources of natural and anthropogenic Hg and Pb on the Faroe Islands. *Geochimica et Cosmochimica Acta*, *69*(1), 1–17. https://doi.org/10.1016/j.gca.2004.06.011

Streets, D. G., Hao, J., Wu, Y., Jiang, J., Chan, M., Tian, H., & Feng, X. (2005). Anthropogenic mercury emissions in China. *Atmospheric Environment*, *39*, 7789–7806. https://doi.org/10.1016/j.atmosenv.2005.08.029

Streets, D. G., Devane, M. K., Lu, Z., Bond, T. C., Sunderland, E. M., Jacob, D. J. (2011). All-time releases of mercury to the atmosphere from human activities. *Environmental Science & Technology, 45*, 10485−10491. https://doi:10.1021/es202765m.

Streets, D. G., Horowitz, H. M., Jacob, D. J., Lu, Z., Levin, L., Ter Schure, A. F. H., & Sunderland, E. M. (2017). Total Mercury Released to the Environment by Human Activities. *Environmental Science & Technology, 51*, 5969–5977. https://doi.org/10.1021/acs.est.7b00451

Streets, D. G., Horowitz, H. M., Lu, Z., Levin, L., Thackray, C. P., & Sunderland, E. M. (2019). Five hundred years of anthropogenic mercury: Spatial and temporal release profiles. *Environmental Research Letters, 14*(8), 84004. https://doi.org/10.1088/1748-9326/ab281f

Ullrich, S. M., Tanton, T. W., & Abdrashitova, S. A. (2001). Mercury in the aquatic environment: a review of factors affecting methylation. *Critical Reviews in Environmental Science & Technology, 31*(3), 241–293. https://doi.org/10.1080/20016491089226

United States Environmental Protection Agency. (1997). *Mercury Study Report to Congress*. Washington. Retrieved from https://www3.epa.gov/airtoxics/112nmerc/volume1.pdf

Woitrin-Bibot, E., Martínez-Arredondo, J. C., & Ramos-Arroyo, Y. R. (2015). Crecimiento urbano e incremento de riesgos hidrológicos en la ciudad de Guanajuato, México. *L'Ordinaire Des Amériques*, *218*. https://doi.org/10.4000/orda.1937 (in Spanish with English abstract).

Zhang, Y., Jaeglé, L., Thompson, L. A., & Streets, D. G. (2014). Six centuries of changing oceanic mercury. *Global Biogeochemical Cycles*, *28*(11), 1251–1261. https://doi.org/10.1002/2014GB004939

Zheng, J. (2015). Archives of total mercury reconstructed with ice and snow from Greenland and the Canadian High Arctic. *Science of the Total Environment*, *509–510*, 133–144. https://doi.org/10.1016/j.scitotenv.2014.05.078

CHAPTER TWO: WIDESPREAD, ELEVATED CONCENTRATIONS OF GASEOUS ELEMENTAL MERCURY IN GUANAJUATO, MEXICO, CENTURIES AFTER HISTORICAL SILVER REFINING BY MERCURY AMALGAMATION

This chapter is a manuscript submitted to and under review by the journal *Environmental Science & Technology*. The citation is as follows:

Loria, A., Ramos-Arroyo, Y. R., Rocha, D., Cruz-Jiménez, G., Razo Soto, I., Alfaro de la Torre, M. C., Guerrero, S., Armstrong, D., & Wang, F. Elevated concentrations of gaseous elemental mercury in air and surface soil from the historical silver mining region of Guanajuato, Mexico. *Environmental Science & Technology* (In Review).

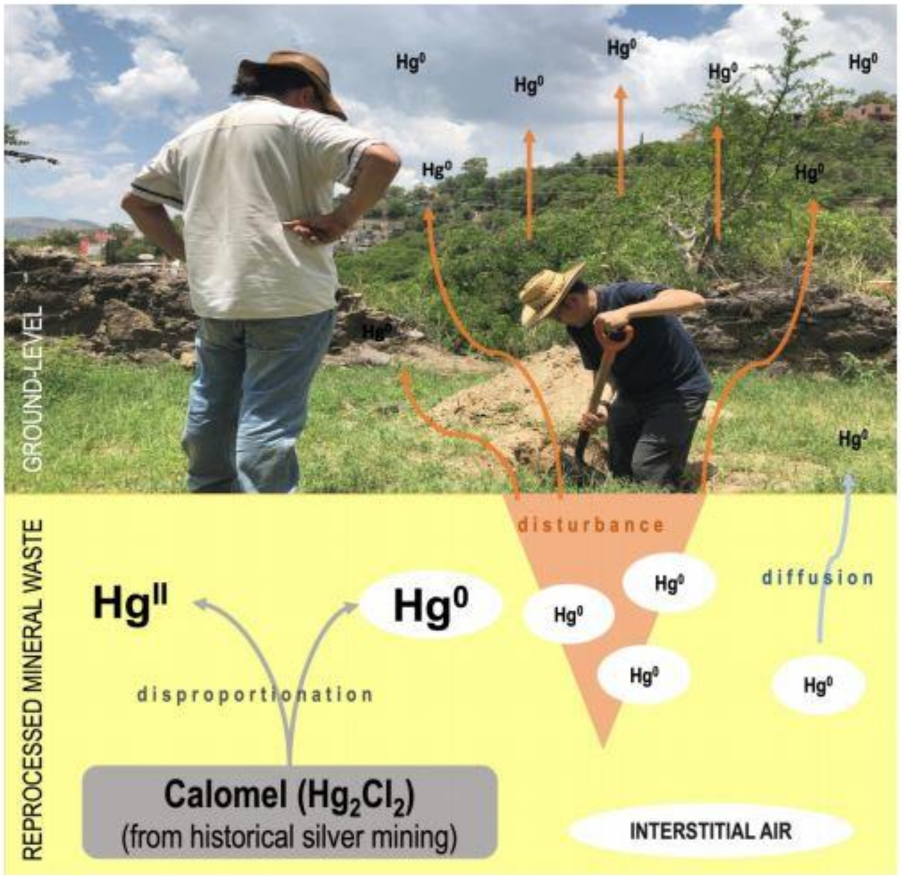

Figure 2-1. *Graphical abstract for the manuscript submitted to Environmental Science & Technology.*

ABSTRACT

Silver (Ag) production in Hispanic America between the 16th and 19th century is thought to be one of the largest sources of anthropogenic mercury (Hg) emissions in history. Recent reviews of the chemistry behind the patio process employed during that time reveal that a large amount of the Hg may not have been immediately released to the atmosphere; instead, it may have been captured in the form of calomel (Hg_2Cl_2, in which Hg exists as monovalent Hg^I) and remained in the local environment. Here we show that the Hg used in the patio process centuries ago in the Guanajuato Mining District of Mexico contributes to highly elevated present-day concentrations of gaseous elemental mercury (GEM) throughout the region. In the ground-level air, GEM ranged from 8 to 454 ng m^{-3}, exceeding the Northern Hemispheric average (~1.4 ng m^{-3}) by over two orders of magnitude. Much higher concentrations, up to 44,700 ng m^{-3}, were found in the interstitial air of reprocessed patio mineral waste, sediment, and soil. We further show that these highly elevated present-day GEM values are caused by the legacy calomel, as supported by the presence of Hg^I in the reprocessed waste and by the GEM release pattern from calomel disproportionation. Our results imply that the contribution of historical Ag refining to atmospheric Hg emissions must be re-evaluated to account for calomel and its subsequent disproportionation and release of GEM to the present-day. Long-term Hg monitoring and human health studies are also urged to assess the chronic impact of the legacy Hg in historical Ag mining regions that employed the patio process.

Keywords: calomel, gaseous elemental mercury, emissions, silver mining, Spanish Colonial era

Synopsis: Much of the mercury used during historical silver refining in Hispanic America has remained as calomel in the local environment with long-lasting impacts to the present-day.

2.1. Introduction

Mercury (Hg) is a global contaminant that is emitted into the atmosphere by various natural and anthropogenic sources, such as volcanic activities, coal combustion, and silver (Ag) and gold (Au) refining processes that employ Hg amalgamation (AMAP/UNEP, 2019). To protect human health and the environment from the adverse effects of Hg, a global treaty, the Minamata Convention, entered into force in 2017 to reduce anthropogenic Hg emissions (AMAP/UNEP, 2019). One of the major challenges in evaluating the effectiveness of the Minamata Convention is the uncertainties associated with Hg released from historical anthropogenic activities, especially from Hg-aided Ag refining in Hispanic America from the late 16th to the end of the 19th centuries (Outridge et al., 2018). Whereas some estimates (Amos et al., 2013; Nriagu, 1993; Streets et al., 2011, 2017) placed Ag refining in Hispanic America as one of the largest anthropogenic Hg sources in history, other studies hinted its contribution might be much smaller (Guerrero, 2012, 2016, 2018; Outridge et al., 2018; Streets et al., 2019; Zhang et al., 2014).

Nriagu (1993) was the first to recognize the global significance of Hg releases from Ag mining in Hispanic America, estimating a total of 2.0×10^5 t of Hg being released to the atmosphere during the period 1570 to 1900, which would have accounted for ~13% of the global total anthropogenic Hg releases throughout human history (Streets et al., 2017). This and subsequent studies (Carmago, 2002; Hagan et al., 2011; Nriagu, 1993, 1994) based their estimates on the assumption that the Hg emission process from Ag mining in Hispanic America was similar to that in artisanal Au mining, during which 60–85% of the Hg was emitted to the atmosphere, with only a small fraction lost to local land and water bodies. Even with a conservative emission factor of 40–52%, global Hg budget models show that Ag refining in Hispanic America would have contributed substantially to the present-day, global atmospheric and oceanic Hg concentrations and inventories (Amos et al., 2013; Streets et al., 2011, 2017).

However, by reviewing the chemistry behind the Ag refining process in Hispanic America, known as the patio process, Guerrero (2012, 2016, 2018) brought attention to the fact that the amalgamation processes involved in Ag and Au extraction were fundamentally different. Gold is typically present in ore in its elemental form which can be directly extracted by amalgamation with elemental Hg (Hg^0). The amalgam would be heated to recover the Au with Hg^0 being released as a vapour, some of which would be recovered and reused in future refining cycles and the rest lost to the atmosphere. In contrast, most of the Ag in deep ore deposits in the Americas occurs as monovalent Ag^I (acanthite (Ag_2S) and chlorargyrite (AgCl)) (Guerrero, 2016; Silitoe, 2009) that does not amalgamate directly with Hg^0. As such, the patio process involved a redox reaction with Hg^0 to convert Ag^I into Ag^0 to allow amalgamation, producing calomel (Hg_2Cl_2, in which Hg exists as monovalent Hg^I) as a by-product (Johnson and Whittle, 1999). Based on this premise, Guerrero (2012, 2016) calculated that as much as 66–93% of the Hg used in Ag extraction by the patio process was transformed into calomel, with no more than 7–34% lost as Hg^0 to the soil, waterways, or via volatilization. Measurements carried out in the 19th century in Mexican and U.S. Ag refining centers suggested that only up to 3% of Hg was emitted directly to the atmosphere during operations (Guerrero, 2018); Guerrero (2018) estimated that the rest was lost to local land and water bodies in the form of calomel (84%) or liquid Hg^0 (13%).

Applying Guerrero’s low emission factor, more recent global Hg modeling reveals that the contribution of Ag mining in Hispanic America to the global atmospheric and oceanic Hg levels and inventories would be much lower than previous thought (Outridge et al., 2018; Streets et al., 2018, 2019; Zhang et al., 2014). This would be in better agreement with historical atmospheric Hg deposition data derived from sediment core records from remote lakes and Hg measurements in the deep ocean, both of which indicate only modest Hg emissions from mining activities during the pre-industrial era (Engstrom et al., 2014; Outridge et al., 2018). However, the presence of calomel in historical Ag mining regions has not been experimentally studied.

As part of an international collaborative effort to understand the local to global implications of Hg releases from historical Ag mining in Hispanic America, here we report highly elevated present-day GEM concentrations in ground-level air and in the interstitial air of reprocessed mineral waste from former patio sites (known locally as *haciendas*), sediment and soil in Guanajuato, Mexico. We further provide evidence to support that the high GEM concentrations are caused by the disproportionation of calomel formed during the historical patio process.

2.2. Materials and Methods

2.2.1. Study Area

The Guanajuato Mining District (GMD) (Figure 2-2), Mexico, was recognized as one of the most lucrative Ag-producing regions in the world during the Spanish Colonial era, producing more than 8000 t of Ag for the period from 1654 to 1805 alone (Guerrero, 2017). The patio process was used until the 19th century when it was gradually replaced by cyanidation, and by flotation since 1946 (Ramos-Arroyo et al., 2004). More details of the GMD and regional information are provided in Appendix A - Supporting Information (Text A1 and Figure A1).

Twenty-six sites in GMD were studied in July 2019 (Figure 2-1, Table A-1), 22 of which are located within the City of Guanajuato, a narrow valley that hosts the renowned Ag mines that were exploited throughout the Colonial era. The study sites include reprocessed mineral waste, sediment/soil, and other sites that may be historically significant to the amalgamation process (e.g., former haciendas, mine areas). Many of the sites are frequented daily by residents and tourists alike, whereas others are more secluded.

The reprocessed waste sites are all former amalgamation wastes from haciendas that has since been reprocessed by either cyanidation or flotation to obtain residual amounts of Ag. Some mineral wastes have been discarded on mountain tops on the outskirts of the city (e.g., La Perlita), while others have been deposited in residential areas (e.g., Cerro del Cuarto). The sediment/soil sites are mostly related to water bodies (e.g., rivers, dams, reservoirs), although some are included in this category based on consistency of the sampling matrix. The sites along the river in the urban area (e.g., Río Guanajuato, Río Pastita and Plaza Ranas) are in proximity of former haciendas, which are known to have spanned the riverside. *Haciendas* housed the amalgamation process and from there the Hg-containing waste would be discarded into the urban river. Conversely, hydrological sites that are not in the urban area (e.g., Puentecillas and La Purísima) are located downstream at the end of the regional basin approximately 20 km south of the city (Figure A1). Other sites include parks in the vicinity of old mines, former haciendas that have been re-purposed (e.g., parkades, hotels), and constituents of the famous underground traffic tunnels of Guanajuato which runs the original course of the Guanajuato River.

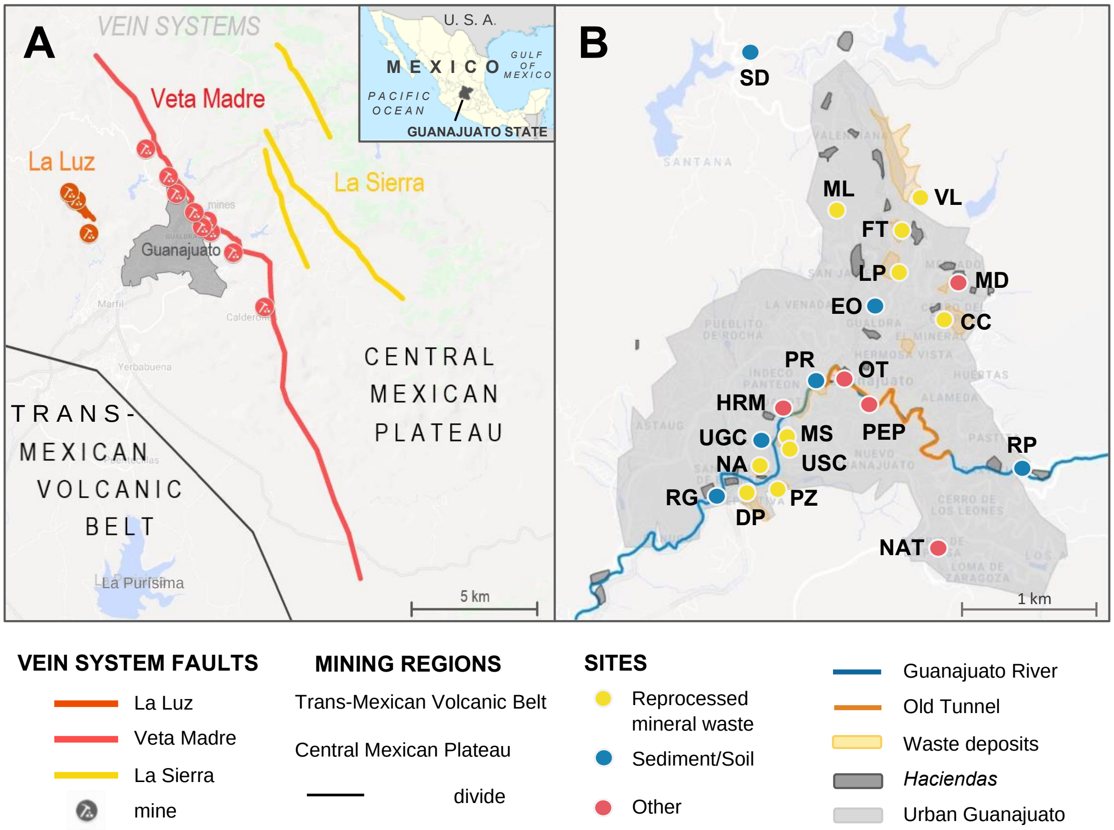

Figure 2-2. *Maps showing A) the silver-bearing veins in the Guanajuato Mining District, Mexico, and B) the study sites in and near the city of Guanajuato (shaded in gray). Details of the study sites are shown in Tables A1 and A2. Base maps were modified from Google Maps and Google Earth.*

2.2.2. Measurement of GEM

In-situ, real-time concentrations of GEM in the ground-level air and interstitial air were measured by Zeeman atomic absorption spectroscopy on a Lumex RA-915M Hg analyzer (Lumex Instruments, Mission, Canada) (Shoulupov et al., 2004). Measurements were taken in the data logger mode to cross-check with the field notes, at a resolution of every second to capture any rapid changes in the GEM concentration. The detection limit was 1 ng m^{-3} and the working GEM range was up to 20,000 ng m^{-3} (Lumex Instruments, n.d.). Quality assurance and quality control (QA/QC) was done by daily verification of the deviation value (± 20% with the stated manufacturer range) and by running a zero check every 15 minutes.

Two types of measurements were made: Surveys and Profiles. At Survey sites, GEM was measured for 5–120 min in the ground-level air only, including the ambient air (at approximately 100 cm above the ground surface), at the ground surface (both undisturbed and when disturbed by gently kicking over the topsoil), in crevasses, and near walls and other features of structures that may pertain to the historical amalgamation process (e.g., Figure 2-3A). At Profile sites, in addition to the ground-level air measurement, GEM was also measured in the interstitial air of reprocessed mineral waste, and sediment/soil. Successive depth excavations, typically in increments of 5 cm, were made from the ground surface downwards, reaching a maximum depth of up to 150 cm as permitted by the substrate. The excavations were done using a Dutch auger and were followed immediately by a GEM measurement at the given depth. The GEM value typically increased to a maximum within a minute or so before it decreased and stabilized (e.g., Figure 2-3B). A measurement was considered complete once the signal stabilized, and the maximum value at each excavated depth was recorded as the GEM concentration in the interstitial air at that depth.

2.2.3. *Measurement of Total Hg and Hg^I in Reprocessed Mineral Waste, Soil, and Sediment*

Where applicable, reprocessed mineral waste, soil and sediment samples were collected on the same day of the GEM measurements for the analysis of total Hg (Hg_T) concentration and for the occurrence of Hg^I. The samples were collected into Whirl-pak bags and shipped in coolers to the University of Manitoba.

A total of 42 samples were analyzed for Hg_T by atomic absorption spectroscopy on a direct Hg analyzer (Hydra-IIc, Teledyne Leeman Labs) following U.S. EPA Method 7473 (U.S. EPA, 2007). Between 1 and 50 mg of sample were weighed into a quartz boat using a microbalance (MS104S, Mettler Toledo). Calibration and QA/QC were done with certified reference materials including MESS-4 (marine sediment, $Hg_T = 90 \pm 40$ ng g^{-1} (average ± standard deviation) and PACS-3 (marine sediment, $Hg_T = 2980 \pm 360$ ng g^{-1}) from the National Research Council of Canada, and NIST 2709A (San Joaquin soil, HgT = 900 ± 200 ng g^{-1}) from the National Institute of Standards and Technology of the U.S.

Twenty-nine of the samples were further analyzed for Hg^I following a recently published qualitative method involving 2-mercaptoethanol (2-ME) extraction (Wang et al., 2020). Briefly, the freeze-dried samples were extracted with a 0.2% (v/v) 2-ME solution for 2 hr on a mechanical shaker at 200 rpm at room temperature, and filtered with 0.2 μm polyethersulfone filters (Puradisc 25, Whatman). Separation of Hg^I from divalent Hg^{II} in the filtrates was achieved on an ion chromatograph (IC) (ICS 5000+, Dionex) with a C18 column (Agilent InfinityLab Poroshell 120 EC-C18) and a 0.5% 2-ME mobile phase, which was interfaced with an inductively coupled plasma-mass spectrometer (ICP-MS; Agilent 8900 triple quadrupole) for Hg detection. More details are provided in the Appendix A (Text A2).

2.2.4. *Calomel Disproportionation Experiment*

A laboratory experiment was carried out to examine the GEM release pattern from calomel disproportionation in the presence of UV-visible light. Approximately 0.1 g of calomel (99% pure, Alfa

Aesar) was weighed into a glass beaker. The beaker was inserted into the chamber of a SunTest XLS+ solar simulator (Atlas, Mount Prospect, USA) for an hour ($\lambda = 300 - 800$ nm, irradiance = 700 W m^{-2}). GEM produced from calomel disproportionation was measured by placing the inlet tubing of the Lumex Hg analyzer near the outflow grid of the solar simulator, following the same QA/QC procedures as described above. Prior to the experiment, GEM was also measured in the laboratory ambient air away from the solar simulator, near the outflow of the solar simulator, and inside the solar simulator chamber to allow comparisons.

2.2.5. Data Analysis

GEM concentrations in the ground-level air were reported as arithmetic means of the ambient air, disturbed and undisturbed surface measurements when the data followed a normal distribution, and as medians otherwise. GEM concentrations in the interstitial air were reported as the maximum values at specific depths. Medians and ranges of GEM were also reported for each site category and across the entire study area as the data did not follow a normal distribution. Statistical analyses were done using SigmaPlot v13 (SysStat Software Inc.). The ANOVA on ranks and the Mann-Whitney Rank Sum analyses were conducted at a significance level of 0.05.

2.3. Results

Examples of time-series patterns of GEM data are shown in Figure 2-3. Examples of vertical distribution patterns of GEM in the interstitial air are shown in Figure 2-4. A summary of ground-level and interstitial air GEM values from each study site is shown in Figure 2-5 and Table A-2.

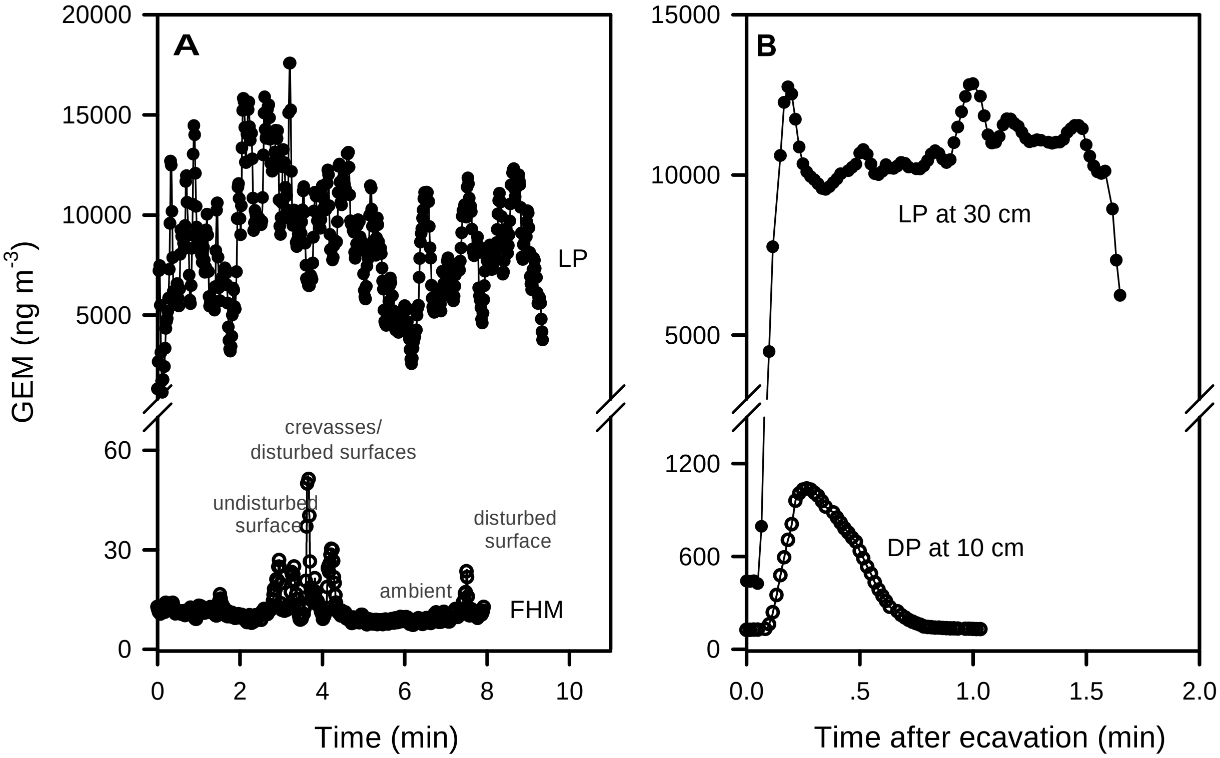

Figure 2-3. *Examples of time series patterns of gaseous elemental mercury (GEM) concentrations in A) the ground-level air at a Survey site, FHM (former hacienda Mellado, a present-day tourist look-out site on the grounds of the preserved ruins of a former hacienda) as the surface went through various disturbances, and at a Profile site, LP (La Perlita, a mountain site where reprocessed mineral waste was discarded), upon surface disturbance on a hot, sunny day; B) the interstitial air at site LP at a depth of 30 cm and at another Profile site, DP (Deportiva, near a present-day sports complex containing discarded reprocessed mineral wastes) at 10 cm.*

2.3.1. GEM in Ground-Level Air

At Survey sites, GEM values in the ground-level air are generally stable but tend to increase upon disturbance of the surface or during measurements in crevasses of walls (Figure 2-3A). At Profile sites, the ground-level air measurement is comprised of the mean of the stabilized ambient air measurement and stabilized surface measurements (Figure 2-3A).

Across the entire study area in Guanajuato, the median GEM concentration in the ground-level air was 28 ng m^{-3}, ranging from 7 ng m^{-3} at the New Access Tunnel (NAT) to 454 ng m^{-3} at the Cerro del Cuarto (CC) (Figure 2-5, Table A-2). Among site categories, the median GEM values in the ground-level air were generally lower at the sediment/soil (21 ng m^{-3}) and other (23 ng m^{-3}) sites than at the reprocessed mineral waste sites (56 ng m^{-3}), although the differences between the groups were not statistically significant (ANOVA on ranks, $p = 0.11$). Spatially, the ground-level air GEM concentrations were generally higher in the urban area (range: 7 to 454 ng m^{-3}) than those in rural areas (range: 8 to 200 ng m^{-3}) such as Puentecillas (PC) and La Purísima (PP).

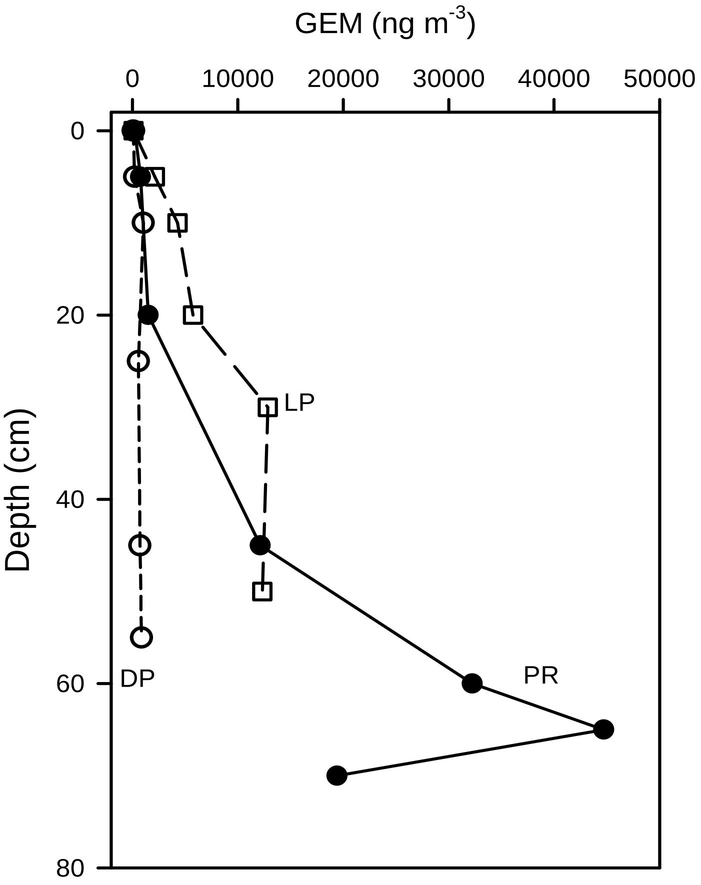

Figure 2-4. *Examples of vertical distribution patterns of maximum gaseous elemental mercury (GEM) concentrations at three Profile sites DP (Deportiva), LP (La Perlita), and PR (Plaza Ranas, near a former hacienda along the old path of the Guanajuato River).*

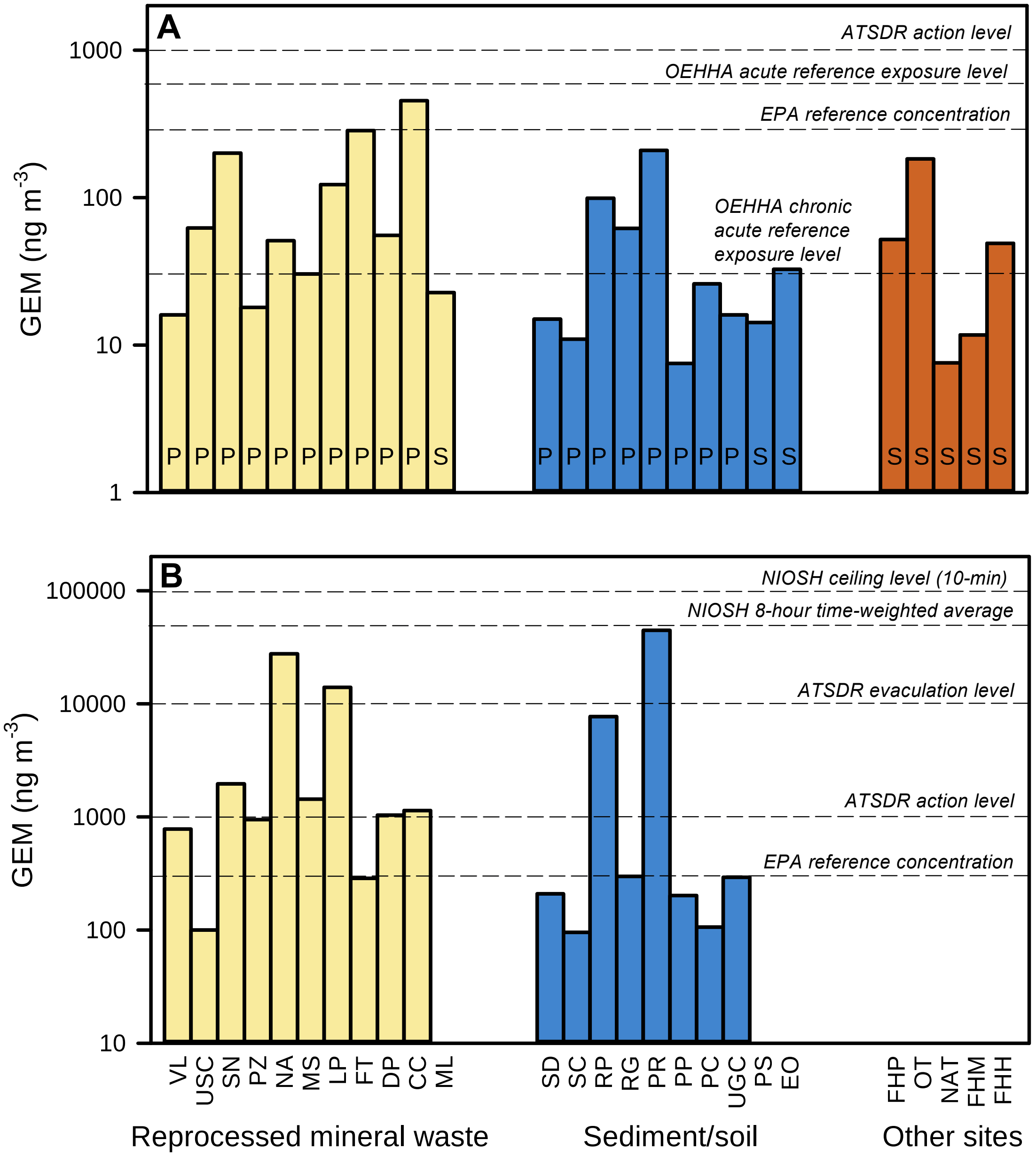

Figure 2-5. *Summary of gaseous elemental mercury (GEM) concentrations in and around the city of Guanajuato, Mexico. A) Mean or median GEM concentrations in the ground-level air. B) Maximum GEM concentrations in the interstitial air. Bars labelled with a "P" refer to Profile sites, and those with an "S" refer to the Survey site data. Dashed lines indicate various air quality guidelines for GEM. ATSDR: U.S. Agency for Toxic Substances and Disease Registry; EPA: U.S. Environmental Protect Agency; NIOSH: U.S. National Institute for Occupational Safety and Health; OEHHA: California Office of Environmental Health Hazard Assessment.*

2.3.2. GEM in the Interstitial Air

At most of the Profile sites, the GEM concentration in the interstitial air increased rapidly following the excavation of the reprocessed mineral waste, sediment or soil material, and then decreased within seconds (e.g., Site DP in Figure 2-3B). One exception is the La Perlita (LP) reprocessed waste site where elevated GEM concentrations at each depth were sustained for more than one minute before decreasing (Figure 2-3B). At the same site, a sustained, elevated GEM signal (consistently between 2,000 and 18,000 ng m^{-3} over 10 min) was also observed at the disturbed surface of the waste (Figure 2-3A).

With two exceptions (Sites FT and CC), GEM concentrations in the interstitial air at all other Profile sites were higher than at the surface or in the ambient air (Figure 2-4, Table A-2). No apparent trend was found between depth and GEM concentrations in the interstitial air of waste, sediments and soils, as the depth where the interstitial GEM concentration peaked varied greatly from 10 cm at DP to 270 cm at PC. The maximum GEM values in the interstitial air varied between 95 ng m^{-3} at Santana Creek (SC) and 44,700 ng m^{-3} at Plaza Ranas (PR), with a median value of 865 ng m^{-3}. The maximum GEM of 44,700 ng m^{-3} was observed downtown at Plaza Ranas near a former hacienda along the old path of the Guanajuato River, which has since been paved into a road. Note that this maximum concentration exceeded the upper limit of the working range (20,000 ng m^{-3}) of the Lumex Hg analyzer, so it is possible that the actual concentration could be higher.

The site category with the highest median GEM concentration in the interstitial air was the reprocessed waste sites (1,090 ng m^{-3}), followed by the sediment/soil sites (251 ng m^{-3}), though the differences between the mean values were not statistically significant (Mann-Whitney Rank Sum Test, $p = 0.198$). Interstitial air measurements were not measured at the other sites, as they were all Survey sites.

2.3.3. Hg_T and Hg^I in waste, soil, and sediment

The Hg_T concentrations in the 42 waste, sediment, and soil samples varied over five orders of magnitude, ranging from 0.068 μg g^{-1} at Puentecillas to 622 μg g^{-1} at the Pastita River (Table A-3), with a median value of 7.04 μg g^{-1}. The Hg_T concentrations were higher in urban areas (median: 14.7 μg g^{-1}, range: 0.177 to 620 μg g^{-1}) than rural areas (median: 7.04 μg g^{-1}, range: 0.068 to 10.6 μg g^{-1}). These values are in good agreement with Hg concentrations found in present-day soil near historical Ag mining sites in Potosí of Bolivia (up to 155 μg g^{-1}) (Hagan et al., 2011; Higueras et al., 2012) and in the vicinity of former haciendas in Cedral of Mexico (up to 116 μg g^{-1} in soil and 548 μg g^{-1} in amalgamation waste) (Leura Vicencio et al., 2017; Morton-Bermea et al., 2015).

The 2-ME extraction method showed the presence Hg^I (and Hg^{II}) in all the 29 samples analyzed (Table A-3). Example IC-ICP-MS chromatograms are shown in Figure 2-6, which clearly shows the presence of both Hg^I and Hg^{II} in the extracted soil sample from Plaza Ranas (PR), as their respective peaks were well separated with retention times matching those of the Hg^I and Hg^{II} standards.

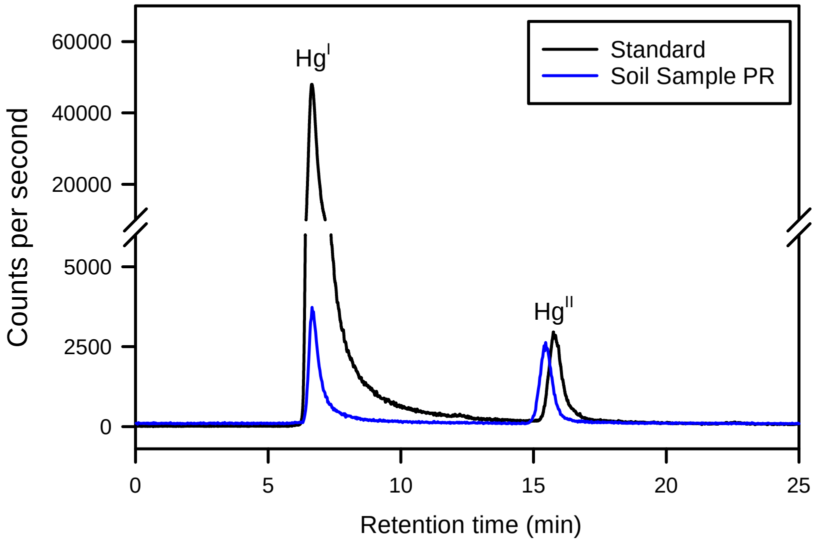

Figure 2-6. *Ion chromatography-inductively coupled plasma-mass spectrometry (IC-ICP-MS) chromatograms of* ^{202}Hg *from a mixed* Hg^I *(100 μg* L^{-1}*) and* Hg^{II} *(10 μg* L^{-1}*) standard solution (black line) and the 2-mercaptoethanol extract of the Plaza Ranas (PR) soil sample (blue line), showing the presence of* Hg^I *(and* Hg^{II}*) in the soil sample.*

2.3.4. Calomel Disproportionation Experiment

Results from the calomel disproportionation experiment are shown in Figure 2-7. GEM measurements taken in the laboratory and outside of the solar simulator prior to the experiment are indicative of background concentrations of the laboratory and showed little variation (Figure 2-7A, B), with a mean of 2.9 and 2.8 ng m^{-3}, respectively. The mean GEM value measured inside the solar simulator chamber prior to the photodegradation experiment was 6 ng m^{-3} (Figure 2-7C). As soon as the calomel sample was placed inside the solar simulator and the light was activated, the GEM signal rose rapidly and peaked at 102 ng m^{-3} within minutes (Figure 2-7D). GEM then decreased slowly over the next 30 min before plateauing at a sustained and elevated concentration of 50 ng m^{-3} for the remainder of the one-hour experiment.

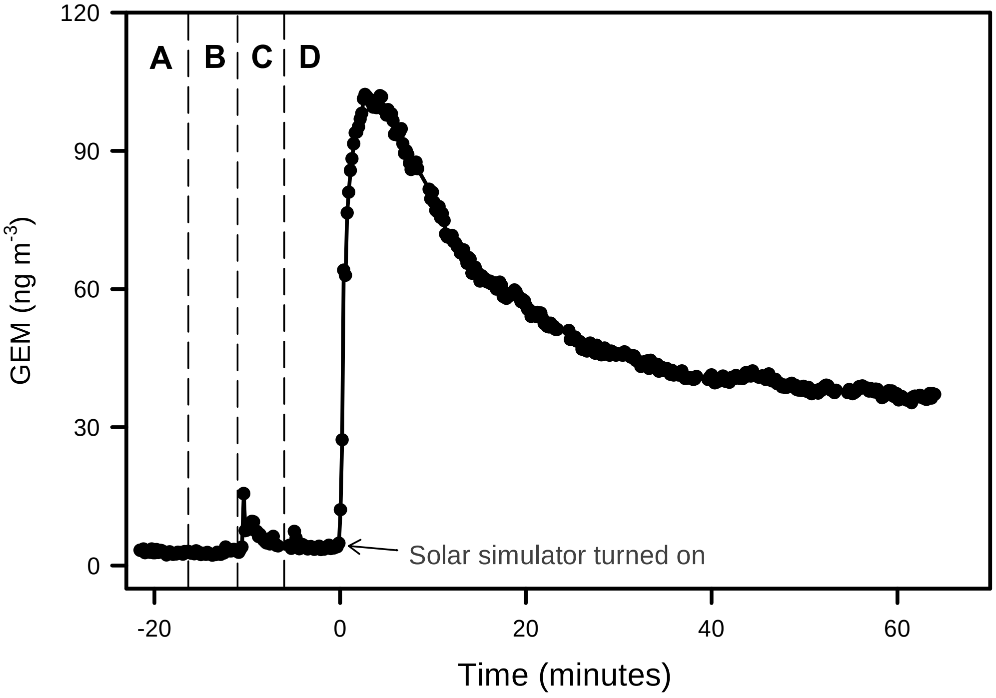

Figure 2-7. *Release of gaseous elemental mercury (GEM) from calomel disproportionation inside a solar simulator, showing GEM concentrations of A) the ambient laboratory air prior to the start of the experiment, B) near the outflow of the solar simulator prior to the start of the experiment, C) the chamber of the solar simulator prior to the start of the experiment, and D) near the outflow of the solar simulator during the experiment. Time zero denotes when the solar simulator was turned on.*

2.4. Discussion

2.4.1. Widespread Incidences of Highly Elevated GEM Values Across the GMD

From Figure 2-5 and Table A-2, it is clear that GEM concentrations in the ground-level ambient air throughout the study area consistently exceeded the global average in the Northern Hemisphere (1.3 to 1.5 ng m^{-3}, AMAP/UNEP, 2019), often by one to two orders of magnitude, in public, residential, and secluded spaces. Much higher GEM concentrations are found in the interstitial air at the reprocessed mineral waste and sediment/soil sites. To our knowledge, the maximum GEM value of 44,700 ng m^{-3} observed at Plaza Ranas near a former *hacienda* is the highest present-day GEM concentration reported for any former Hispanic-American Ag mining regions. It is over an order of magnitude higher than that reported beneath the topsoil of a former patio site at the Cerro Rico mine in Potosí, Bolivia (3,000 ng m^{-3}, Higueras et al., 2012).

2.4.2. Source and Processes Causing the Elevated Air Hg Concentrations

Based on the geology and mineralogy of the ores in the GMD, there are no significant natural sources of Hg in this region, as Hg concentrations in the epithermal veins are reportedly less than 1 μg g^{-1} (Randall-Roberts et al., 1994). The widespread, present-day high concentrations of GEM in the ground-level ambient air and interstitial air can thus only be attributed to the legacy Hg used in historical Ag refining. This is consistent with Guerrero's postulations that the direct loss of volatilized Hg to the air was minimal during the patio process and that most of the Hg used in historical Ag amalgamation formed calomel and remained in the local environment (Guerrero, 2012, 2016, 2018).

Based on the work of Johnson and Whittle (1999), Guerrero (2018), and the results from this study, the chemical reactions involved in the patio process can be summarized in Figure 2-8. $Ag_2S(s)$ in the ore was first converted to AgCl(s) in the presence of Cu^{2+} and Cl^- in aqueous solution:

$$2Cu^{2+}(aq) + Ag_2S(s) + 8Cl^-(aq) \rightleftharpoons 2AgCl(s) + 2[CuCl_3]^{2-}(aq) + S(s) \qquad (1)$$

Hg^0 was then added, reducing AgCl(s) to Ag^0, while itself being oxidized to calomel:

$$2AgCl + 2Hg^0 \rightleftharpoons 2Ag^0 + Hg_2Cl_2(s) \quad (2)$$

Subsequently, the amalgam was formed from the reaction of Ag0 with excess Hg0.

$$2Ag^0 + nHg^0 \rightleftharpoons Ag_2Hg_n \quad (3)$$

The amalgam was then heated to recover Ag. Some of the Hg^0 was recycled, with the rest rapidly lost to the air, or as residual liquid Hg^0 to the soil and waterways where it may eventually be re-volatilized to the air.

In contrast to Guerrero's hypothesis that the calomel would function as a permanent chemical sink for most of the Hg used in Ag refining (Guerrero, 2017), our results suggest that the calomel in the local environment has been slowly degrading and generating GEM over time. As a Hg^I compound, calomel is known to be susceptible to a disproportionation reaction, producing GEM and Hg^{II} (Schlüter, 2000):

$$Hg_2Cl_2 \rightleftharpoons Hg^0 + HgCl_2 \quad (4)$$

The formed $HgCl_2$ would likely be converted to the more stable HgS(s) in reprocessed mineral waste deposits or river sediment where sulfide is present, as demonstrated by a sequential extraction study (Morton-Bermea et al., 2015).

It is possible that a small fraction of the calomel could have disproportionated during or shortly after the patio process, which we refer to as "instantaneous emissions". The patios were open-air chemical reactors, where the amalgamation slurry was mixed by the feet of workers and hooves of animals for several weeks (Guerrero, 2017), and exposed to the elements such as sunlight that could have induced calomel disproportionation. A large amount of calomel, however, would have been discarded into the river with the rest of the refining waste, and/or buried in soil and sediments, where it slowly degrades and emits GEM through disproportionation to the present-day, which we refer to as "cumulative emissions".

The GEM formed from calomel disproportionation would be initially confined to the interstitial air within the encompassing matrices, but can be slowly emitted to the ambient air via diffusion or more rapidly upon physical disturbance to the matrix (e.g., Figure 2-3), contributing to the elevated ground-level GEM concentrations observed present-day. GEM releases from interstitial air to the ambient air occurs by means of diffusion or physical disturbance. Estimating the mass budget of calomel over the past several hundred years would require a better knowledge of the factors that may affect the rate of the calomel disproportionation reaction including temperature, precipitation, exposure to sunlight, presence of certain elements, and the reprocessing of the waste.

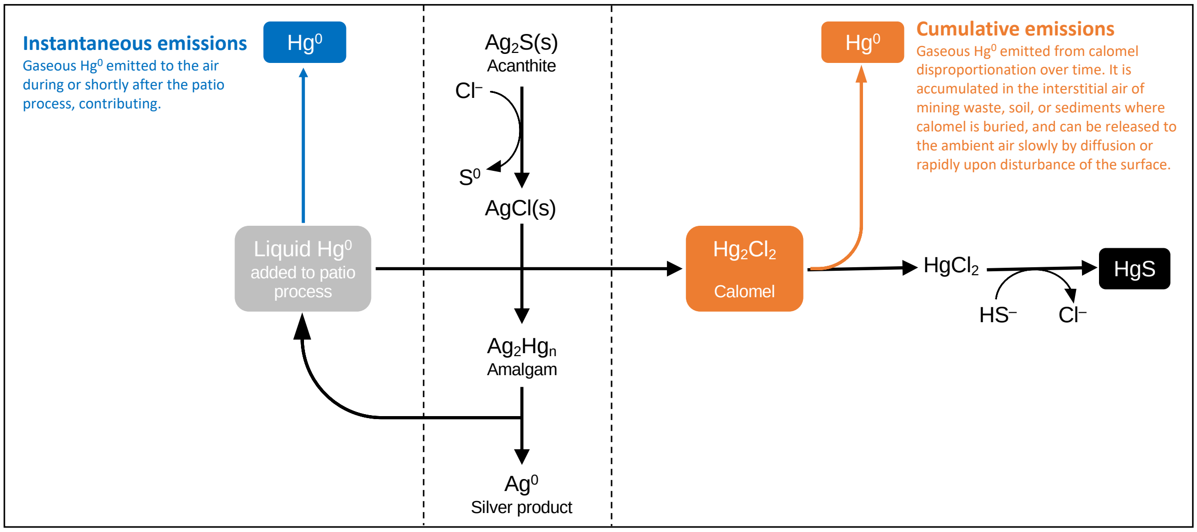

Figure 2-8. *An updated scheme, based on Johnson and Whittle (1999), Guerrero (2018), and this work, of major chemical reactions involved in the patio process of historical silver (Ag) refining in Hispanic America. The central dashed box highlights reactions involving Ag. Some of the liquid mercury added to the patio process was emitted to the air in the form of elemental mercury (Hg^0) during or shortly after the process ("instantaneous emissions", shown in the left panel), whereas the rest was converted to calomel (Hg_2Cl_2) and remained in the local environment, continuing to release Hg^0 (and Hg^{II}) to the present-day via disproportionation ("cumulative emissions", shown in the right panel).*

2.4.3. Further Support for the Role of Calomel

Standard mineralogical analytical techniques, including X-ray diffraction, scanning and transmission electron microscopy, were unable to identify calomel in the soil/mineral waste samples, due to limitations by total Hg concentrations. Instead, the presence of calomel is supported by two independent and indirect lines of evidence. First, the occurrence of calomel in the sediment and soil containing mineral waste is supported by the Hg^I peak in all the waste, soil, and sediment samples analyzed (Figure 2-7, Table A-2). Although the method is not capable of quantifying the Hg^I content (Wang et al., 2020), the chromatograms explicitly revealed the presence of Hg^I in the samples. While the chemical structures and stabilities of possible Hg^I compounds in the environment remain poorly studied, calomel is the most probable Hg^I compound in the Guanajuato samples given the chemical reactions involved in the patio process (Figure 2-8).

The second line of evidence is the calomel disproportionation experiment. Both the in-situ GEM measurements at La Perlita (Figure 2-3A) and the GEM pattern from the laboratory calomel disproportionation experiment (Figure 2-7) exhibit a consistent and elevated GEM signal that is sustained beyond the ambient baseline for an extended period of time. The La Perlita measurements were conducted at the top of a mountain on a hot and sunny day where the freshly exposed surface of the waste was exposed immediately under the sunlight, the conditions that are conducive to calomel disproportionation. The GEM pattern measured can be readily explained by calomel disproportionation under a solar simulator (Figure 2-7).

2.4.4. Human Exposure Implications

As shown in in Figure 2-5, ground-level GEM concentrations at 14 of the 26 study sites surpass the California Office of Environmental Health Hazard Assessment (OEHHA) chronic reference exposure level (REL) (30 ng m^{-3}), while one site exceeds the U.S. Environmental Protect Agency (EPA) reference concentration of 300 ng m^{-3}. The maximum interstitial air GEM values surpassed the U.S. Agency for

Toxic Substances and Disease Registry (ATSDR) evacuation level (10,000 ng m^{-3}) at three sites, including Noria Alta (NA), La Perlita (LP) and Plaza Ranas (PR). The maximum GEM value of 44,700 ng m^{-3} at Plaza Ranas approaches the U.S. National Institute for Occupational Safety (NIOSH) and Health 8-hour time-weighted average guideline at 50,000 ng m^{-3}.

The ground-level air GEM measurements are concentrations that the public are readily and likely chronically exposed to, as they represent ambient air measurements from above-ground surveys and upon surface disturbance of the mineral waste, soil, or sediment. Conversely, the interstitial air GEM measurements are potential concentrations that people may be exposed to as an acute exposure event when a disruption of the encompassing matrix occurs. The maximum GEM concentrations in the interstitial air of reprocessed mineral waste, and sediment/soil are often observed at depth (Table A-1), implying that the population is not readily exposed to these high GEM concentrations without matrix disturbance. However, the waste may slowly emit GEM by diffusion over time. Disturbance events, such as heavy rainfall or construction activities, may initiate GEM releases of higher concentration, thereby increasing the potential for exposure as waste retaining high concentrations of GEM are consistently dispersed throughout the urban area of Guanajuato in high traffic areas, including the university campus, residential areas, and downtown (e.g., Plaza Ranas). A recent study from another Ag refining region (Cedral, Mexico) indeed attributed inhalation as the most significant exposure route of Hg to the local human population (Morton-Bermea et al., 2021).

Therefore, long-term Hg monitoring of Hg in the air and human health studies (e.g. measuring Hg in hair, blood, or urine as exposure biomarkers) are recommended in the Guanajuato region to assess the potential health impact on local residents who may have been chronically exposed to Hg and to determine whether and which mitigation measures are required. Similar studies should also be considered for other historical Ag mining regions that employed the patio process. For example, elevated Hg concentrations have been reported in the soil and river sediment in the vicinity of former haciendas in Cedral of Mexico

(Leura Vicencio et al., 2017; Morton-Bermea et al., 2015), Potosí of Bolivia (Hagan et al., 2011; Higueras et al., 2012; Hudson-Edwards et al., 2001), and Puno of Peru (Kennedy and Kelloway, 2020).

Our results reveal that much of the Hg used in historical Ag refining in Hispanic America persists in the local environment to the present day, centuries after the use of Hg for Ag refining, in the form of calomel and its disproportionation products, GEM and Hg^{II}. Our findings support Guerrero's postulation that GEM releases to the atmosphere during the patio process were much less than the high emission factors estimated from Au mining (60 to 85% (Camargo, 2002; Hagan et al., 2011; Nriagu, 1993, 1994; Robins et al., 2012)) or those used in earlier global Hg models (40 to 52% (Amos et al., 2013; Streets et al., 2011; Streets et al., 2017)). Despite a much lower emission factor during the patio process, the cumulative GEM emissions to the atmosphere from the disproportionation of calomel over centuries is potentially substantial, and may have been chronically affecting the health of local residents. Further studies are needed to determine the amount of calomel formed during the patio process and its disproportionation kinetics in the environment to better quantify both the instantaneous and cumulative release of Hg to local soils, waterways, and the local and global atmosphere. This could result in major changes to global anthropogenic Hg emission inventories, and affect the effectiveness of Hg emission controls prescribed in the Minamata Convention.

ACKNOWLEDGEMENTS

This work was supported by the Natural Sciences and Engineering Research Council of Canada and the Canada Research Chairs Program (F.W.) and a graduate fellowship from the University of Manitoba (A.L.). We thank Diego Díaz Barriga, José Carlos Zárate Valdovinos, José Adolfo Chávez García, Fátima Nicasio Gutiérrez, María Yanely Zavala Guzman, Daniel Ramos-Matehuala and Xebastian Ramos-Alvarez for volunteering their time, efforts, and enthusiasm in the field.

REFERENCES

AMAP/UN Environment. (2019). Technical Background Report for the Global Mercury Assessment 2018. Retrieved from Arctic Monitoring and Assessment Programme, Oslo, Norway / UN Environment Programme, Chemicals and Health Branch, Geneva, Switzerland.

Amos, H. M., Jacob, D. J., Streets, D. G., & Sunderland, E. M. (2013). Legacy impacts of all-time anthropogenic emissions on the global mercury cycle. *Global Biogeochemical Cycles*. 27, 410–421. https://doi.org/10.1002/gbc.20040

Camargo, J. A. (2002). Contribution of Spanish-American silver mines (1570−1820) to the present high mercury concentrations in the global environment: a review. *Chemosphere*, 48, 51–57. https://doi.org/10.1016/S0045-6535(02)00047-4

Engstrom, D. R., Fitzgerald, W. F., Cooke, C. A., Lamborg, C. H., Drevnick, P. E., Swain, E. B., Balogh, S. J., & Balcom, P. H. (2014). Atmospheric Hg emissions from preindustrial gold and silver extraction in the Americas: A reevaluation from lake-sediment archives. *Environmental Science & Technology*, 48, 6533–6543. https://doi.org/10.1021/es405558e

Guerrero, S. (2012). Chemistry as a tool for historical research: Identifying paths of historical mercury pollution in the Hispanic New World. *Bulletin for the History of Chemistry*, 37, 61–70.

Guerrero, S. (2015). The Environmental History of Silver Refining in New Spain and Mexico, 16c to 19c: A Shift of Paradigm. (Ph.D). McGill University, Montreal.

Guerrero, S. (2016). The history of silver refining in New Spain, 16C to 18C: back to the basics. *History and Technology*, 32, 2–32. https://doi.org/10.1080/07341512.2016.1191864

Guerrero, S. (2018). The environmental history of silver production, and its impact on the United Nations Minimata Convention on mercury. In *Session on Global Production and Distribution of Silver, World Economic History Congress*. Boston, USA. Retrieved from http://wehc2018.org/wp-content/uploads/2018/04/WEHCguerreroMinamata-2.pdf

Hagan, N., Robins, N., Hsu-Kim, H., Halabi, S., Morris, M., Woodall, G., Zhang, T., Bacon, A., Richter, D. D. B., & Vandenberg, J. (2011). Estimating historical atmospheric mercury concentrations from silver mining and their legacies in present-day surface soil in Potosí, Bolivia. *Atmospheric Environment*, 45, 7619–7626. https://doi.org/10.1016/j.atmosenv.2010.10.009

Higueras, P., Llanos, W., García, M. E., Millán, R., & Serrano, C. (2012). Mercury vapor emissions from the Ingenios in Potosí (Bolivia). *Journal of Geochemical Exploration*, 116, 1–7. https://doi.org/10.1016/J.GEXPLO.2011.05.004

Hudson-Edwards, K. A., Macklin, M. G., Miller, J. R., & Lechler, P. J. (2001). Sources, distribution and storage of heavy metals in the Río Pilcomayo, Bolivia. *Journal of Geochemical Exploration*. 72, 229–250. https://doi.org/10.1016/S0375-6742(01)00164-9

Johnson, D. A., & Whittle, K. (1999). The chemistry of the Hispanic-American amalgamation process. *Journal of the Chemical Society, Dalton Transactions*, 4239–4243. https://doi.org/10.1039/A905612B

Kennedy, S. A., & Kelloway, S. J. (2020). Identifying metallurgical practices at a colonial silver refinery in Puno, Peru, using portable X-Ray fluorescence spectroscopy (pXRF). *Journal of Archaeological Science Reports*, 33, 102568. https://doi.org/102510.101016/j.jasrep.102020.102568.

Leura-Vicencio, A. K., Carrizales Yañez, L., & Razo Soto, I. (2017). Mercury pollution assessment of mining wastes and soils from former silver amalgamation area in North-Central Mexico. *Revista Internacional de Contaminación Ambiental*, 33, 655–669. https://doi.org/10.20937/rica.2017.33.04.09

Lumex Instruments. (n.d.). RA-915M: Direct determination of mercury content in ambient air. Retrieved from https://www.lumexinstruments.com/metodics/16AE08.01.01-1.pdf.

Morton Bermea, O., Castro-Larragoitia, J., Arellano Álvarez, Á. A., Pérez-Rodríguez, R. J., Leura-Vicencio, A., Schiavo, B., Salgado-Martínez, E., Razo Soto, I., & Hernández Álvarez, E. (2021). Mercury in blood of children exposed to historical residues from metallurgical activity. *Exposure and Health*, 13, 281–292. https://doi.org/10.1007/s12403-021-00382-z

Morton-Bermea, O., Jiménez-Galicia, R. G., Castro-Larragoitia, J., Hernández-Álvarez, E., Pérez-Rodríguez, R., García-Arreola, M. E., Gavilán-García, I., & Segovia, N. (2015). Anthropogenic impact of the use of Hg in mining activities in Cedral S.L.P. Mexico. *Environmental Earth Sciences*, 74, 1161–1168. https://doi.org/10.1007/s12665-015-4102-7

Nriagu, J. O. (1993). Legacy of mercury pollution. *Nature*, 363, 589.

Nriagu, J. O. (1994). Mercury pollution from the past mining of gold and silver in the Americas. *Science of the Total Environment*, 149, 167–181.

Outridge, P., Mason, R., Wang, F., Guerrero, S., & Heimburger-Boavida, L.-E. (2018). Updated global and oceanic mercury budgets for the United Nations Global Mercury Assessment 2018. *Environmental Science & Technology*, 52, 11466–11477. https://doi.org/10.1021/acs.est.8b01246

Ramos-Arroyo, Y. R., Prol-Ledesma, R. M., & Siebe-Grabach, C. (2004). Características geológicas y mineralógicas e historia de extracción del Distrito de Guanajuato, México. *Revista Mexicana de Ciencias Geologicas*, 21, 268–284.

Randall-Roberts, J. A., Saldaña, E., & Clark, K. F. (1994). Exploration in a volcano-plutonic center at Guanajuato, México. *Economic Geology*, 89, 1722–1751. https://doi.org/10.2113/gsecongeo.89.8.1722

Robins, N. A., Hagan, N., Halabi, S., Hsu-Kim, H., Espinoza Gonzales, R. D., Morris, M., Woodall, G., Richter, D. dB., Heine, P., Zhang, T., Bacon, A., & Vandenberg, J. (2012). Estimations of historical atmospheric mercury concentrations from mercury refining and present-day soil concentrations of total mercury in Huancavelica, Peru. *Science of the Total Environment*, 426, 146–154. https://doi.org/10.1016/j.scitotenv.2012.03.082

Schlüter, K. (2000). Review: evaporation of mercury from soils. An integration and synthesis of current knowledge. *Environmental Geology*, 39, 249–271.

Sholupov, S., Pogarev, S., Ryzhov, V., Mashyanov, N., & Stroganov, A. (2004). Zeeman atomic absorption spectrometer RA-915+ for direct determination of mercury in air and complex matrix samples. *Fuel Processing Technology*, 85, 473–485.

Silitoe, R. (2009). Supergene silver enrichment reassessed. In: Titley SR, editor. Supergene Environmental, Processes and Products. *Society of Economic Geologists, Special Publication*, 14, 15–32.

Streets, D. G., Devane, M. K., Lu, Z., Bond, T. C., Sunderland, E. M., & Jacob, D. J. (2011). All-time releases of mercury to the atmosphere from human activities. *Environmental Science & Technology*, 45, 10485–10491. https://doi.org/10.1021/es202765m

Streets, D. G., Horowitz, H. M., Jacob, D. J., Lu, Z., Levin, L., ter Schure, A. F. H., & Sunderland, E. M. (2017). Total mercury released to the environment by human activities. *Environmental Science & Technology*, 51, 5969–5977. https://doi.org/10.1021/acs.est.7b00451

Streets, D. G., Horowitz, H. M., Lu, Z., Levin, L., Thackray, C. P., & Sunderland, E. M. (2019). Five hundred years of anthropogenic mercury: spatial and temporal release profiles. *Environmental Research Letters*. 14, 084004. https://doi.org/084010.081088/081748-089326/ab084281f.

U.S. EPA. (2007). Method 7473 (SW-846): Mercury in Solids and Solutions by Thermal Decomposition, Amalgamation, and Atomic Absorption Spectrophotometry. United States Environmental Protection Agency, Washington, DC.

Wang, Y., Liu, G. L., Li, Y. B., Liu, Y. W., Guo, Y. Y., Shi, J. B., Hu, L., Cai, Y., Yin, Y., & Jiang, G. B. (2020). Occurrence of mercurous [Hg(I)] species in environmental solid matrices as probed by mild 2-mercaptoethanol extraction and HPLC-ICP-MS analysis. *Environmental Science & Technology Letters*, 7, 482–488. https://doi.org/10.1021/acs.estlett.0c00329

Zhang, Y., Jaeglé, L., Thompson, L., & Streets, D. G. (2014). Six centuries of changing oceanic mercury. *Global Biogeochemical Cycles*, 28, 1251–1261. https://doi.org/10.1002/2014GB004939

CHAPTER THREE: ONWARDS – ADDITIONAL ANALYSES

3.1. Introduction

This chapter includes the methodology and results from microscopy analyses that were conducted but not included in the manuscript (Chapter 2), as well as additional commentary and information from the method development of the Hg(I) analysis that was presented in the previous chapter. Details on our attempt at quantification during the Hg(I) speciation analysis are also denoted here. The results of the Hg(I) method development present the issues that we encountered, the modifications that we attempted, and the corresponding results obtained. We also discuss the implications of the flaws in this method, explore the possible causes, and discuss suggestions for improvements. This information regarding the Hg(I) method is presented with the intention to help anyone wanting to further refine the method in our laboratory, without having to repeat conditions that we have already attempted.

A summary of the sites at which waste/sediment/soil samples were collected in relation to the sites referenced in Chapter 2 are outlined in Table 3-1. Site descriptions and coordinates can be found in Appendix A in Table A-1. A list of the waste/sediment/soil samples collected and the analyses that were conducted on the respective samples is defined in Table 3-2.

Table 3-1. *Summary of soil, sediment, mineral waste data collected by site from Guanajuato, Mexico*

Location	**Site ID**	**Site Type**	**Data Collected**	
			Air	**Solid samples**
Monte de San Nicolás	SN	Reprocessed mineral wastes	x	
Murcielagos	ML	Reprocessed mineral wastes	x	
Meteorological Station	MS	Reprocessed mineral wastes	x	x
University Sports Center	USC	Reprocessed mineral wastes	x	
Noria Alta	NA	Reprocessed mineral wastes	x	
Pozuelos	PZ	Reprocessed mineral wastes	x	
Deportiva	DP	Reprocessed mineral wastes	x	
La Perlita	LP	Reprocessed mineral wastes	x	x
Filtros	FT	Reprocessed mineral wastes	x	
Cerro del Cuarto	CC	Reprocessed mineral wastes	x	x
Valenciana	TV	Reprocessed mineral wastes	x	
Plaza Ranas	PR	Sediment/soil	x	x
Presa Purísima	PP	Sediment/soil	x	x
Presa Santana	PS	Sediment/soil	x	x
Puentecillas	PC	Sediment/soil	x	x
Río Guanajuato	RG	Sediment/soil	x	
Río Pastita	RP	Sediment/soil	x	x
Santana Creek	SC	Sediment/soil	x	
Soledad Dam	SD	Sediment/soil	x	
Campus	UGC	Other	x	x
El Orito	EO	Other	x	
Parking El Patrocinio	FHP	Other	x	
Hotel Real de Minas	FHH	Other	x	
Medallo	FHM	Other	x	
New Access Tunnel	NAT	Other	x	
Old Tunnel	OT	Other	x	

Refer to Table A-1 for a more detailed site description and Figure 2-2 for the map.

Table 2-2. *Summary of waste, sediment, and soil samples collected and the analyses conducted*

Location	Sample name	Depth (m)	Analyses		
			THg	Hg(I)	SEM/TEM
Puentecillas	PC-1	3.17-3.60	x		
Puentecillas	PC-2	2.70-3.17	x		
Puentecillas	PC-3	2.30-2.70	x		
Puentecillas	PC-4	2.05-2.30	x		
Puentecillas	PC-5	1.59-2.05	x		
Puentecillas	PC-6	1.45-1.59	x		
La Presa Purisima	PP2-1	0	x		
La Presa Purisima	PP2-2	0.1	x		
La Presa Purisima	PP2-3	0.2	x		
La Perlita	LP top - 1	0.00-0.18	x	x	
La Perlita	LP top - 2	0.18-0.32	x	x	
La Perlita	LP top - 3	0.32-0.60	x	x	
La Perlita	LP bottom - 1	0.00-0.12	x	x	
La Perlita	LP bottom - 2	0.12-0.25	x	x	
La Perlita	LP bottom - 3	0.25-0.40	x	x	
La Perlita	LP bottom - 4	0.40-0.54	x	x	
La Perlita	LP bottom - 5	0.54-0.70	x	x	
Presa Santana	PS-1	0.00-0.13	x		
Presa Santana	PS-2	0.13-0.23	x		
Presa Santana	PS-3	0.23-0.31	x		
Presa Santana	PS-4	0.31-0.50	x		
Campus	UGC	0.0-0.60	x	x	
Meterological Station	MS2	0.50-0.60	x	x	
Noria Alta	NA-1	0.00-0.02	x	x	
Noria Alta	NA-2	0.02-0.22	x	x	
Noria Alta	NA-3	0.22-0.30	x	x	
Noria Alta	NA-4	0.30-0.41	x	x	
Noria Alta	NA-5	0.41-0.50	x	x	
Plaza Ranas	PR-1	0.00-0.20	x	x	
Plaza Ranas	PR-2	0.20-0.40	x	x	
Plaza Ranas	PR-3	0.40-0.60	x	x	
Río Pastita	RP end - 1	0.00-0.20	x	x	
Río Pastita	RP end - 2	0.20-0.40	x	x	
Río Pastita	RP end - 3	0.40-0.60	x	x	
Río Pastita	RP middle - 1	0.00-0.20	x	x	
Río Pastita	RP middle - 2	0.20-0.40	x	x	
Río Pastita	RP middle - 3	0.40-0.60	x	x	
Río Pastita	RP trees - 1	0.00-0.10	x	x	
Río Pastita	RP trees - 2	0.10-0.28	x	x	
Río Pastita	RP trees - 3	0.28-0.42	x	x	
Río Pastita	RP trees - 4	0.42-0.54	x	x	
Río Pastita	RP trees - 5	0.54-0.70	x	x	x

3.2. Methods

3.2.1. Scanning Electron Microscopy

Characterization of mineralogical phases at the nano-scale requires a thorough pre-characterization at the micrometer-scale to first 1) identify textural relationship between Hg-bearing phases and common minerals in the soil sample and 2) to locate areas of interests for the subsequent preparation of transmission electron microscopy (TEM) samples. Following previous analytical protocols (Schindler & Hochella, 2017; Mantha et al., 2020), a soil sample from the Pastita River (RP trees – 5) was chosen for analysis, as it exhibited the highest total Hg concentration in this study. It was first characterized with scanning electron microscopy (SEM). During the SEM analysis, suitable sites of interest were identified for TEM analysis and were subsequently prepared for TEM using the focused ion beam (FIB) technology, followed by TEM investigations. The RP trees – 5 sample corresponds to a riverbank profile site along the Pastita River, upon which trees had grown (Figure 3-1). The 5 refers to the fifth collected sample of the profile at a depth of 0.54 m to 0.70 m from the ground surface of the riverbank (Table 3-2).

SEM is an imaging technique that can provide qualitative information about a sample. It enables the user to obtain images of a sample by scanning the surface of the sample with a focused electron beam at high vacuum. Three different types of electrons are generated in an SEM analysis: backscattered electrons (BSE), secondary electron (SE) and Auger electrons (AE) (Vernon-Parry, 2000). BSE and SE were used in this study to characterize samples and will be discussed in greater detail.

BSE are elastically scattered electrons of the primary electron beam by atoms in the upper 3 to 5 μm of a sample. Samples with higher electron density tend to scatter electrons to a greater extent, thus producing a stronger, brighter signal in comparison to samples with lower electron density. Because the number of scattered electrons is proportional to the atomic number (Z), information on electron density can be deduced. BSE images are thus helpful to locate Hg-bearing phases in soil samples. In contrast, SE are electrons emitted by excited atoms near the surface of the sample. As a result, SE images are useful to visualize topographic features on the surface of a sample. Concurrently, X-ray microanalysis, such as energy-dispersive x-ray spectroscopy (EDS), is used to characterize the chemical composition of a sample. Spot analysis or mapping can be done to determine the elemental distribution and estimate relative abundance of elements (i.e. semi-quantitative analysis). The ratio of the relative abundance of elements was then used to infer the oxidation states and the chemical compounds present in the sample.

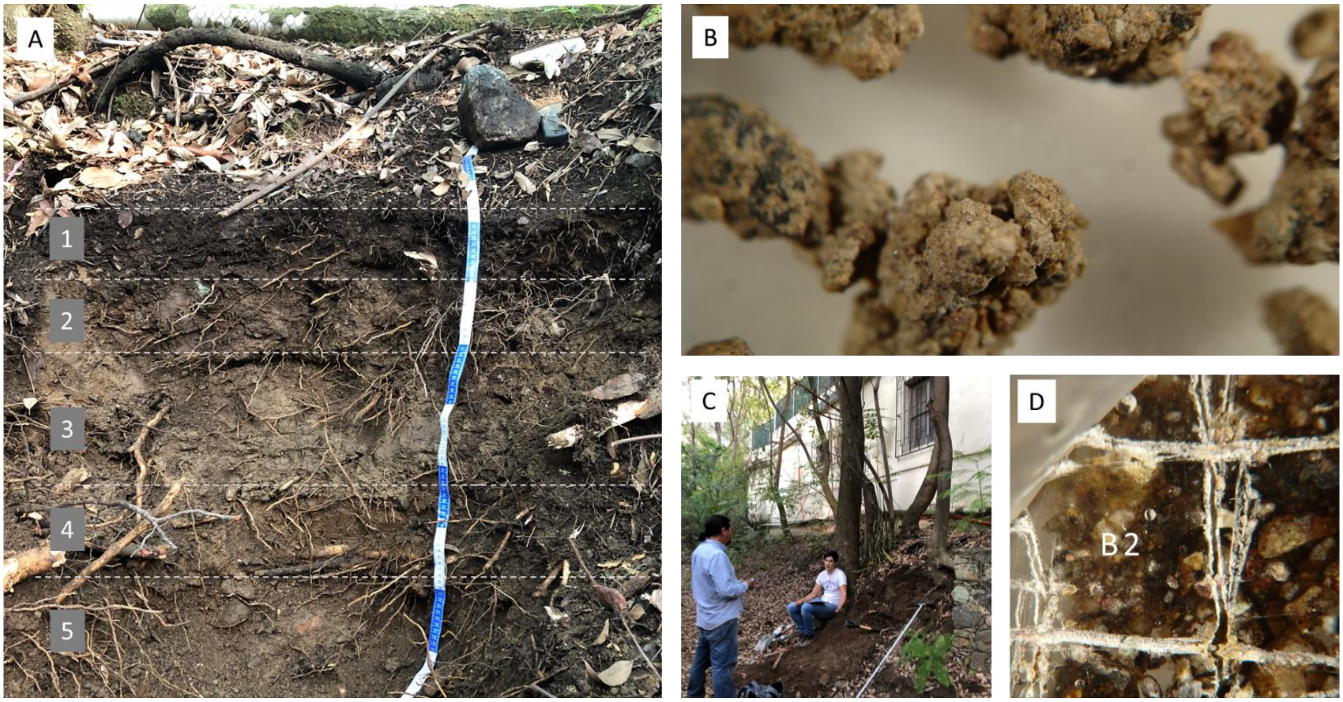

Figure 3-1. *Pastita River sampling at the RP trees site. A) The RP trees profile. Numbers 1 through 5 refer to the RP trees samples taken (see Table 3-2). B) Clusters of granules coated in fine waste and/or sand material (unmounted RP trees – 5 sample). C) The RP trees site. The profile was taken on the riverbank near an old building near the trees. D) RP trees – 5 sample settled in epoxy, prior to carbon coating for SEM analysis.*

To prepare for this analysis, a fraction of the soil sample, RP trees – 5, was embedded into an epoxy puck and carefully ground and polished. A grid system was scratched into the surface of the puck to locate grains during the subsequent preparation of the TEM samples (Figure 3-2). The puck surface was subsequently coated with carbon prior to SEM analysis.

The analysis was done with a FEI Quanta 650 FEG scanning electron microscope (ThermoFisher Scientific) at the Manitoba Institute for Materials at the University of Manitoba. The sample was analyzed systematically at magnifications up to 25,450X. Chemical distribution maps generated from EDS spectra were recorded for areas containing elevated concentration of Cl and Hg. Again, the ratio of the relative abundance of elements was then used to infer the chemical compounds present in the sample.

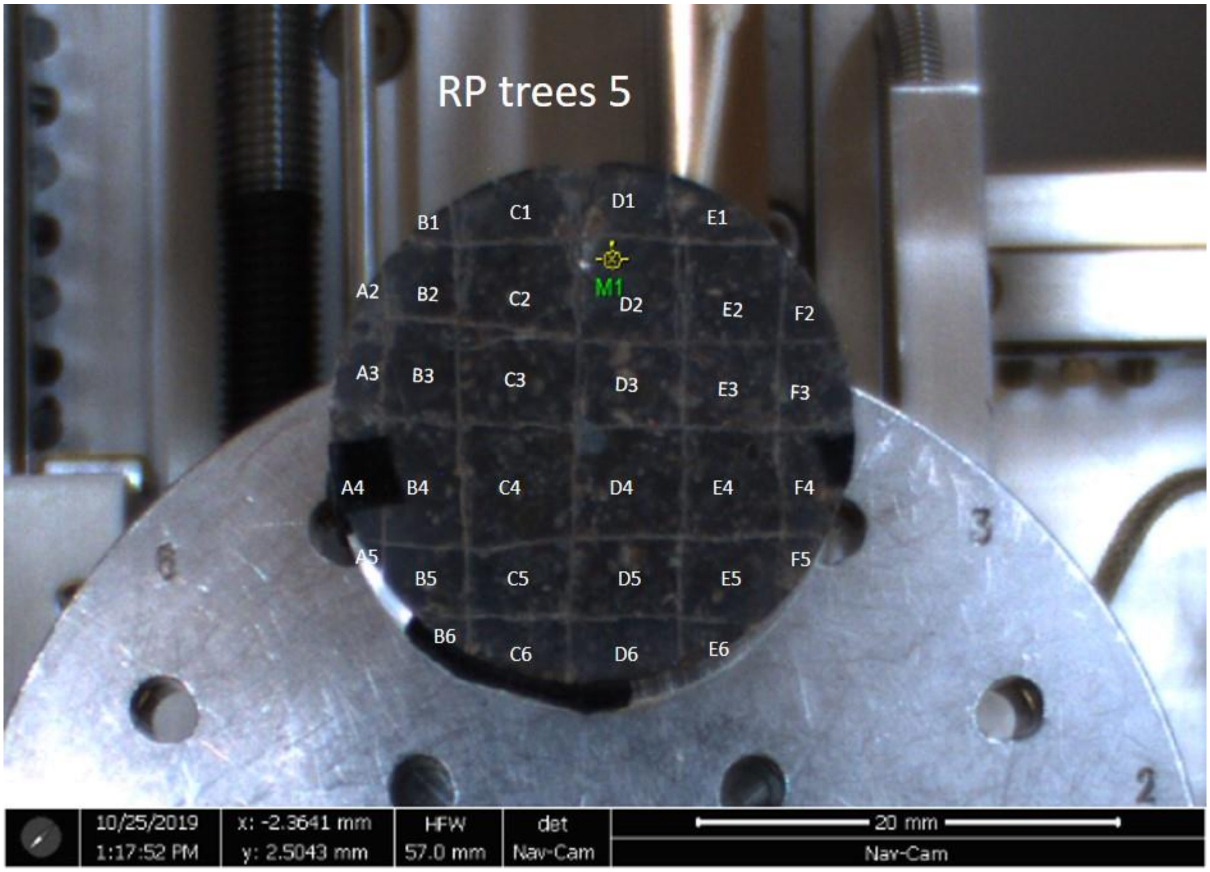

Figure 3-2. *Pastita River sample (RP trees – 5) during SEM analysis. The puck is coated in carbon and organized into quadrants (A to F for the columns and 1 to 6 for the rows).*

3.2.2. Preparation of the TEM with Focused Ion Beam Technology

The FIB technology uses most commonly a combination of SEM and a focused gallium (Ga) ion beam to extract thin and precise samples for subsequent TEM analyses (Wirth, 2004). The samples are mounted onto a TEM grid coated with carbon and are then ready for analysis. The benefit of FIB extraction in preparation for TEM analyses is that site-specific samples identified during SEM can be analyzed in greater detail due to the additional capacities and resolution TEM allows. The promptness at which a TEM sample can be prepared is also of great benefit (Wirth, 2004).

Two FIB sections were extracted from selected areas containing elevated concentrations of mercury and chloride using a FEI Dualbeam 235 SEM-FIB (ThermoFisher Scientific) at 4D Labs, Simon Fraser University, BC, Canada. The extracted sections were subsequently lifted using a platinum gas-glue and thinned to electron transparency by ion gas milling with Ga ions.

3.2.3. Transmission Electron Microscopy

As the name implies, TEM is an imaging technique that detects transmitted electrons from the electron beam passing through the thin section of the extracted sample. As electrons are transmitted rather than scattered, the configuration of a TEM is similar to that of an optical microscope. The shorter wavelength of the electrons allows a higher resolution and thus allows the recording of structural, textural and compositional features at the nanometer scale. Common operating capabilities during TEM include callcilay TEM imaging, scanning TEM imaging (STEM), selected area electron diffraction (SAED), and energy dispersive spectroscopy in STEM mode (e.g., EDS-STEM). Here, TEM was used to enhance image resolution to deduce whether calomel was present in the form of nanoparticles on two selected sites from the RP trees – 5 sample.

The TEM analyses were conducted using the FEI Talos F200X S/TEM (ThermoFisher Scientific) at the Manitoba Institute for Materials at the University of Manitoba. The two FIB sections s were mapped at low magnification to get a preliminary idea of where mercury was located. TEM images, STEM-EDS mapping, and SAED were conducted at sites where Hg and Cl overlapped with adequate density. The ratio of the relative abundance of elements was then used to infer the oxidation states of the elements and the chemical compounds present in the sample.

3.2.4. Hg(I) Analysis

A recently published method by Wang et al. (2020) claimed to be effective in extracting and qualitatively identifying Hg(I) compounds. In short, 2-mercaptoethanol (2-ME) is used to extract the Hg compounds from the solid matrix, which is followed by high performance liquid chromatography paired to inductively coupled plasma-mass spectrometry (HPLC ICP-MS). We attempted to replicate the Wang et al. (2020) Hg(I) analysis in our lab by following the optimal conditions, as outlined in their study. First, 0.05 g of freeze-dried sample was digested in 2 mL 0.2% 2-ME (pH at approximately 6.5) and shaken on a mechanical shaker (Benchmark Orbi-Shaker Jr) at 200 rpm for 2 hours at room temperature. The sample was then passed through a 0.2 μm polyethersulfone (PES) syringe filter (Puradisc 25, Whatman) and analyzed by coupling a Dionex ICS-5000+ ion chromatography (IC) system to an Agilent 8900 triple-quadrupole inductively coupled plasma mass spectrometer (ICP-MS). The separation of Hg(I) and Hg(II) was done using reverse-phased chromatography with 0.5% 2-ME as a mobile phase and a C_{18} column (Agilent InfinityLab Poroshell 120 EC-C_{18}). The Hg(I) standards were prepared from mercurous nitrate ($HgNO_3$, Sigma Aldrich) or calomel (Alfa Aesar). The Hg(II) standard was from SPEX CertiPrep. Data was collected from monitoring the ^{202}Hg isotope.

In addition to reproducing their method, we also attempted quantitation. During the method development, several modifications were tested to optimize results. These included a column change (from the Zorbax to the Poroshell), making fresh stock solutions every day (rather than every week), method run time, extraction solution, pH of the mobile phase and of the extraction solution, length of the mechanical digest, and the length of time between the digest and sample injection for analysis. More specifically, idle times (to ensure freshness of the sample) of less than 20 minutes were achieved by conducting sequential digests and timing them to coincide within minutes of the injection. The mechanical shaking times of 15, 30, and 60 minutes were all tested, as well as extraction solutions with a pH of 6 (unadjusted) versus a more basic solution with a pH of 8. A test using water as the extraction solution was also attempted.

Observational stability tests for the Hg(I) digest were also conducted by adding pH variations of the 0.2% 2-ME digest solution to a vial with calomel, mechanically shaking the vials, and scanning for visible signs of degradation.

3.3. Results

3.3.1. Scanning Electron Microscopy

The RP trees – 5 sample was chosen for SEM analysis because it exhibited the highest mean total Hg concentration at 622 μg g^{-1}. The sample was comprised of clusters of granules coated in fine mineral waste and/or sand (Figure 3-1).

A summary of the areas containing Hg in the RP trees – 5 SEM sample is outlined in Table 3-3. The quadrants refer to those outlined in Figure 3-2. Examples of BSEI, SEI, and EDS chemical mapping are illustrated in Figures 3-3 through 3-5.

The results of our SEM analysis of the soil sample from the Pastita River showed no clear or direct evidence for calomel. However, many (approximately 33) distinct areas containing both mercury and sulfur overlap were observed, ranging from 0.5 to 8 μm in size, all of which are listed in Table 3-3 and an example is illustrated in Figure 3-3. This result is suggestive of the presence of HgS(s) (cinnabar and/or metacinnabar), which supports our calomel degradation via disproportionation hypothesis and is similar to results observed in waste samples from Cedral, which determined HgS (90%; Bayer, 2013) or insoluble mercury corresponding to HgS and/or HgO (Morton-Bermea et al., 2015) as the predominant mercury compounds in wastes. In instances where mercury was not present as discrete structures with mercury-sulfur overlap, it was found within a larger structure (often iron) typically with copper, silver, sulfur, and chloride (e.g. Figures 3-4 and 3-5). Two sites with seemingly high overlap between both mercury and chloride were SEM areas M2 (Figure 3-4) and M3 (Figure 3-5). These two sites were selected for subsequent analysis by TEM for improved resolution to determine if calomel was present as nanoparticles.

Table 3-3. *Summary of Hg observed during SEM analysis of RP trees – 5 sample*

Quadrant	Area Name	EDS	Notes	Count	
				HgS	Other Hg
D2	M1	Hg, S, Ag, Se, Fe	Cu-S core in the shape of a bean with Fe and Hg shell	0	1
B1	M2*	Hg, S, Cu, Cl, Fe	Fe structure with Cu-S core with HgS and potential HgCl halo	0	1
C3	M3*	Hg, Ag, S, Fe, Ca, Si, O, Cu	Fe core with small aggregate particles of Ag/Hg/S/Cl/Cu/P. All within Fe structure	0	1
C3	M4	Hg, S, Cl, Ag, Fe, Ca, Se	Ag-S with Hg and Cl adhered onto it all within Fe	0	1
D4	M5	Hg, S	HgS, discrete rectangle shape embedded in Fe structure	1	0
D4	M6	Ag, Hg, Cl, S, Al, Fe, Si	Two spots, mostly Ag, low in Hg	0	0
D4	M7	Hg, Se, Fe	HgSe, no S	0	1
B5	M8	Hg, S	HgS in/on Fe	1	0
B5	M9	Ag, Hg, S, Cl, Fe, Cu, Se	AgS with some Hg, Cl, Fe, Cu	0	0
B5	M10	Hg, S, Se	HgS	1	0
B5	M11	Hg, S, Se, Si	HgS	1	0
B5	M12	Hg, S, Ag, Fe, Se	HgS-Ag?, EDS spot map	1	0
B5	M13	Hg, Se, S, Fe	HgSe, EDS spot map	0	1
B5	M14	Hg, Ag, S	HgAgS	0	1
B5	M15	Hg, S, Ag, Fe, P, Ca	HgS, Ag, Fe	1	0
B5	M16	Hg, S, Fe	HgS, 7 um x 4 um	1	0
B5	M17	Hg, S, Fe	HgS, 0.5 um (+2 HgS in area 19)	3	0
C5	M18	Hg, S, Ag, Se, Cl	22: HgAgS, 23: 8 spots in one structure, HgAgS and HgS, ~ 5 μm	5	4
C5	M19	Hg, S, Se, Fe	HgS, 5 μm	1	0
C5	M20	Hg, S, Ag, Fe, Cl	HgS?	1	0
D5	M21	Hg, Se, S,	HgSe, HgS x3 ~5 μm	3	1
D5	M22	Hg, S, Ag, Fe	HgS, 5 of 6 // Ag, 1 of 6 particles	5	0
D5	-	Hg, S, Ag	HgS x2 (lab book)	2	0
E5	M23	Hg, S, Fe	HgS, 8 μm	1	0
E5	M24	Hg, S, Fe, Se	HgS, 5 μm	1	0
E5	-	Hg, S	HgS, 1 μm (lab book)	1	0
E5	M25	Hg, S, Fe	HgS, 5 μm	1	0
C6	M26	Hg, S	HgS, 4 μm discrete small particles clustered	1	0
D6	M27	Hg, S	HgS, <3 μm	1	0
			TOTAL:	33	12

* sites selected for TEM analysis

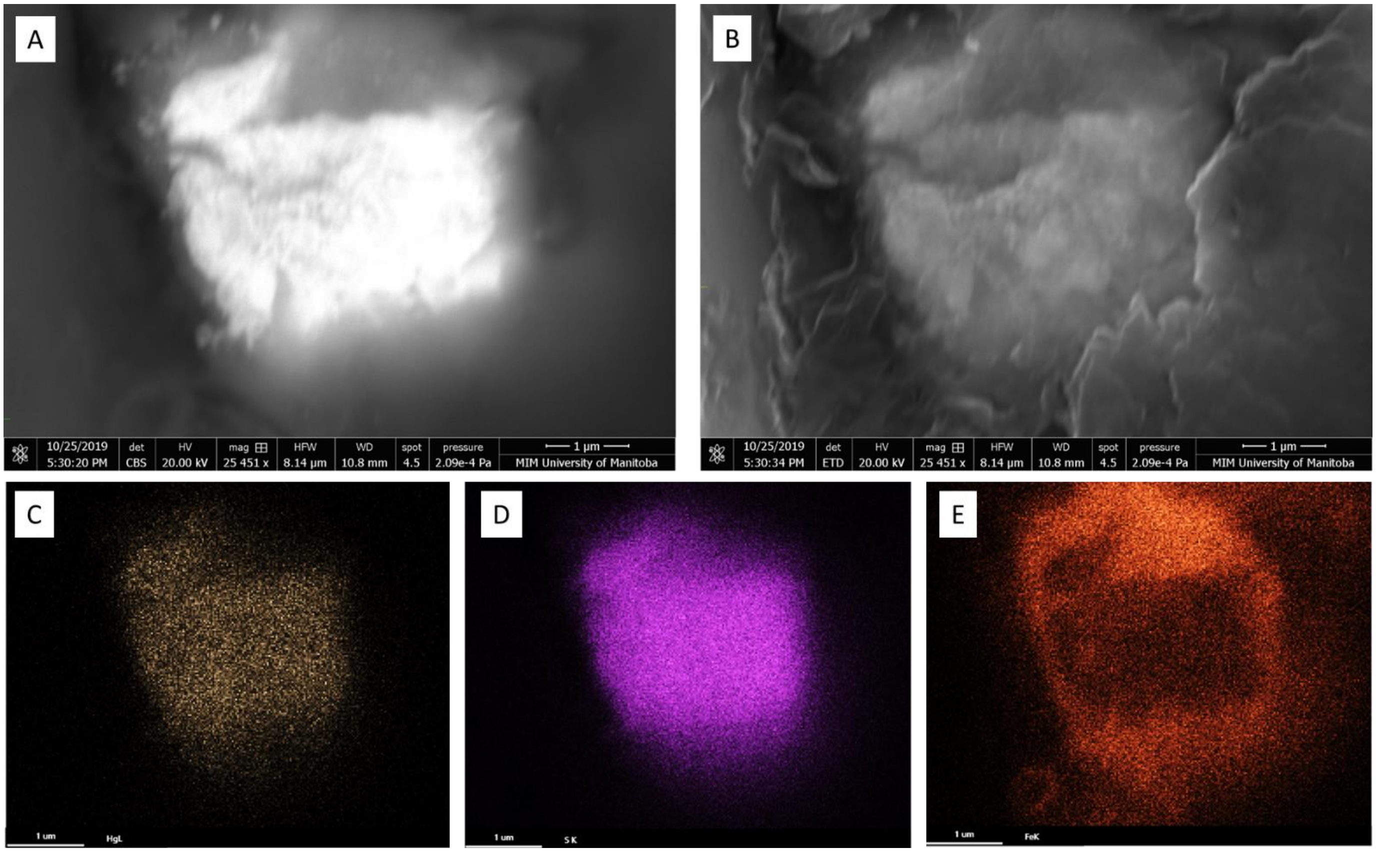

Figure 3-3. *Scanning electron microscopy data of area M5 (Table 3-3) of the RP trees – 5 sample. Example of a discrete HgS particle along the order of 4 µm embedded within an Fe structure. A) Backscatter secondary electron image. B) Secondary electron image. C) Chemical map of Hg. D) Chemical map of S. E) Chemical map of Fe.*

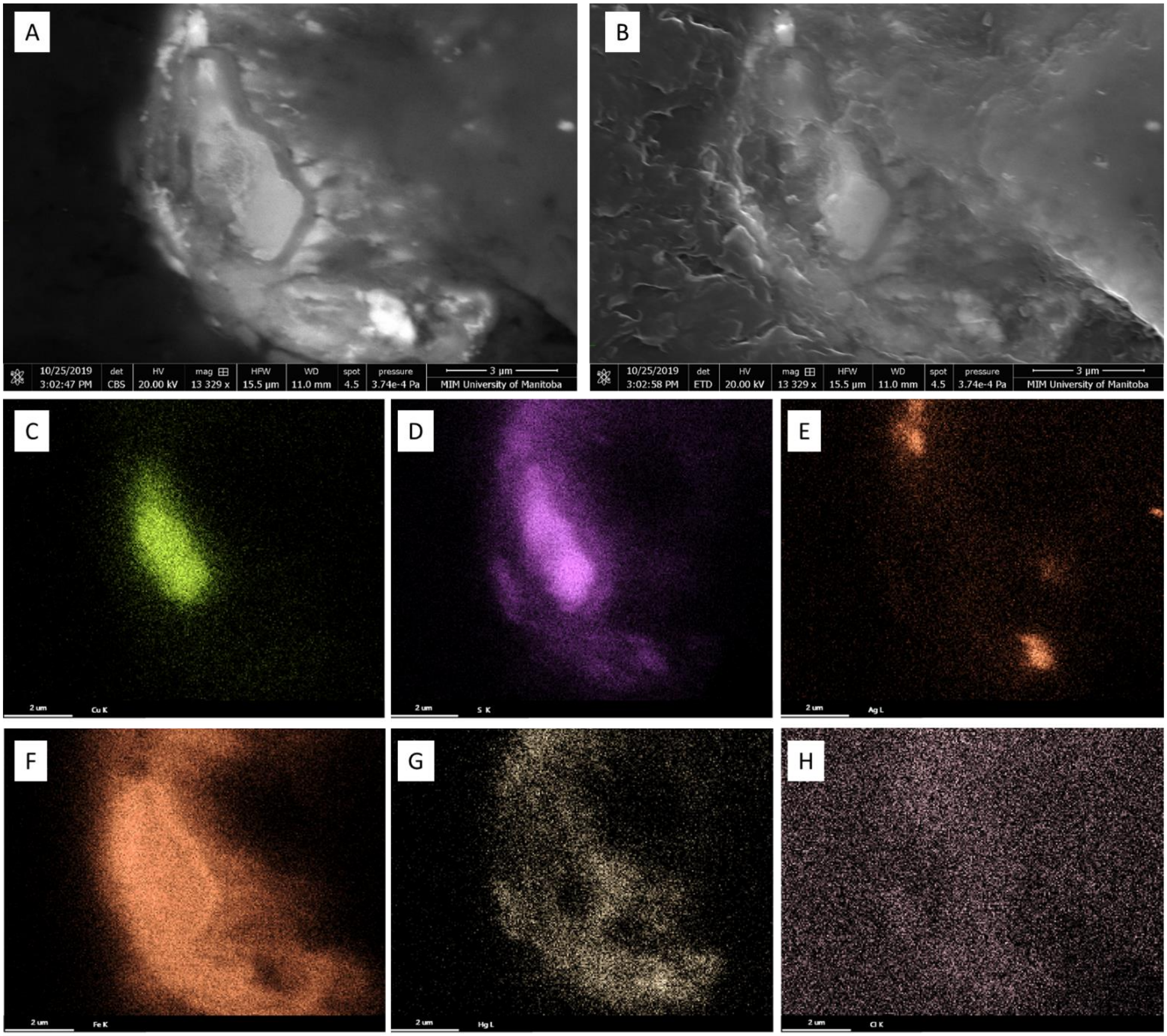

Figure 3-4. *Scanning electron microscopy data of area M2 (Table 3-3) of the RP trees – 5 sample. Also transmission electron microscopy site 1. Example of Hg incorporated into an Fe structure with a Cu-S core. A) Backscatter secondary electron image. B) Secondary electron image. C) Chemical map of Cu. D) Chemical map of S. E) Chemical map of Ag. F) Chemical map of Fe. G) Chemical map of Hg. H) Chemical map of Cl.*

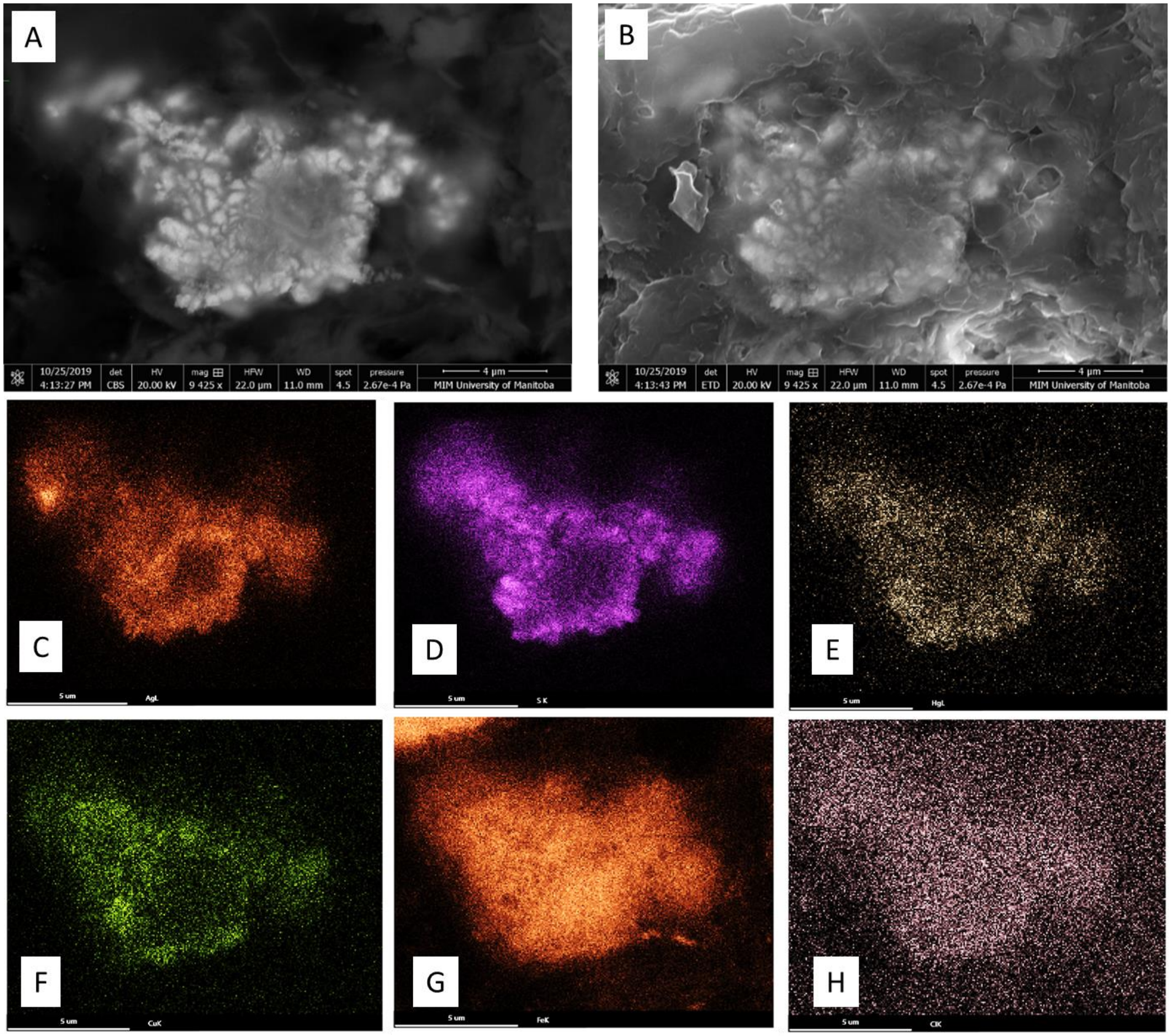

Figure 3-5. *Scanning electron microscopy data of area M3 (Table 3-3) of the RP trees – 5 sample. Also transmission electron microscopy site 2. Example of Hg incorporated into an Fe structure with a Cu core. A) Backscatter secondary electron image. B) Secondary electron image. C) Chemical map of Ag. D) Chemical map of S. E) Chemical map of Hg. F) Chemical map of Ca. G) Chemical map of Fe. H) Chemical map of Cl.*

3.3.2. Transmission Electron Microscopy

The two FIB extracted sites from the RP trees – 5 SEM sample are SEM sites M2 and M3, which correspond to FIB sections 1 and 2 (Figure 3-6). Images, EDS chemical maps, and some EDS spot data are illustrated in Figures 3-7 and 3-8. A summary of the findings from this analysis is tabulated in Table 3-4. Note that this is a not a thorough interpretation of the results (preliminary observations only), as the overarching objective of this analysis was to determine the presence or absence of calomel.

Overall, no calomel was explicitly identified. The preliminary observations on the mineralogy of mercury in the Pastita River sample suggested that mercury was present in all oxidation states: Hg(0) most likely a Ag-Hg alloy, Hg(I) as $(Ag, Hg)_2S$, and Hg(II) as HgS.

On FIB section 1 (Figure 3-6A), there were three areas of interest: crack (top), crack (bottom), and spots (left and right). The crack in the iron matrix going through FIB section 1 is clearly illustrated in Figure 3-6A and 3-7. Chemical mapping showed that the phases trapped in the top half of the crack were comprised of chlorine, silver, mercury, and sulfur (Figure 3-7B, C, D, E, and F). Upon further investigation, the chemical analysis by EDS showed that these minerals contained a higher number and similar proportion of mercury and silver (atomic percentages of 37.02% and 51.69%), with a lower proportion (little to none) of chlorine and sulfur (atomic percentages of 1.47% and 9.82%; Figure 3-7G). A similar result was observed within the minerals in the lower part of the crack. The chemical analysis for the green zone in Figure 3-7H once again shows a high proportion of mercury and silver (atomic percentages of 23.91% and 36.48%) compared to sulfur (atomic percentage of 11.03%). The chlorine-rich phase in red was indiscernible. The mineralogical results from the cracked area with both mercury and silver in similar/equal proportions with little to no anions suggest that silver and mercury may be present together in their respective elemental states; thus, most likely as an alloy.

Also within FIB section 1 was the spots area. Here, two distinct structures are visible. The chemical maps in Figure 3-8 show that the grain on the left contains chlorine, silver, and sulfur, while the structure on the right contain all of the aforementioned elements, plus mercury. The chemical analysis revealed that the grain on the right contained atomic proportions of Hg and Ag of 19.59% and 46.17%, resulting in a cumulative fraction of Hg and Ag of ~66%. Conversely, the atomic percentage of sulfur was 33.65%. Chlorine was not present in significant concentrations. The atomic ratio of Hg and Ag (66%) to S (33%) is 2:1, which suggests that Hg and Ag may both be present in the +1 oxidation states and bound to S, in an oxidation state of –2, in the form of (Ag, Hg)$_2$S.

FIB section 2 (Figure 3-6B) was not characterized in detail due to low concentrations of Cl. EDS chemical analyses showed an atom percent ratio of 30:1 of Hg to Cl. The overall finding from FIB section 2 was that Hg was present in an unknown oxidation state within an iron-rich environment.

Table 4-4. *Summary of Hg observed during TEM analysis of RP trees – 5 sample*

SEM Area Name	**FIB Section**	**FIB Area Name**	**Notes**
M2	1	Crack (top)	Hg(0) in a Hg-Ag alloy; Figure 3-7
M2	1	Crack (bottom)	Hg(0) in a Hg-Ag alloy; Figure 3-7
M2	1	Spots	Hg(I) in (Hg, Ag)$_2$S; Figure 3-8
M2	1	N/A	Hg(II) in HgS
M3	2	N/A	Hg in an unknown valence state in a Fe-rich matrix. Occurrence of cinnabar can be excluded due to Hg>>S (determined by EDS)

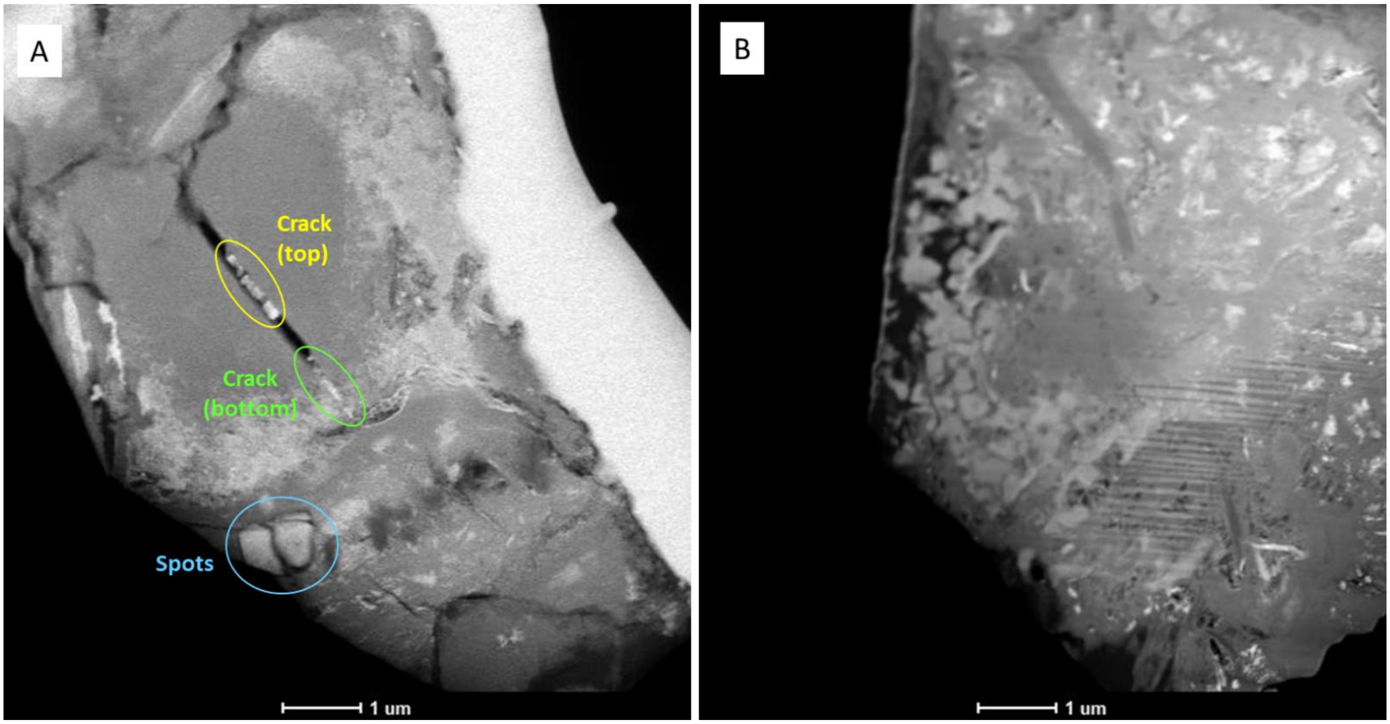

Figure 3-6. *Backscatter electron images of the two FIB extracted sections originating from the RP trees – 5 SEM sample. A) FIB section 1 from SEM M2. Areas of interest are labelled (i.e. crack (top), crack (bottom), and spots. B) FIB section 2 from SEM site M3.*

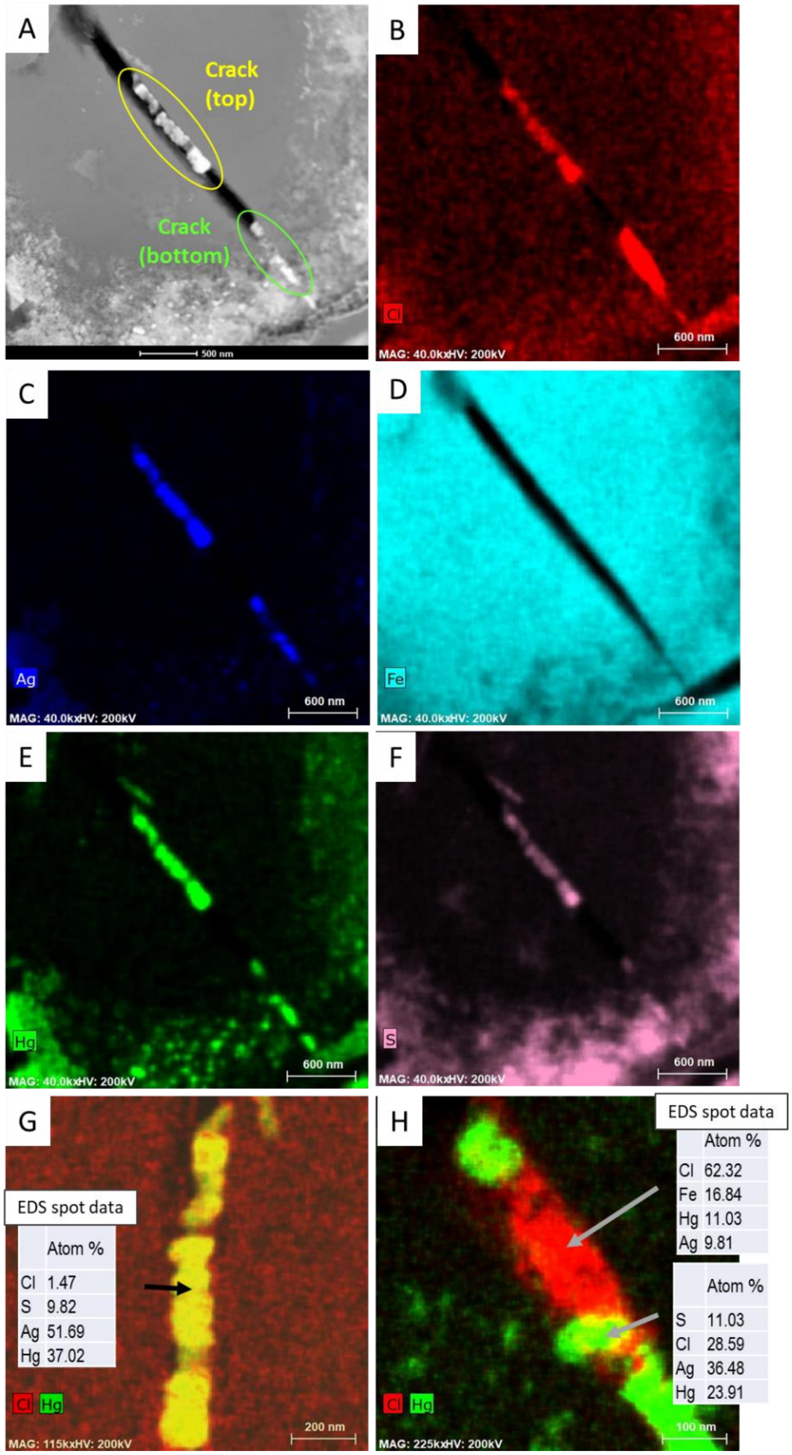

EDS spot data

	Atom %
Cl	1.47
S	9.82
Ag	51.69
Hg	37.02

EDS spot data

	Atom %
Cl	62.32
Fe	16.84
Hg	11.03
Ag	9.81

	Atom %
S	11.03
Cl	28.59
Ag	36.48
Hg	23.91

Figure 3-7. *Transmission electron microscopy data from FIB section 1 (originating from SEM site M2), re entitled crack (top) and (bottom). A) Backscatter electron image. B) Chemical map of Cl. C) Chemical map of Ag. D) Chemical map of Fe. E) Chemical map of Hg. F) Chemical map of S. G) Zoomed in overlay of Hg (green) and Cl (red) chemical maps of TEM area crack (top). H) Zoomed in overlay of Hg (green) and Cl (red) chemical maps of TEM area crack (bottom). EDS chemical analysis is shown for yellow zone in panel G, as well as red and green zones in panel H.*

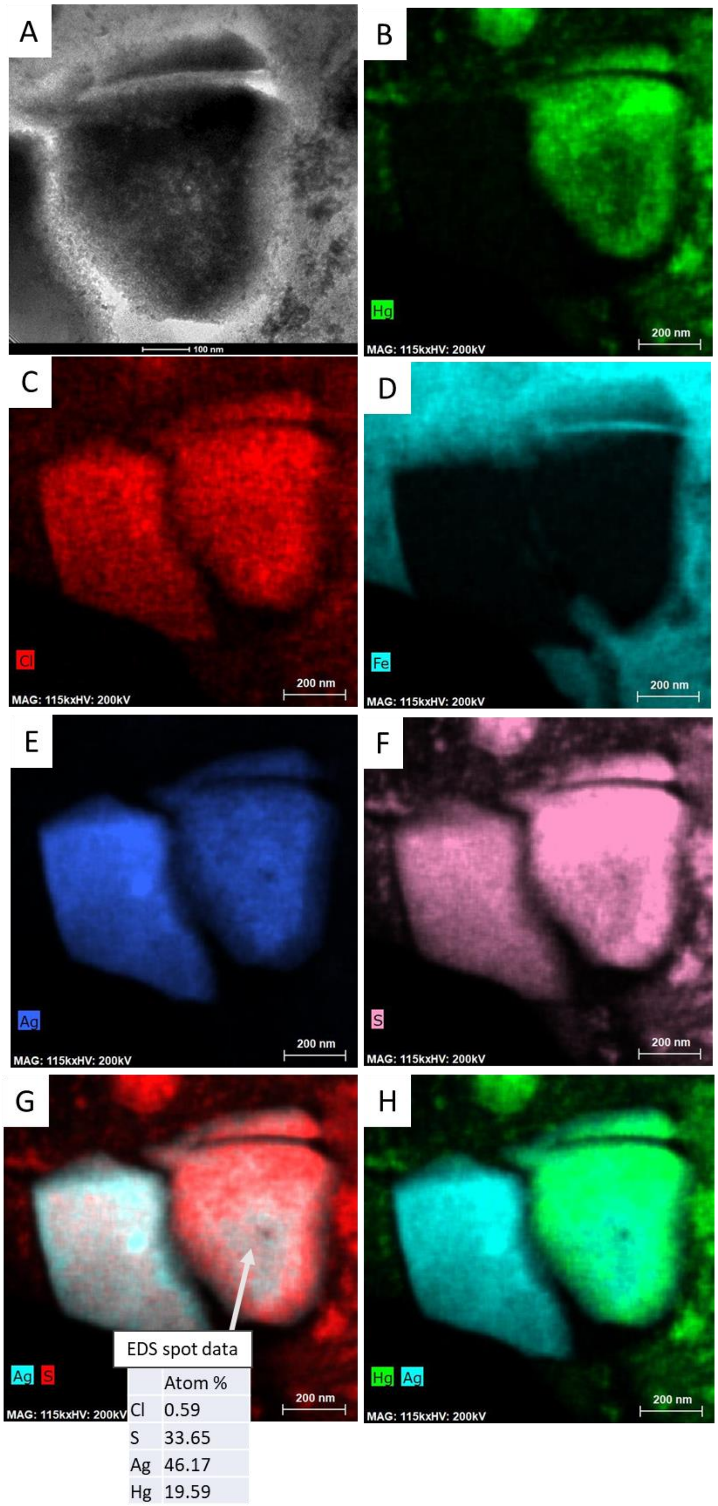

EDS spot data

	Atom %
Cl	0.59
S	33.65
Ag	46.17
Hg	19.59

Figure 3-8. *Transmission electron microscopy data from the SEM area M2 / TEM area spots. A) Zoomed in transmission electron microscope image of right spot. B) Chemical map of Hg. C) Chemical map of Cl. D) Chemical map of Fe. E) Chemical map of Ag. F) Chemical map of S. G) Overlay of Ag (cyan) and S (red) chemical maps. G) Overlay of Hg (green) and Ag (cyan) chemical maps. EDS chemical analysis is shown for right spot in panel G.*

3.3.3. Hg(I) Method Development

3.3.3.1. Issues and Modifications of the Original Wang et al. (2020) Method

Our original attempt at the Hg(I) method followed the optimal conditions described by Wang et al. (2020) and aimed for quantification also. During this endeavour, we encountered many setbacks. A list of the major issues that arose along with the modifications and their corresponding results are listed in Table 3-5.

Some of the difficulties encountered included peak shape and separation. At first, peak separation between Hg(I) and Hg(II) were adequate (retention times of 6.65 and 16.78 minutes), though the Hg(I) peak had a long trailing tail that coincided with the Hg(II) peak. To improve the peak shape, we tried using different proportions of 2-ME in the mobile phase but saw no improvements (Table 3-5). We then decided to try using a different C18 column – namely, the Agilent InfinityLab Poroshell 120 EC-C_{18} (inner diameter of 4 μm), instead of the Agilent Zorbax Eclipse Plus C18 (inner diameter of 5 μm). The Poroshell column improved the peak shape during test sample runs, although no changes were observed during standard runs. We decided to keep using the Poroshell sample from there on. Eventually, we made a new, more dilute Hg(I) stock solution which improved the Hg(I) peak tail. As a result, daily, fresh stock standard solutions became common practice for this method in our lab.

In terms of peak separation, it is normal for retention times to shift closer to one another over time due to less efficient interactions with the column, which are often a result of sample carry over, where sample accumulates and coats the column. Cleaning by pumping mobile phase or acetonitrile may resolve this issue; but if the problem persists, a more extensive cleaning regimen is likely needed (e.g. change or clean cones).

Table 5-5. *Summary of issues and modifications made to the original Wang et al. (2020) protocol during our method development process with the corresponding results.*

Issue	Modification	Result
Peak shape; Hg(I) peak had a long tail (extended into Hg(II) peak)	*Adjust % 2-ME in mobile phase*	
	• 0.5% 2-ME mobile phase *	Hg(I) peak had a long tail *
	• 0.25% 2-ME mobile phase	Hg(I) peak was very wide
	• 1.0% 2-ME mobile phase	Hg(I) and Hg(II) peaks merged
	• 5% methanol in 0.5% 2-ME mobile phase	Hg(I) and Hg(II) peaks merged
	• 0.5% 2-ME mobile phase with pH 4.5	No change observed
	Changed column from the Zorbax to the Poroshell*	
	• Zorbax column *	Hg(I) peak had a tail *
	• Poroshell column	Improved peak shape during sample runs, but no change for standards
	New Hg(I) stock solution	
	• Fresh and more dilute stock every day	Reduced Hg(I) tail
Peak separation; Hg(I) and Hg(II) peaks merged	*Adjust % 2-ME in mobile phase to improve peak separation*	
	• 0.5% 2-ME mobile phase with pH 8.5	No peak separation
	Cleaning	
	• Reverse column then run mobile phase for 2 hours, then follow with 100% acetonitrile for 2 hours. Equilibrate over night.	Improved peak separation
	• Change guard column	Improved peak separation
	• Change cones	Improved peak separation
	• Tune instrument	
Peaking shifting; Bi internal standard	• Extend method length accordingly	Unreasonably long sample runs hindering progress; eliminated Bi internal standard
Quantitation; non-linear Hg(I) curve	*Extend curve to verify that Hg(I) is linear at higher concentrations (> 25 ppb)*	Linear when calibration range is extended
Quantitation; contrast between Hg(I) and Hg(II) concentrations in samples	*Adjust dilution factor of sample*	
	• Dilutions of 500x, 250x, 100x, 50x, and 10x were all attempted	Hg(I) below quantitation limit, Hg(II) beyond upper point of curve.
	• 0x dilution	Best course of action to observe Hg(I) above limit (1 ppb)
	Simultaneously generate Hg(I) and (II) curves on different scales	
	• E.g. Hg(I) curve ranging from 1 ppb to 30 and Hg(II) ranging from 100 ppb to 3000 ppb	Appropriate for anticipatory low Hg(I) and high Hg(II) concentrations in samples

* original method based on Wang et al. (2020).

Another issue that we encountered was peak shifting of the Bi internal standard. Originally, samples and standards were injected with a Bi internal standard. However, the Bi peak shifted often, randomly, and drastically. We would extend the sample run time to compensate, but since the shifts were not incremental, this did not always work, and ended up prolonging our runs beyond a reasonable run time per sample and hindering our progress. With restricted lab hours due to the ongoing COVID pandemic and the need to run only fresh samples (idle less than 4 hours before being loaded), we decided to discontinue the use of Bi.

As mentioned, we also attempted to develop the quantification of this method and eventually deemed it adequate based on our calibration and standard runs. This is ensuring that the standard solutions (stock and running standards) are made fresh daily and do not sit longer than 4 hours before injection, which is approximately the time at which we noticed Hg(I) degradation. Some of the difficulties encountered while developing the quantitation aspect of the method was that the Hg(I) calibration curve only became linear at concentrations greater than 5 μg L^{-1} (Figure 3-9). This is of note for future method users in our lab, as the group that originally published the method had only looked at samples with Hg(I) concentrations below 10 μg L^{-1} (personal communication). On the other hand, the Hg(II) calibration curve was linear within the range of 1 μg L^{-1} to 3 mg L^{-1}. Another issue we encountered was ensuring that sample concentrations would fall onto the calibration curve range. This required trial and error with the dilution factors of the samples and adjustments of the calibration curve ranges. To compensate for the high amounts of Hg(II) and low amounts of Hg(I) in the sample, we made 5 point curves of Hg(I) and Hg(II), simultaneously, on vastly different scales. For example, our Hg(I) curve could range from 1 ppb to 30 ppb, while Hg(II) would range from 100 to 3,000 ppb. Samples were not diluted due to presumed low extracted concentrations of Hg(I), which will be discussed.

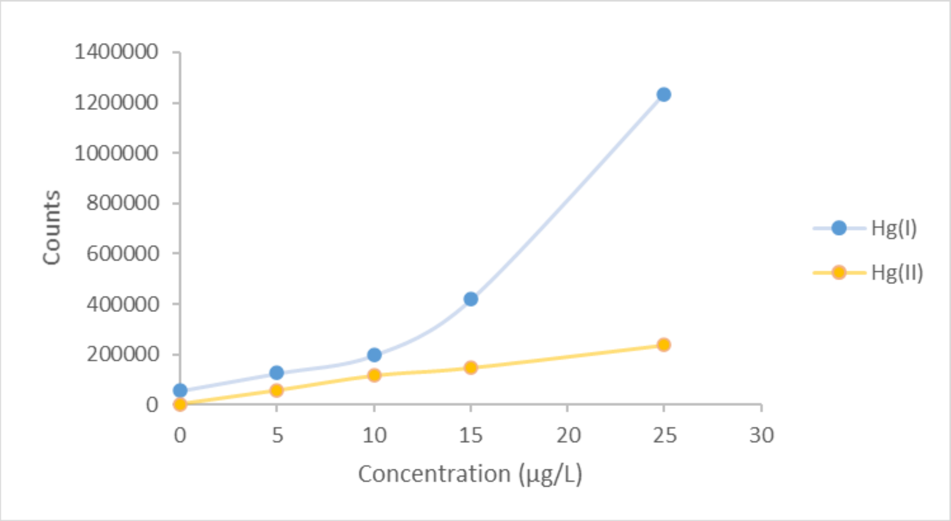

Figure 3-9. ^{202}*Hg(I) and* ^{202}*Hg(II) calibration curves during Hg speciation analysis.*

3.3.3.2. Hg(I) Results and Stability Issues

Our analysis showed that all 33 samples analyzed exhibited Hg(I) concentrations below 4 µg L^{-1} (< 1 µg g^{-1}) (Table 3-6, Appendix B). Despite the low tabulated concentrations, each sample showed both Hg(I) and Hg(II) peaks, suggesting presence of both Hg(I) and Hg(II) in all selected samples from Guanajuato. This is also true for the samples that were analyzed during run 4, which all exhibit concentrations below baseline or close to 0 µg L^{-1} (Table 3-6). Figure 3-10 illustrates the chromatograms resulting from samples 4B and 7B, which show 4 peaks corresponding to Hg(I), Hg(II), and Bi, respectively. The inaccurate quantification near baseline is likely a result of the quadratic shape of the Hg(I) curve at low concentrations that was previously discussed, plus the low amounts of Hg(I) extracted. The cause of the Hg(I) peak splitting is not known, though it could indicate Hg(I) instability/degradation to Hg(II). The chromatograms of analyzed samples can be found in the Appendix.

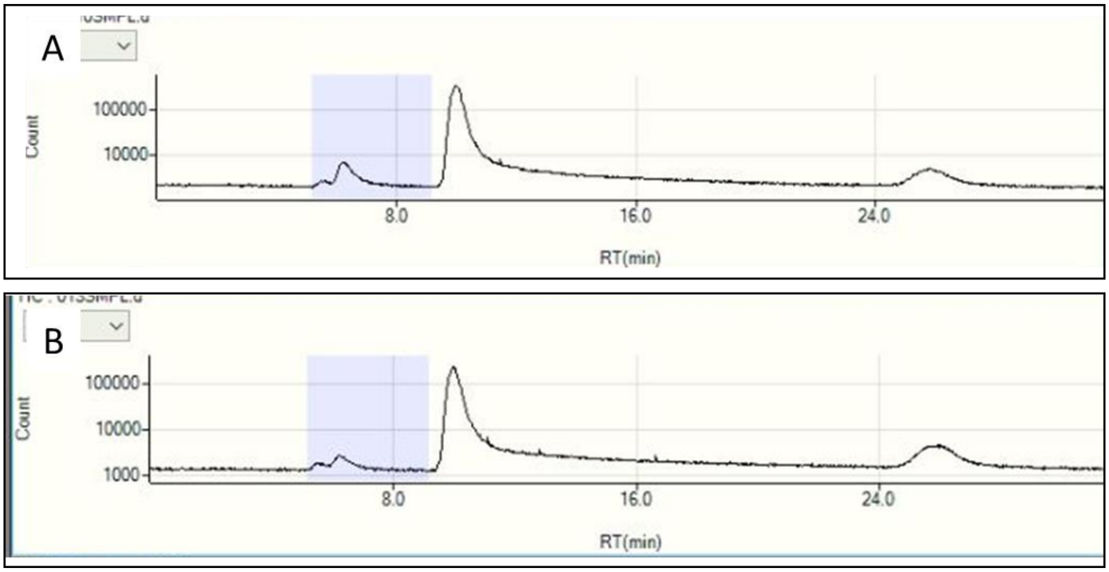

Figure 3-10. *Chromatograms resulting from the IC-ICP analysis of samples A) 4B and B) 7B, both from La Perlita. The chromatogram shows 4 peaks corresponding to Hg(I) (retention time ~ 6.5 min), Hg(II) peak (retention time ~ 10 min), and Bi (retention time ~ 26 min).*

The digestion and analysis of a calomel standard (treated as a sample) indicated that Hg(I) was not stable. The chromatogram showed that calomel had degraded, as indicated by the lack of Hg(I) (concentration < 5 μg L^{-1}) and presence of a very large Hg(II) peak (> 542,000 μg L^{-1}) (Figure 3-11). As calomel is susceptible to disproportionation, it is likely that calomel as Hg(I) degrades to Hg(II) in this way. Another indication of Hg(I) degradation was the noted colour change of the calomel solid from white to grey-black upon the addition of the digest solution, 0.5% 2-ME. The broadness of the Hg(I) peak may be due to Hg(I) degradation. The calomel digest and analysis were repeated four more times on different days and the results were similar, though the Hg(I) peak failed to appear altogether during one of the runs. These results were achieved despite efforts put forth in our timing to ensure that the idle time between the calomel digest and injection for analysis was minimal.

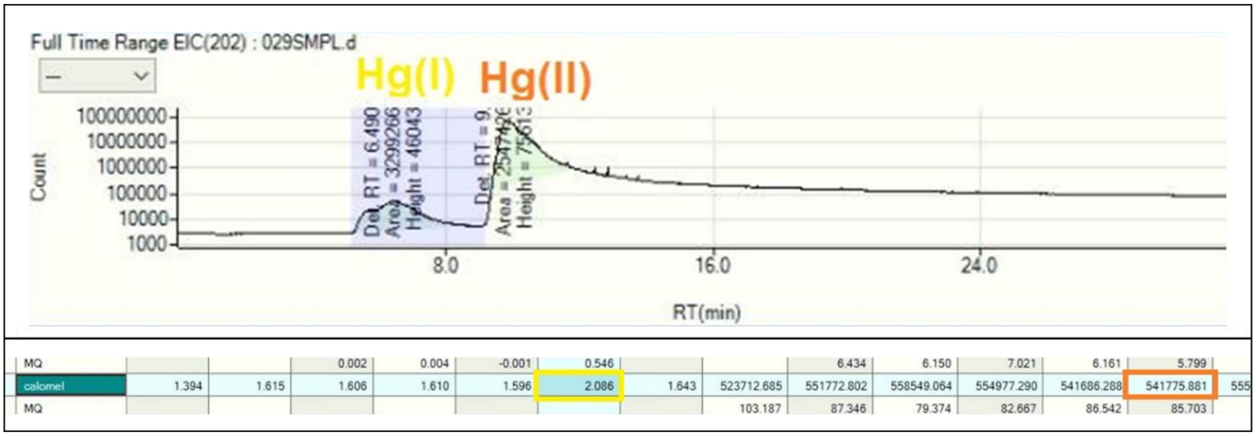

MQ			0.002	0.004	-0.001	0.546			6.434	6.150	7.021	6.161	5.799	
calomel	1.394	1.615	1.606	1.610	1.596	2.086	1.643	523712.685	551772.802	558549.064	554977.290	541686.288	541775.881	555
MQ								103.187	87.346	79.374	82.667	86.542	85.703	

Figure 3-11. *Chromatogram resulting from the Hg(I) analysis of a calomel standard. The chromatogram shows a small Hg(I) peak (retention time ~ 6.5 min) and a large Hg(II) peak (retention time ~ 10 min) with an extended tail. The corresponding Hg(I) and Hg(II) concentrations in ppb are denoted below the chromatogram; Hg(I) is highlighted yellow and Hg(II) is highlighted in orange.*

It is very likely that Hg(I) degrades during the digest portion of the protocol, as chemical reactions may occur when the solid interacts with the extraction solution or when the mixture is agitated during mechanical shaking. To briefly explore the stability of Hg(I) during the digest, observational stability tests were conducted by adding pH variations of the 0.2% 2-ME digest solution to a vial with calomel or mercury nitrate, shaking the vials, and noting the results, particularly signs of degradation – the main indicator being colour change. The results are tabulated in Table 3-7. The results showed that neither of the Hg(I) compounds were stable in any 0.2% 2-ME of the tested pH conditions, based on colour change as the primary indicator of stability. The degree to which degradation occurs is not known based on this observational experiment. These results insinuate that degradation must occur readily in the presence of 2-ME as the colour changes occur instantaneously.

Other modifications to the digest included minimizing idle time between the digest and the injection, length of time the sample undergoes mechanical shaking, using water as the extraction solution rather than 2-ME, and varying the pH of the 2-ME extraction solution. It is unclear whether minimizing idle time or pH adjustments of the 2-ME extraction solution had any effect on the results, though shorter mechanical shaking times did not appear to improve extraction, as no Hg(I) peaks were observed after 15 and 30 minutes. The use of water as opposed to 2-ME as an extraction solution was attempted due to the lack of colour change of calomel, which may suggest that Hg(I) is stable in water. However, water was proven ineffective as an extraction solution, as no Hg(I) peak was observed. Overall, the effect of these modifications on duplicate samples was unclear, as the results were inconsistent, sometimes showing good replication, though this may have more to do with an incomplete extraction, as previously suggested.

Table 6-6. *Hg speciation quantitation results*

Sample Name	Sample	Run	Hg(I) (μg L^{-1})	Hg(II) (μg L^{-1})	Hg(I) (μg g^{-1})	Hg(II) (μg g^{-1})
LP top - 1	1A	4	3.53	2498	0.134	95.0
LP top - 2	2B	4	3.05	3763	0.118	146
LP top - 3	3A	4	3.52	6606	0.138	259
PR-1	16A	4	3.00	5657	0.117	221
PR-2	17B	4	3.00	5611	0.115	215
PR-3	18A	4	3.11	5739	0.118	218
MS2	10C	5	0.05	716	0.000	6.36
LP bottom - 1	4B	5	0.00	436	0.000	4.34
LP bottom - 2	5B	5	0.00	345	0.000	3.43
LP bottom - 3	6B	5	-0.01	302	0.000	2.91
LP bottom - 4	7B	5	-0.01	290	0.000	2.99
LP bottom - 5	8B	5	0.00	1243	0.000	12.4
RP end - 1	19A	5	0.02	523	0.000	5.36
RP end - 2	20B	5	0.00	825	0.000	8.90
RP end - 3	21B	5	-0.01	908	0.000	8.98
RP middle - 1	22A	5	-0.01	712	0.000	7.14
RP middle - 2	23C	5	-0.01	457	0.000	4.63
RP middle - 3	24A	5	-0.01	323	0.000	3.50
UGC	9C	6	0.48	590	0.005	5.82
NA - 1	11C	6	0.46	970	0.004	9.29
NA - 2	12B	6	0.45	174	0.005	1.86
NA - 3	13C	6	0.46	2288	0.004	20.7
NA - 4	14C	6	0.50	16702	0.005	154
NA - 5	15A	6	0.47	11692	0.005	123
NA - 5	15B	6	0.47	11680	0.004	111
RP trees - 1	25A	6	0.46	15531	0.005	157
RP trees - 1	25B	6	0.47	16035	0.004	154
RP trees - 2	26C	6	0.50	22561	0.005	235
RP trees - 3	27A	6	0.47	35168	0.005	377
RP trees - 3	27B	6	0.46	39870	0.004	381
RP trees - 4	28C	6	0.49	13243	0.004	119
RP trees - 5	29A	6	0.47	23317	0.005	237
RP trees - 5	29B	6	0.52	24752	0.005	238

Table 7-7. *Hg(I) observational stability testing in various digest solutions of 2-mercaptoethanol*

Hg(I) Standard	**Weight (g)**	**Extraction Solution**	**pH**	**Observations**
Calomel	0.0545	0.2% 2-ME	9.00	Initially a white powdered solid. Upon addition of extraction solution, the solid immediately turned black-grey in colour. Extraction solution remained clear after shaking for ~ 1 min. Some suspended solid material at the surface.
Calomel	0.0514	0.2% 2-ME	8.27	Initially a white powdered solid. Upon addition of extraction solution, the solid immediately turned black-grey in colour. Extraction solution remained clear after shaking for ~ 1 min. Some white/sparkly suspension.
Calomel	0.0507	0.2% 2-ME	7.00	Initially a white powdered solid. Upon addition of extraction solution, the solid immediately turned black-grey in colour. The extraction solution remained clear. After shaking, some sparkly suspension was present.
Calomel	0.0495	0.2% 2-ME	6.00	Initially a white powdered solid. Upon addition of extraction solution, the solid immediately turned black-grey in colour. Extraction solution remained clear. Suspended white solid powder resulted after shaking.
Mercurous nitrate	0.0589	0.2% 2-ME	9.00	Initially a yellow crystalline solid. Upon addition of extraction solution, the solid turned black and the solution turned grey. Some suspended flaky solids remained after shaking.
Mercurous nitrate	0.0530	0.2% 2-ME	8.27	Initially a yellow crystalline solid. Upon addition of extraction solution and upon shaking, the solution turned grey. Some suspended flaky solids remained after shaking.
Mercurous nitrate	0.0490	0.2% 2-ME	7.00	Initially a yellow crystalline solid. Upon addition of extraction solution and upon shaking, the solution turned grey. Some suspended flaky solids remained after shaking.
Mercurous nitrate	0.0459	0.2% 2-ME	6.00	Initially a yellow crystalline solid. Upon addition of extraction solution and upon shaking, the solution turned grey. Some suspended flaky solids remained after shaking.

3.4. Discussion

3.4.1. Limitations on the Interpretation of Microscopy Results

The microscopy data was limited to results from 1 of the 26 sites at which samples were collected due to limitations imposed by total mercury concentrations. The analyzed sample was from the “trees” site along the Pastita River and chosen because of its total mercury concentration of 622 μg g^{-1}, which is just above the minimum concentration required to resolve elements using mineralogical techniques, such as SEM. Thus, the microscopy work conducted on the Pastita River sample cannot be generalized to the entire area unless: 1) sites with similar or higher total mercury concentrations are found and 2) similar microscopy results were achieved in various other locations in throughout Guanajuato or other historical silver mining regions in Mexico. Here we acknowledge that although the results are interesting, further investigations are required before making conclusive statements on the mineralogy of mercury long after the *patio* process, as well as the presence or absence of calomel.

3.4.2. Takeaways for the Continued Development of the Hg(I) Method

Despite the challenges encountered when attempting to reproduce the Wang et al. (2020) Hg(I) method, the method ultimately operated as it was intended – i.e., as a qualitative Hg(I) analysis. As indicated by Wang et al. (2020) and noted in our own results, 2-ME does extract Hg(I) from solid samples, in comparison to other extraction solutions, such as water. Thus, if Hg(I) is present in environmental samples, 2-ME can extract some quantity of it, which indicates its presence by a peak at the corresponding retention time for the Hg(I) standard on the chromatogram.

Conversely, repeat digests and analyses of calomel showed that inconsistent amounts of Hg(I) were extracted from the solid into the 2-ME solution. Thus, the mechanical shaking digest in 0.2% 2-ME results in incomplete Hg(I) extraction from solids, which prohibits accurate quantitation. Moreover, Hg(I), particularly in the form of calomel and mercurous nitrate, showed signs of degradation (namely, colour change) upon the addition of the extraction solution, 2-ME, which may further contribute to inaccurate quantitation of Hg(I) in the original sample.

Based on our experience with this method, we obtained the best results by preparing fresh stock solutions of Hg(I) and Hg(II) every day and by timing our digests to ensure that the idle time between the digest and injection was no more than 4 hours. We used 0.2% 2-ME as an extraction solution and a mechanical shaker to digest the samples for 1 hour. The digest was done underneath a garbage bag to protect the samples from light.

To date, 2-ME is the only reported extraction solution that can extract Hg(I) from solid samples, though our observations suggest that 2-ME and mechanical shaking may still elicit Hg(I) degradation, albeit inconsistently, to an unknown degree. This method should continue to undergo development to evaluate the degree to which 2-ME may affect degradation of Hg(I) in solid samples and whether there are variations that can be implemented to minimize degradation. This would eventually allow for quantitative analysis of Hg(I).

3.4.3. Other Methods Considered

The possibility of conducting powder x-ray diffraction (PXRD) was considered, but ultimately discarded based on the necessary high total mercury concentrations. This analysis would require calomel concentrations to be in the 100s to 1000s ppm ($\mu g\ g^{-1}$) range to be able to discern the spectrum among other sample constituents. Prior to sample collection, we tested to see whether the minimum amount of calomel (approximately 10% by weight) in a mix of typical minerals in the region, based on proportions reported by Carillo-Chavez (2003) (i.e., quartz, feldspar, and calcite), would be discernable. One of the concerns was that the abundance of quartz in the sample would very likely overshadow any signal from mercury compounds. The test run showed that the software was able to identify calomel, though the peaks of the spectrum were weak and it would probably not be visible if the concentration of calomel was any lower or if the sample matrix was more complex, which would likely be the case in a real sample (and based on our microscopy results, this was likely the case). In another test run, we used a clay separation method to the sample prior to analysis to see if it was effective at separating out calomel by density. Though the main calomel peak was larger, it did not improve the resolution to a significant degree. With these results, we were not convinced that this method would be useful alone. Based on the total mercury concentrations, we figured it was unlikely that even if calomel was present, concentrations would probably not be high enough to be discernable, leading to the decision not to conduct this analysis.

Another analysis that we considered was thermal desorption. This technique can be done using a direct mercury analyzer. Thermal release profiles of different mercury compounds can be compared to those resulting from an environmental sample to infer which species may be present. This method has been developed using the Milestone DMA-80 (e.g. Windmöller et al., 1996, 2017; Rumayor et al., 2013, 2016), though no studies have attempted this technique using the Teledyne Hydra-IIc. Because we would have to develop a method ourselves on the Hydra-IIc to conduct this analysis, we decided to forego thermal desorption, and focus on the Hg(I) IC-ICP-MS analysis instead. Future studies on this topic should consider thermal desorption as a potential mercury characterization technique for samples with total mercury concentrations below the typical mineralogical analysis threshold.

Sequential extraction analysis (e.g. Ebinghaus et al., 1999; Bloom et al., 2003; Morton-Bermea et al., 2015) was also considered to infer the presence of calomel, though calomel has been shown to separate into two different fractions in almost even proportions (Kim et al., 2003), which would not unequivocally demonstrate the presence of absence of calomel among other fraction constituents.

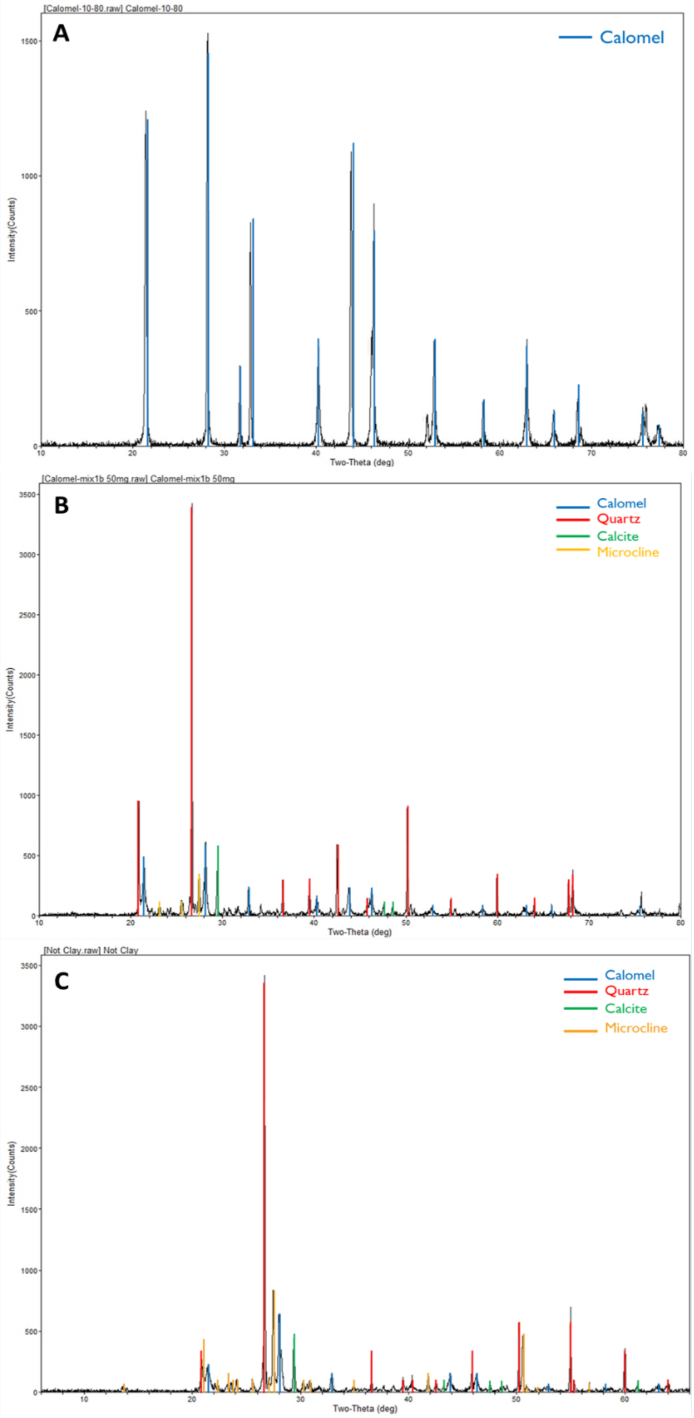

Figure 3-12. *Diffraction patterns of: A) calomel, B) calomel 10% (by weight) in Mixture A (60% quartz, 30% feldspar, 10% calcite), and C) calomel 10% (by weight) in Mixture A (60% quartz, 30% feldspar, 10% calcite) after a density separation.*

3.5. Conclusions

The supplementary analyses and attempts outlined in this chapter may serve to provide insight on future directions of this work. To summarize, calomel was not explicitly identified during either of the microscopy analyses, but the SEM and TEM results did suggest that Hg was present in all valence states in the Pastita River sample: Hg(0) likely as an alloy (Ag-Hg), Hg(I) likely in the form of $(Ag, Hg)_2S$, and Hg(II) likely as HgS. The overwhelming majority of Hg observed via SEM was in the form of HgS, supporting the calomel disproportionation hypothesis asserted in Chapter 2. The results from the microscopy analyses should not be regarded as conclusive evidence or generalized, as there is not enough data representative of the entire region.

The Hg(I) HPLC-ICP analysis by Wang et al. (2020) served its purpose as a qualitative Hg(I) method. Our attempt at quantification was overall unsuccessful due to the digestion with 2-ME, which showed inconsistent and incomplete extraction of Hg(I) from the solid samples, though the calibration aspect of our quantitation was satisfactory at concentrations greater than 5 ug L^{-1}. The development of this method should be continued to improve the extraction efficacy of the Hg(I) to eventually allow for quantitative analysis.

REFERENCES

Bayer, F. M. (2013). *Quecksilberspeziation von Bergbaurückständen aus Fresnillo und Cedral, Mexiko Erklärung*. Karlsruhe Institute of Technology.

Bloom, N. S., Preus, E., Katon, J. G., & Hiltner, M. (2003). Selective extractions to assess the biogeochemically relevant fractionation of inorganic mercury in sediments and soils. *Analytica Chimica Acta*, 479(2), 233–248. https://doi.org/10.1016/S0003-2670(02)01550-7

Carrillo-Chavez, A., Morton-Bermea, O., Gonzalez-Partida, E., Rivas-Solomon, H., Oesler, G., Garcia-Meza, V., Hernandez, E., Morales, P., & Cienfuegos, E. (2003). Environmental geochemistry of the Guanajuato Mining District, Mexico. *Ore Geology Reviews, 23*, 277–297. https://doi.org/10.1016/S0169-1368(03)00039-8

Ebinghaus, R., Turner, R. R., de Lacerda, L. D., Vasiliev, O., & Salomons, W. (1999). Mercury Contaminated Sites. Springer: New York.

Kim, C. S., Bloom, N. S., Rytuba, J. J., & Brown, G. E. J. (2003). Mercury speciation by x-ray absorption fine structure spectroscopy and sequential chemical extractions: a comparison of speciation methods. *Environmental Science & Technology*, 37, 5102–5108.

Mantha, H., Schindler, M., & Hochella, M. F. (2019). Occurrence and formation of incidental metallic Cu and CuS nanoparticles in organic-rich contaminated surface soils in Timmins, Ontario. *Environmental Science Nano, 6*, 163–179. https://doi.org/10.1039/c8en00994e

Rumayor, M., Diaz-Somoano, M., Lopez-Anton, M. A., & Martinez-Tarazona, M. R. (2013). Mercury compounds characterization by thermal desorption. *Talanta*, *114*, 318–322. https://doi.org/10.1016/j.talanta.2013.05.059

Rumayor, M., Lopez-Anton, M. A., Díaz-Somoano, M., Maroto-Valer, M. M., Richard, J.-H., Biester, H., & Martínez-Tarazona, M. R. (2016). A comparison of devices using thermal desorption for mercury speciation in solids. *Talenta*, *150*, 272–277. https://doi.org/10.1016/j.talanta.2015.12.058

Schindler, M., & Hochella, M. F. (2017). Sequestration of Pb-Zn-Sb-and As-bearing incidental nanoparticles by mineral surface coatings and mineralized organic matter in soils. *Environmental Science Processes and Impacts*, *19*, 1016–1027. https://doi.org/10.1039/c7em00202e

United States Environmental Protection Agency. (2002). EPA Method 1631, Revision E: Mercury in Water by Oxidation, Purge and Trap, and Cold Vapor Atomic Fluorescence Spectrometry. Retrieved January 5, 2019, from https://www.epa.gov/sites/production/files/2015-08/documents/method_1631e_2002.pdf

Vernon-Parry, K. D. (2000). Scanning electron microscopy: an introduction. *III-Vs Review*, *13*(4), 40–44. https://doi.org/10.1016/S0961-1290(00)80006-X

Wang, Y., Liu, G. L., Li, Y. B., Liu, Y. W., Guo, Y. Y., Shi, J. B., Hu, L., Cai, Y., Yin, Y., & Jiang, G. B. (2020). Occurrence of mercurous [Hg(I)] species in environmental solid matrices as probed by mild

2-mercaptoethanol extraction and HPLC-ICP-MS analysis. Environmental Science & Technology Letters, 7, 482–488. https://doi.org/10.1021/acs.estlett.0c00329

Wirth, R. (2004). Focused Ion Beam (FIB): A novel technology for advanced application of micro- and nanoanalysis in geosciences and applied mineralogy. *European Journal of Mineralogy*, *16*(6), 863–876. https://doi.org/10.1127/0935-1221/2004/0016-0863

Windmöller, C. C., Silva, N. C., Andrade, P. H. M., Mendes, L. A., & Magalhães Do Valle, C. (2017). Use of a direct mercury analyzer® for mercury speciation in different matrices without sample preparation. *Analytical Methods*, *9*, 2159. https://doi.org/10.1039/c6ay03041f

Windmöller, C. C., Wilken, R.-D., & De Figueiredo Jardim, W. (1996). Mercury speciation in contaminated soils by thermal release analysis. *Water, Air, and Soil Pollution*, *89*, 399–416. https://doi.org/10.1007/BF00171644

CHAPTER FOUR: CONCLUSIONS AND RECOMMENDATIONS

4.1. Summary

The work presented in this thesis investigates whether there was evidence of calomel in historical silver amalgamation wastes from Guanajuato, Mexico. The first chapter contains introductory and background information necessary to understand the scope of the research. It includes the context, thesis objective and structure, background information on mercury, silver amalgamation, calomel, the Guanajuato region and a literature review. The second chapter was written in the form of a manuscript that was submitted to *Environmental Science & Technology* for peer review. It reports widespread, elevated GEM concentrations observed in the ground-level air and in the interstitial air of soils, sediments, and refining wastes. We propose that the elevated GEM concentrations are attributed to calomel disproportionation, which is supported by a qualitative Hg(I) analysis of a soil/waste sample and a laboratory monitoring experiment involving calomel photodegradation in a sun simulator. Chapter 3 presents data from additional analyses that were not included in the manuscript, including SEM, TEM, and details on the Hg(I) IC-ICP method development. The microscopy analyses suggested evidence of mercury present in all valence states, with Hg(II) in the form of HgS being the most prevalent species. However, the microscopy results are limited to data from a single site, and therefore cannot be generalized to the area, due to total mercury concentration requirements for the analysis.

4.2. Conclusions and Future Recommendations

The research outlined in this thesis shows evidence of present-day, widespread, elevated GEM concentrations observed in the ground-level air air (range: 8 to 454 ng m^{-3}) and in the interstitial air of reprocessed mineral wastes, soils, and sediments (maximum: 44,700 ng m^{-3}) throughout the historical silver mining region of Guanajuato, Mexico. Such high elevated GEM concentrations are hypothesized to be a result of calomel disproportionation, forming Hg(0) (GEM) and Hg(II). This hypothesis is supported by several subsequent analyses including the Hg(I) analysis, the calomel photodegradation/disproportionation experiment, and microscopy analyses. The mineralogical analyses indicated that HgS was the most dominant solid-phase mercury species. The prevalence of HgS combined with the elevated GEM concentrations in ground-level and interstitial air in Guanajuato, and the supporting Hg(I) and photodegradation analyses, suggest that calomel may have once been present, but due to its susceptibility to disproportionation, the majority of it has since degraded leaving a legacy of mercury in the form of GEM held within the interstitial air of the wastes and in the solid form of HgS.

The findings of this work highlight the need to further investigate calomel's environmental stability during and long after the *patio* process. An accurate account of the fate of calomel will improve the uncertainty regarding mercury emission factors from historical silver refining processes on the global mercury budget. This work should also provide grounds for the implementation of long-term mercury monitoring in Guanajuato and in other historical silver mining regions to assess the local health and safety risks. Because inhalation is the most important exposure pathway of mercury from historical silver mining operations (GEM and particulate mercury < 2.5 um), the risk associated with the GEM retained in the wastes should be assessed as a potential present-day mercury emission/exposure source to the population.

The major shortcoming of the work presented here was the concentration limitation imposed by mineralogical analyses that would have provided direct evidence of calomel (if present). Mineralogical analyses require a relatively high concentration of the mineral of interest to be present in the sample for characterization. Our total mercury results hindered mineralogical analysis by SEM/TEM of all but one sample in and around the Guanajuato area, prohibiting a thorough investigation of the Guanajuato area. As such, calomel was not unequivocally identified in our mineralogical analyses on the Pastita River sample; although if present in any of our samples, it would likely be in extremely low quantities.

Thus, future studies should attempt less common speciation methods that may potentially have the capability to identify low concentrations of calomel, such as thermal desorption. Additionally, follow up work should attempt to better characterize calomel in the laboratory to improve our understanding its properties, especially the degradation kinetics via disproportionation, and better predict its behaviour in the environment. All of the conditions that evoke disproportionation should also be characterized and reviewed, then the patio process could be conducted in a simulated environmental setting to monitor calomel and the timing of its fate. Only once the physical properties of calomel are well-understood can it be accurately incorporated into emission estimates to refine the global mercury budget. The Hg(I) analysis method should also be further refined so that the digest results are consistent enough to allow for quantification. Various other historical silver refining areas should be investigated to compare whether similar results in terms of GEM and mineralogy are achieved.

APPENDIX A: SUPPLEMENTARY INFORMATION

Text A1. Details about the Guanajuato Mining District

The Guanajuato Mining District (GMD) is located between the Central Mexican Plateau and the Mexican Volcanic Belt in a temperate sub-humid climate (Figure A-1) (Woitrin-Bibot et al., 2015). The region has a mean annual air temperature of 18.7°C (range: 5–35°C) (Ramos-Arroyo et al., 2004), and is subjected to intense convective and orographic rainfalls, especially in summer (Martinex-Arredondo et al., 2015). Encompassing an area of 490 km^2, the GMD is part of the Lerma River basin hydrological system, and is bound by the Guanajuato River with La Purísima dam as the exit point of the basin. Most of the historical silver (Ag) mining waste deposits are located within or near the urban area of the city of Guanajuato (area: 57 km^2; population of about 184,000), which is a UNESCO World Heritage Site for its historical importance as an economic centre, culture, and picturesque, colonial architecture.

The GMD was recognized as one of the most lucrative Ag-producing regions in the world during the Spanish Colonial era (Guerrero, 2017). From 1654 to 1805 over 8,000 t of Ag were produced (prior to 1654, Ag production from Guanajuato was registered with the district of Mexico). The Ag ores at the GMD are hosted in three vein systems, including La Luz, Veta Madre, and La Sierra (Figure A-1) (Antuñez-Echegaray, 1964; Randall-Roberts et al., 1994). Four different extraction processes were applied over time: smelting (*fundición* or *plata de fuego*) and Hg amalgamation (patio process or *plata de azogue*) from the 17th until the end of the 19th century, which were replaced gradually by cyanidation in the 19th century, and by flotation since 1946 (Ramos-Arroyo et al., 2004).

Much of the waste generated from these mining processes was discarded and accumulated in the waterways. Some of the amalgamation waste that was initially dumped into the rivers were hauled back to land and reprocessed by cyanidation or flotation to extract the remaining Ag (Ramos-Arroyo et al., 2004). Although various efforts were put forth by the municipal government to clean the rivers in the 18th century, the disposal of mining waste only became regulated in 1930 (Antuñez-Echegaray, 1964). After re-processing, the waste generated was discarded around the city in the form of mineral waste deposits.

Text A2. Methodological details on the Hg^I analysis

Environmental studies on Hg have almost exclusively focussed on Hg^0 and Hg^{II}, under the general assumption that Hg^I is not stable enough to be of environmental significance. Recently Wang et al. (2020) developed a liquid chromatography (LC) - inductively coupled plasma mass spectrometer (ICP-MS) method following 2-mercaptoethanol (2-ME) extraction, and for the first time detected the presence of Hg^I in environmental solid samples including fly ash, soil and macroalgae. We carried out extensive tests in our laboratory to see whether we could improve the method to allow quantitative measurement, but unfortunately it was not successful due to the instability of Hg^I observed during the extraction and analysis. Therefore, our analysis of Hg^I in the waste, sediment, and soil samples from Guanajuato was considered qualitative only, which is sufficient to address our question about the presence or absence of Hg^I in these samples.

Below we provide our methodological details based on Wang et al. (2020) and our optimizations.

Sample Preparation: Solid samples were freeze-dried, ground with a mortar and pestle, and sieved prior to analysis.

Reagents: The stock solutions were made from Hg^I ($HgNO_3$, Sigma Aldrich) and Hg^{II} (SPEX CertiPrep) at 10 or 100 mg L^{-1}. The stock solutions were stored at 4°C. Each day, dilute working solutions were made fresh from the stock solutions in deionized water (18 MΩ cm; Milli-Q Element, from Millipore). 2-ME (Acros Organics) was used to make the 0.5% (v/v) mobile phase and the 0.2% (v/v) extraction solution in the Milli-Q water.

Extraction: Approximately 0.05 g of the freeze-dried sample were weighed into a 20 mL scintillation vial, to which 2 mL of 0.2% 2-ME was added. The vials were capped and secured in the sample holder on a Benchmark Orbi-Shaker Jr mechanical shaker, and shaken at 200 rpm for 2 hr at room temperature. The sample was then filtered by passing the extraction mixture through 0.2 μm polyethersulfone syringe filters (Puradisc 25, Whatman).

Analysis: The filtrates were analyzed by coupling a Dionex ICS-5000+ ion chromatography system to an Agilent 8900 triple-quadrupole ICP-MS. The separation of Hg^{I} and Hg^{II} was done via reverse-phased chromatography with 0.5% 2-ME as a mobile phase and a C_{18} column (Agilent InfinityLab Poroshell 120 EC-C_{18}).

FIGURES

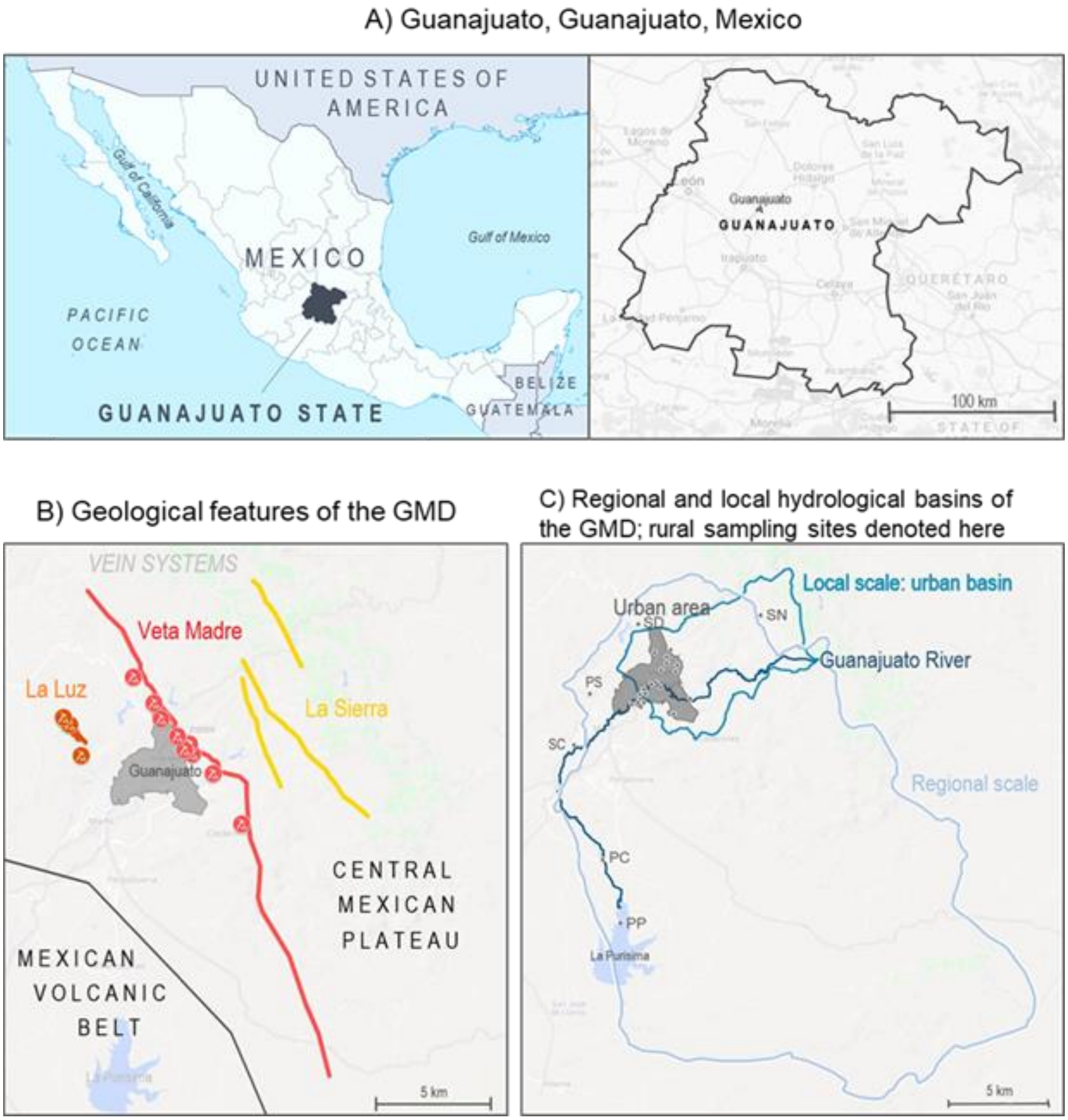

Figure A-1. *Geographical, geological and hydrological settings of the Guanajuato Mining District, Mexico. Base maps were based on Google Maps and Google Earth.*

TABLES

Table A-1. Study sites in Guanajuato, Mexico and the analyses conducted: gaseous elemental mercury (GEM), total mercury (Hg_T), and monovalent Hg (Hg^I).

Location	Depth (cm)	GEM	Hg_T	Hg^I
Monte de San Nicolás	Surface	x		
Murcielagos	Surface	x		
University Sports Center	Surface	x		
Pozuelos	Surface	x		
Deportiva	Surface	x		
Filtros	Surface	x		
Cerro del Cuarto	Surface	x		
Valenciana	Surface	x		
Río Guanajuato	Surface	x		
Santana Creek	Surface	x		
Soledad Dam	Surface	x		
El Orito	Surface	x		
Former *hacienda* (parkade)	Surface	x		
Former *hacienda* (hotel)	Surface	x		
Former *hacienda* (Mellado)	Surface	x		
New Access Tunnel	Surface	x		
Old Tunnel	Surface	x		
Puentecillas	317–360	x	x	
Puentecillas	270–317	x	x	
Puentecillas	230–270	x	x	
Puentecillas	205–230	x	x	
Puentecillas	159–205	x	x	
Puentecillas	145–159	x	x	
La Presa Purisima	0	x	x	
La Presa Purisima	10	x	x	
La Presa Purisima	20	x	x	
La Perlita	0–180	x	x	x
La Perlita	180–320	x	x	x
La Perlita	32–60	x	x	x
La Perlita	0–12	x	x	x
La Perlita	12–25	x	x	x
La Perlita	25–40	x	x	x
La Perlita	40–54	x	x	x
La Perlita	54–70	x	x	x
Presa Santana	0–13	x	x	
Presa Santana	13–23	x	x	
Presa Santana	23–31	x	x	
Presa Santana	31–50	x	x	

Campus	0–60	x	x	x
Meteorological Station	50–60	x	x	x
Noria Alta	0–2	x	x	x
Noria Alta	2–22	x	x	x
Noria Alta	22–30	x	x	x
Noria Alta	30–41	x	x	x
Noria Alta	41–50	x	x	x
Plaza Ranas	0–20	x	x	x
Plaza Ranas	20–40	x	x	x
Plaza Ranas	40–60	x	x	x
Río Pastita	0–20	x	x	x
Río Pastita	20–40	x	x	x
Río Pastita	40–60	x	x	x
Río Pastita	0–20	x	x	x
Río Pastita	20–40	x	x	x
Río Pastita	40–60	x	x	x
Río Pastita	0–10	x	x	x
Río Pastita	10–28	x	x	x
Río Pastita	28–42	x	x	x
Río Pastita	42–54	x	x	x
Río Pastita	54–70	x	x	x

Table A-2. Concentrations of gaseous elemental mercury (GEM) in the ground-level air and the maximum concentrations of GEM in the interstitial air in Guanajuato, Mexico. The study sites are grouped by category: reprocessed mineral wastes, sediment and soil, and other sites.

Site Code	Location	Coordinates	Method	Ground-level air GEM (ng m^{-3})[a]	Maximum Interstitial air GEM (ng m^{-3})[b] and Depth of its Occurrence	Site Description
Reprocessed Mineral Waste Sites:						
SN	Monte de San Nicolás	21°3'12.78" N, 101°12'13.49" W	Profile	200	1,960 at 20 cm	Amalgamation waste reprocessed by cyanidation. Wastes located on mountain next to community. Ore originating from the La Sierra vein.
MS	Meteorological Station	21°0'51.08" N, 101°15'58.85" W	Profile	30	1,440 at 70 cm	Amalgamation waste reprocessed by cyanidation. Wastes located near the university meteorological station. Ore originating from the Veta Madre vein.
USC	University Sports Center	21°0'48.72" N, 101°15'57.71" W	Profile	62	100 at 220 cm	Amalgamation waste reprocessed by cyanidation. Wastes located on the university sports center. Ore originating from the Veta Madre vein.
NA	Noria Alta	21°0'38.93" N, 101°16'7.45" W	Profile	51*	27,700 at 40 cm	Amalgamation waste reprocessed by cyanidation. Mixed mineral and construction waste and located on university campus. Ore originating from the Veta Madre vein.
PZ	Pozuelos	21°0'33.00" N, 101°16'1.00" W	Profile	18	950 at 85 cm	Amalgamation waste reprocessed by cyanidation. Wastes located in a residential area. Ore originating from the Veta Madre vein.
DP	Deportiva	21°0'32.76" N, 101°16'12.19" W	Profile	56	1,040 at 10 cm	Amalgamation waste reprocessed by cyanidation. Wastes located near sports complex. Ore originating from the Veta Madre vein.
LP	La Perlita	21°1'44.48" N, 101°15'15.99" W	Profile	113*	14,000 at 35 cm	Amalgamation waste reprocessed by cyanidation. Wastes located on a mountain. Ore originating from the Veta Madre vein.
FT	Filtros	21°1'56.74" N, 101°15'15.62" W	Profile	285	285 at 0 cm	Amalgamation waste reprocessed by flotation. Wastes located in a residential area. Ore originating from the Veta Madre vein.
CC	Cerro del Cuarto	21°1'29.24" N, 101°14'58.59" W	Profile	454	1,140 at 0 cm	Amalgamation waste reprocessed by flotation. Wastes located in a residential area. Ore originating from the Veta Madre vein.
VL	Valenciana	21°2'9.07" N, 101°15'8.93" W	Profile	16*	780 at 20 cm	Amalgamation waste reprocessed by flotation. Wastes were located near a school. Ore originating from the Veta Madre vein.
ML	Murcielagos	21°2'4.00" N, 101°15'40.00" W	Survey	20*	N/A	Low grade, unprocessed material near La Valenciana mine.
All Reprocessed Mineral Waste Sites (Median and range)				56 (18 to 454)	1,090 (100 to 27,700)	

Sediment/Soil Sites:						
PR	Plaza Ranas	21°1'7.11" N, 101°15'46.25" W	Profile	209	44,700 at 65 cm	Soil/sediment downtown near old *hacienda* ruins along the former path of the Guanajuato River (currently paved over).
PP	La Purísima	20°53'51.64" N, 101°16'46.47" W	Profile	8	202 at 20 cm	Sediment near dam and reservoir at the end of the regional basin.
PC	Puentecillas	20°55'46.84" N, 101°17'20.93" W	Profile	26	106 at 270 cm	Sediment from exposed bank edge near river near the head of the Purísima reservoir.
RG	Río Guanajuato	21°0'30.07" N, 101°16'24.51" W	Profile	62	298 at 20 cm	Sediment from river in which mineral waste from amalgamation was originally discarded.
RP	Río Pastita	21°0'39.52" N, 101°14'30.77" W	Profile	95	7,740 at 20 cm	Sediment from river in which mineral waste from amalgamation was originally discarded.
SC	Santana Creek	20°59'16.00" N, 101°18'16.00" W	Profile	11	95 at 20 cm	Sediment from creek that receives mine drainage. Located near a garbage dump.
SD	Soledad Dam	21°2'55.80" N, 101°16'12.30" W	Profile	15	209 at 40 cm	Soil / sediment from old *hacienda* ruins.
UGC	Campus	21°0'47.90" N, 101°16'7.61" W	Profile	16	293 at 40 cm	Soil from site on the university campus.
PS	Presa Santana	21° 0'49.80" N, 101°17'45.18" W	Survey	13*	N/A	Sediment near dam upstream of Santana Creek, which is associated with mine drainage.
EO	El Orito	21°1'32.41" N, 101°15'26.72" W	Survey	25*	N/A	Ambient air and surface soil along pathway of municipal park near old mines.
All Sediment/Soil Sites (Median and range)				21 (8 to 209)	251 (95 to 44,700)	
Other Sites:						
FHP	Former *hacienda* (Parkade)	21°1'0.69" N, 101°15'26.79" W	Survey	41*	N/A	Ambient air around parkade, near walls and above water well of a present-day car park (former *hacienda*).
FHH	Former *hacienda* (Hotel)	21°0'57.60" N, 101°16'0.11" W	Survey	23*	N/A	Ambient air in lobby, in restaurant and parking lot surface of a present-day hotel (former *hacienda*).
FHM	Former *hacienda* (Mellado)	21°1'40.64" N, 101°14'54.68" W	Survey	11*	N/A	Ambient air around site and surface of a present-day preserved look-out site (former *hacienda*).
NAT	New Access Tunnel	21°0'12.73" N, 101°15'1.88" W	Survey	7*	N/A	Ambient air in traffic tunnel.
OT	Old Tunnel	21°1'9.50" N, 101°15'37.18" W	Survey	83*	N/A	Ambient air in tunnel, near walls and in crevasses of the Old Tunnel (former course of the Guanajuato River).
All Other Sites (Median and range)				23 (7 to 83)	N/A	
Entire Study Area (Median and range)				28 (7 to 454)	865 (95 to 44,700)	

[a] Arithmetic means of the ambient air, undisturbed and disturbed surface (Profile sites), except those marked with * which are median values at the data did not follow a normal distribution.

[b] Maximum observed GEM interstitial air value reported (at given depth) for Profile sites only. Interstitial air measurements are not applicable (N/A) to Survey sites.

Table A-3. Total Hg (Hg_T) concentrations and the occurrence of monovalent Hg (Hg^I) in mining wastes, soil and sediment samples from Guanajuato, Mexico. N/A: Not analyzed.

Sample ID	**Location**	**Hg_T ($\mu g\ g^{-1}$)**	**Hg^I occurrence**
Urban sites:			
LP top - 1	La Perlita	92.7	Yes
LP top - 2	La Perlita	174	Yes
LP top - 3	La Perlita	187	Yes
LP bottom - 1	La Perlita	7.38	Yes
LP bottom - 2	La Perlita	4.71	Yes
LP bottom - 3	La Perlita	4.6	Yes
LP bottom - 4	La Perlita	7.26	Yes
LP bottom - 5	La Perlita	14	Yes
UGC	Campus	1.7	Yes
MS2	Meteorological Station	0.177	Yes
NA-1	Noria Alta	14.7	Yes
NA-2	Noria Alta	1.63	Yes
NA-3	Noria Alta	18	Yes
NA-4	Noria Alta	121	Yes
NA-5	Noria Alta	293	Yes
PR-1	Plaza Ranas	197	Yes
PR-2	Plaza Ranas	218	Yes
PR-3	Plaza Ranas	215	Yes
RP end - 1	Río Pastita	6.81	Yes
RP end - 2	Río Pastita	5.27	Yes
RP end - 3	Río Pastita	6.12	Yes
RP middle - 1	Río Pastita	12.6	Yes
RP middle - 2	Río Pastita	4.06	Yes
RP middle - 3	Río Pastita	3.74	Yes
RP trees - 1	Río Pastita	143	Yes
RP trees - 2	Río Pastita	213	Yes
RP trees - 3	Río Pastita	520	Yes
RP trees - 4	Río Pastita	125	Yes
RP trees - 5	Río Pastita	622	Yes
Median		*14.7*	
Min		*0.177*	
Max		*622*	
Rural sites:			
PC-1	Puente Cillas	0.068	N/A
PC-2	Puente Cillas	2.88	N/A
PC-3	Puente Cillas	3.47	N/A
PC-4	Puente Cillas	2.15	N/A
PC-5	Puente Cillas	1.46	N/A
PC-6	Puente Cillas	0.457	N/A

PP2-1	La Presa Purisima	9.11	N/A
PP2-2	La Presa Purisima	6.15	N/A
PP2-3	La Presa Purisima	10.6	N/A
PS-1	Presa Santana	0.2	N/A
PS-2	Presa Santana	0.3	N/A
PS-3	Presa Santana	0.15	N/A
PS-4	Presa Santana	0.09	N/A
Median		*7.04*	
Min		*0.068*	
Max		*10.6*	
All Sites:			
Median		***7.04***	
Min		***0.068***	
Max		***622***	

REFERENCES

Antuñez-Echegaray, F. (1964). Monografía Histórica y Minera del Distrito Minero de Guanajuato: México: Consejo Nacional de Recursos Naturales no Renovables, Publicación 17-E (in Spanish).

Guerrero, S. (2017). Silver by Fire, Silver by Mercury: A Chemical History of Silver Refining in New Spain and Mexico, 16th to 19th Centuries. Leiden, the Netherlands: Brill, 2017.

Martinez-Arredondo, J. C., Jofre Meléndez, R., & Ortega Chávez, V. M. (2015). Descripción de la variabilidad climática normal (1951-2010) en la cuenca del río Guanajuato, centro de México. Acta Universitaria 2015; 25: 31–47 (in Spanish).

Ramos-Arroyo, Y. R., Prol-Ledesma, R. M., & Siebe-Grabach, C. (2004). Características geológicas y mineralógicas e historia de extracción del Distrito de Guanajuato, México. *Revista Mexicana de Ciencias Geologicas*, 21, 268–284 (in Spanish with English abstract).

Randall-Roberts, J. A., Saldaña, E., & Clark, K. F. (1994). Exploration in a volcano-plutonic center at Guanajuato, México. *Economic Geology*, 89, 1722–1751. https://doi.org/10.2113/gsecongeo.89.8.1722

Wang, Y., Liu, G. L., Li, Y. B., Liu, Y. W., Guo, Y. Y., Shi, J. B., Hu, L., Cai, Y., Yin, Y., & Jiang, G. B. (2020). Occurrence of mercurous [Hg(I)] species in environmental solid matrices as probed by mild 2-mercaptoethanol extraction and HPLC-ICP-MS analysis. *Environmental Science & Technology Letters*, 7, 482–488. https://doi.org/10.1021/acs.estlett.0c00329

Woitrin-Bibot, E., Martínez-Arredondo, J. C., & Ramos-Arroyo, Y. R. (2015). Crecimiento urbano e incremento de riesgos hidrológicos en la ciudad de Guanajuato, México. *L’Ordinaire Des Amériques*, 218.

APPENDIX B: Hg(I) CHROMATOGRAMS

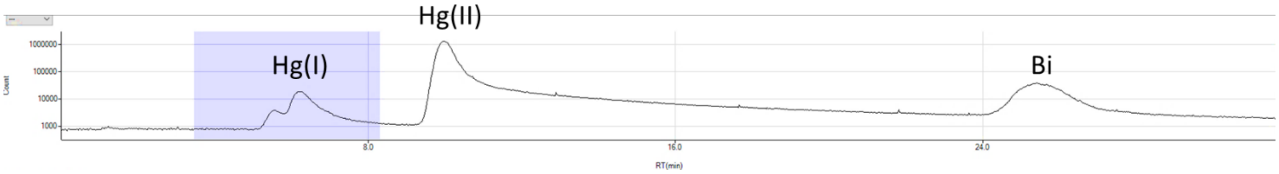

Figure B-1. *Chromatogram of sample 1A from La Perlita (LP top – 1). Run 4.*

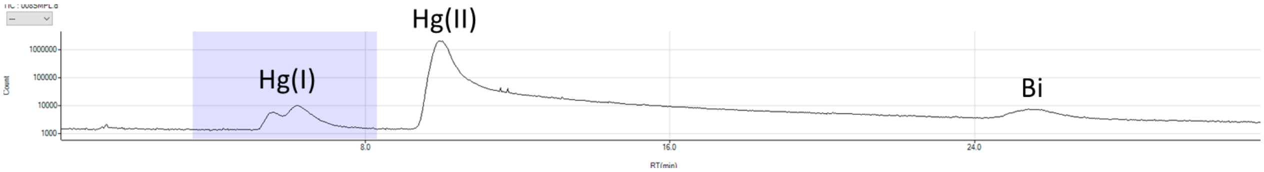

Figure B-2. *Chromatogram of sample 2B from La Perlita (LP top – 2). Run 4.*

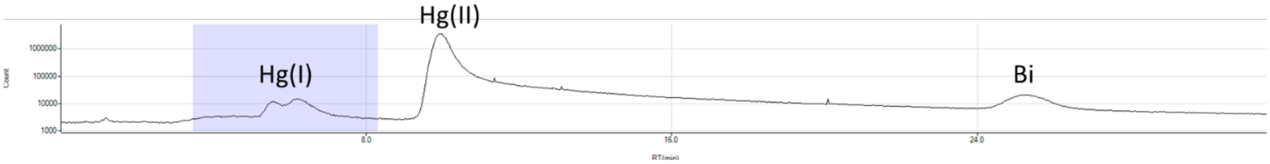

Figure B-3. *Chromatogram of sample 3A from La Perlita (LP top – 3). Run 4.*

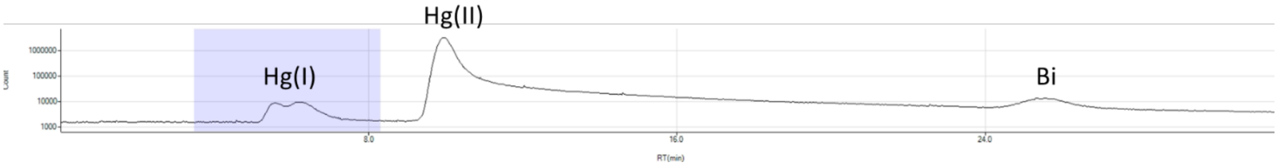

Figure B-4. *Chromatogram of sample 16A from Plaza Ranas (PR – 1). Run 4.*

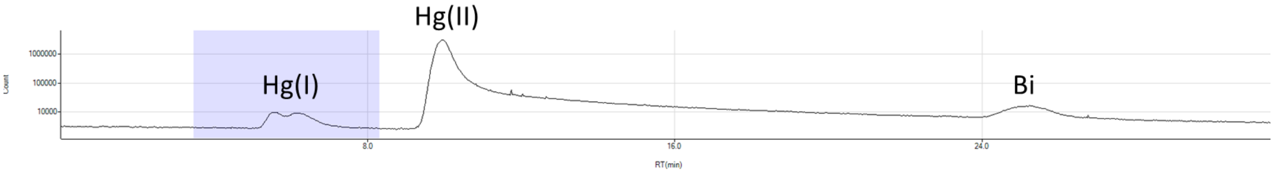

Figure B-5. *Chromatogram of sample 17B from Plaza Ranas (PR – 2). Run 4.*

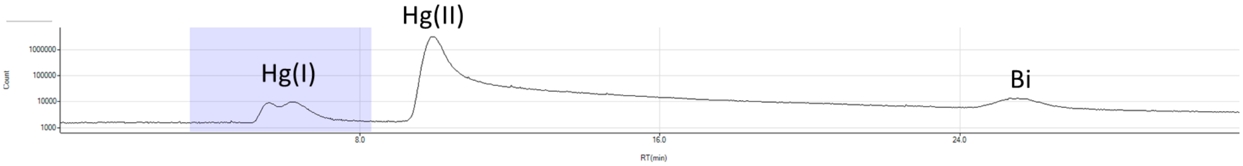

Figure B-6. *Chromatogram of sample 18A from Plaza Ranas (PR – 3). Run 4.*

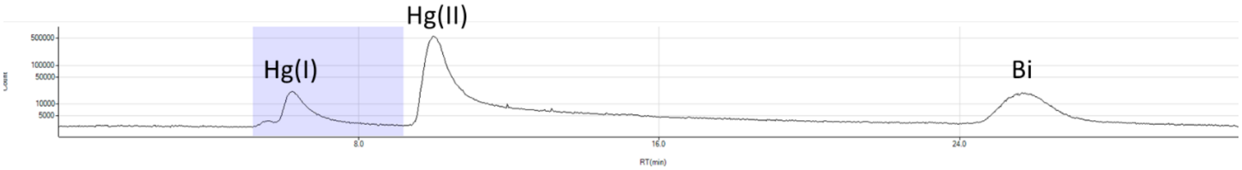

Figure B-7. *Chromatogram of sample 10C from the Meteorological Station (MS2). Run 5.*

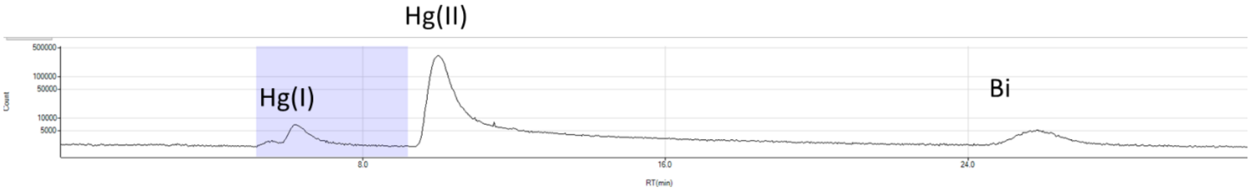

Figure B-8. *Chromatogram of sample 4B from La Perlita (LP bottom – 1). Run 5.*

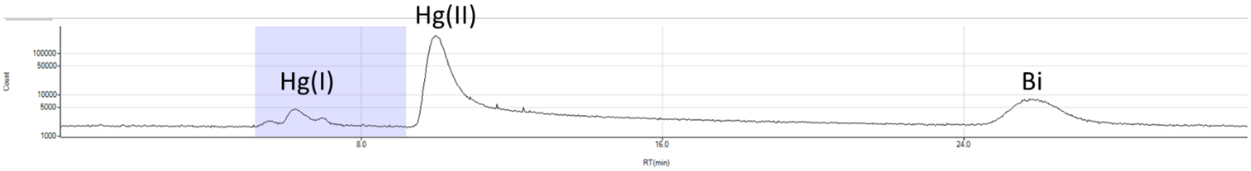

Figure B-9. *Chromatogram of sample 5B from La Perlita (LP bottom – 2). Run 5.*

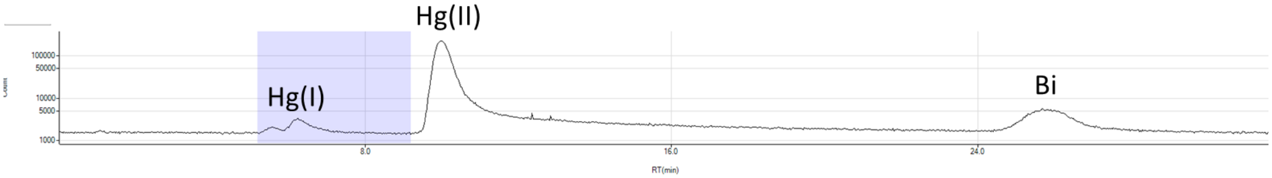

Figure B-10. *Chromatogram of sample 6B from La Perlita (LP bottom – 3). Run 5.*

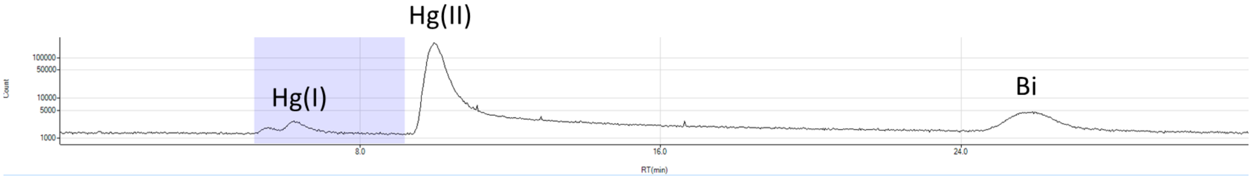

Figure B-11. *Chromatogram of sample 7B from La Perlita (LP bottom – 4). Run 5.*

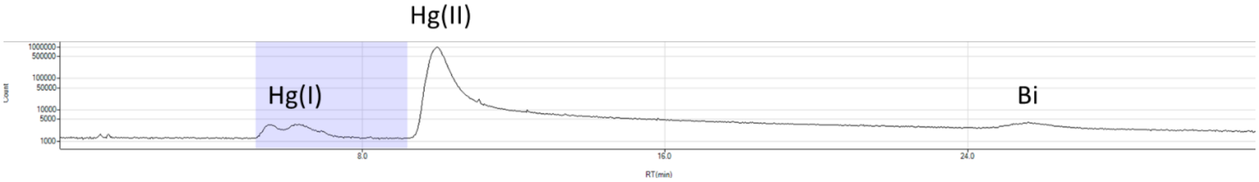

Figure B-12. *Chromatogram of sample 8B from La Perlita (LP bottom – 5). Run 5.*

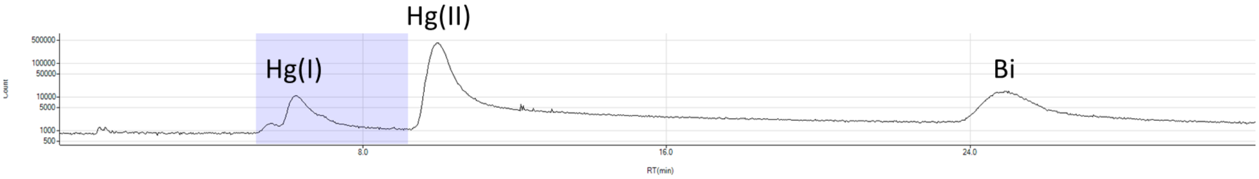

Figure B-13. *Chromatogram of sample 19A from the Pastita River (RP end – 1). Run 5.*

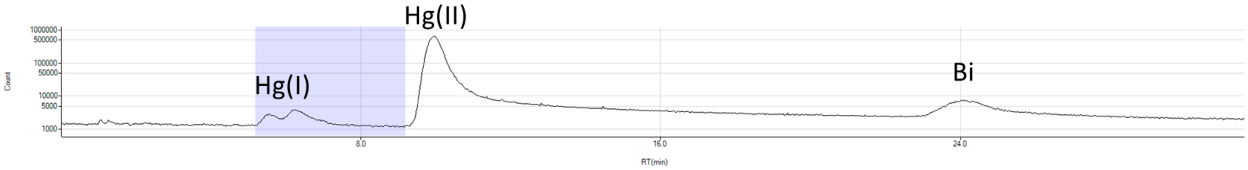

Figure B-14. *Chromatogram of sample 20B from the Pastita River (RP end – 2). Run 5.*

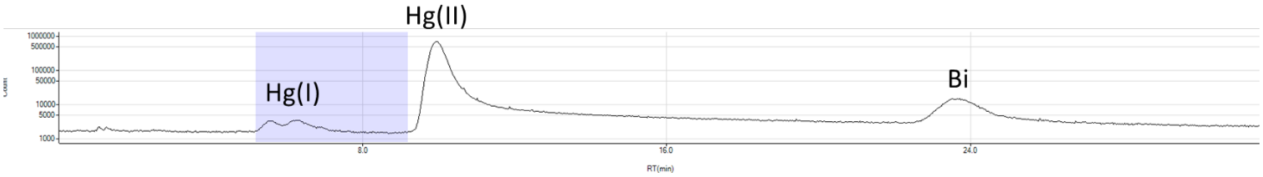

Figure B-15. *Chromatogram of sample 21B from the Pastita River (RP end – 3). Run 5.*

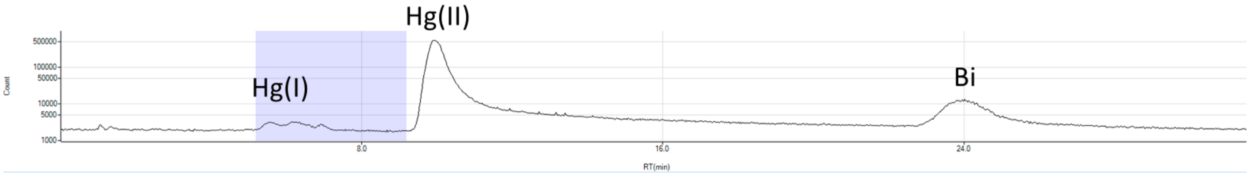

Figure B-16. *Chromatogram of sample 22A from the Pastita River (RP middle – 1). Run 5.*

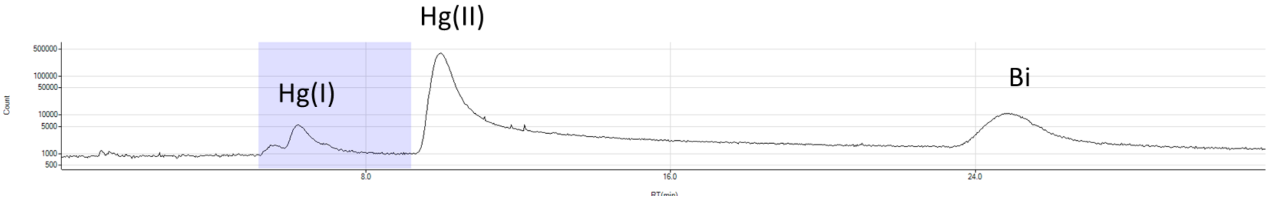

Figure B-17. *Chromatogram of sample 23C from the Pastita River (RP middle – 2). Run 5.*

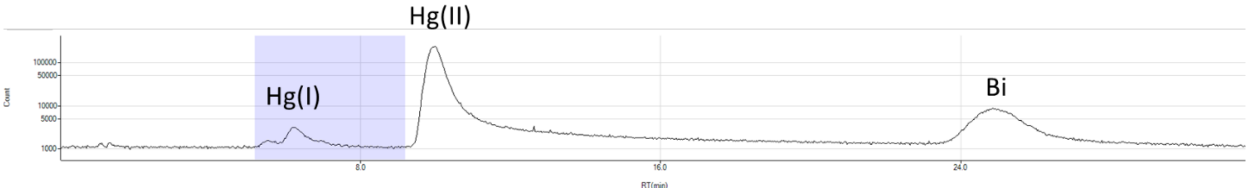

Figure B-18. *Chromatogram of sample 24A from the Pastita River (RP middle – 3). Run 5.*

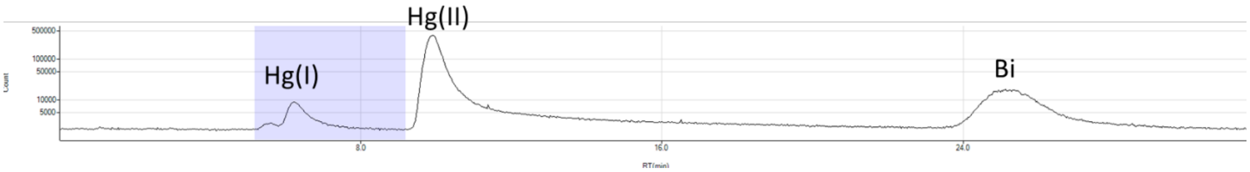

Figure B-19. *Chromatogram of sample 9C from the University of Guanajuato campus (UGC). Run 6.*

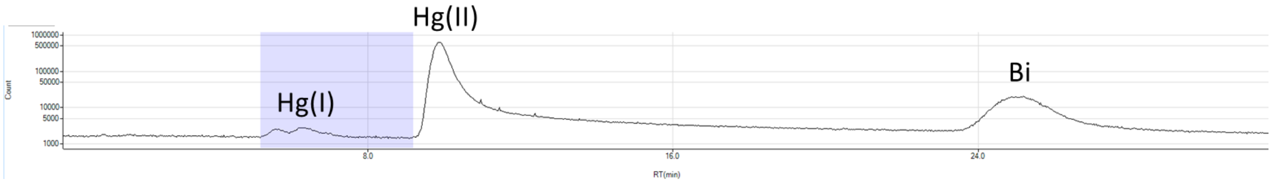

Figure B-20. *Chromatogram of sample 11C from Noria Alta (NA – 1). Run 6.*

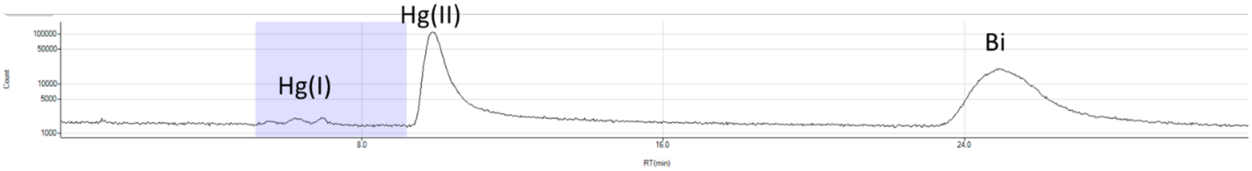

Figure B-21. *Chromatogram of sample 12B from Noria Alta (NA – 2). Run 6.*

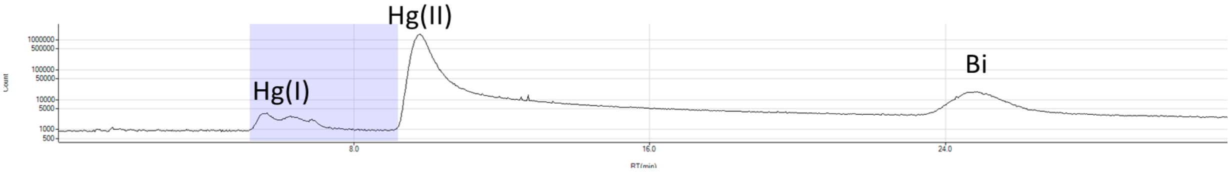

Figure B-22. *Chromatogram of sample 13C from Noria Alta (NA – 3). Run 6.*

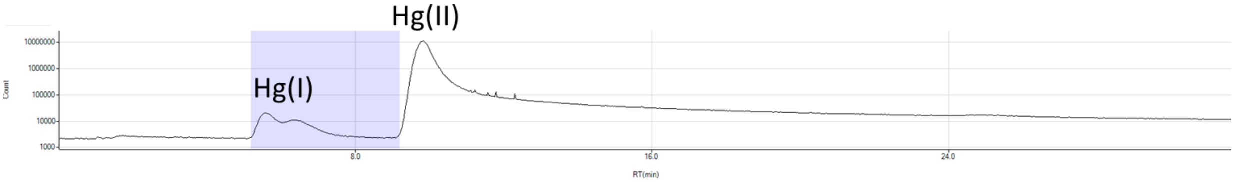

Figure B-23. *Chromatogram of sample 14C from Noria Alta (NA – 4). Run 6.*

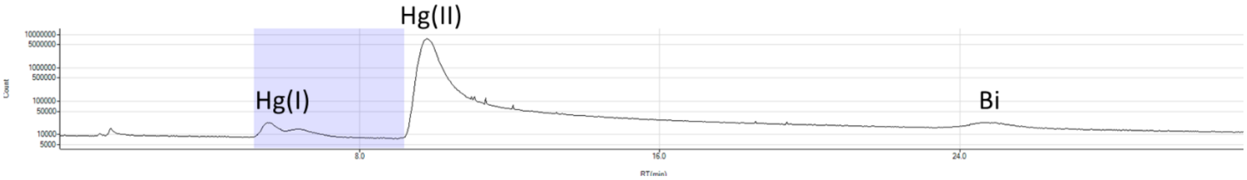

Figure B-24. *Chromatogram of sample 15A from Noria Alta (NA – 5). Run 6.*

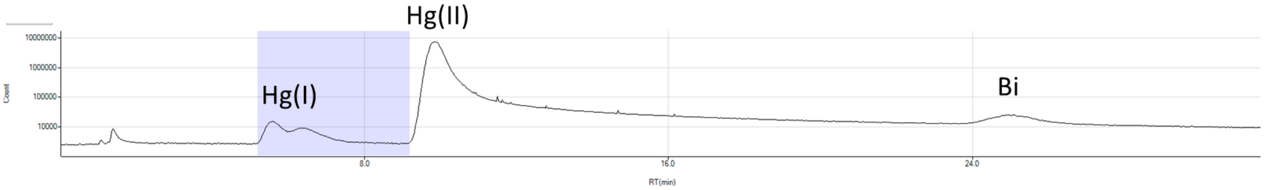

Figure B-25. *Chromatogram of sample 15B from Noria Alta (NA – 5). Run 6.*

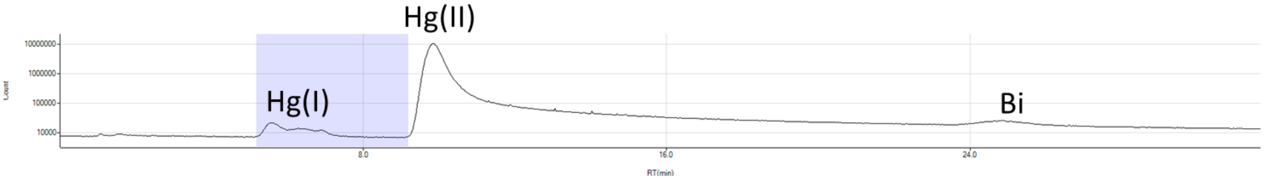

Figure B-26. *Chromatogram of sample 25A from the Pastita River (RP trees – 1). Run 6.*

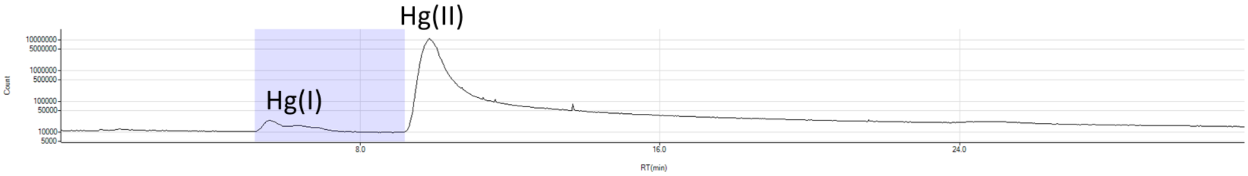

Figure B-27. *Chromatogram of sample 25B from the Pastita River (RP trees – 1). Run 6.*

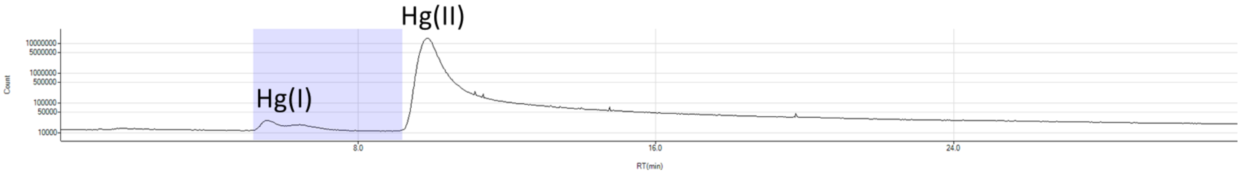

Figure B-28. *Chromatogram of sample 26C from the Pastita River (RP trees – 2). Run 6.*

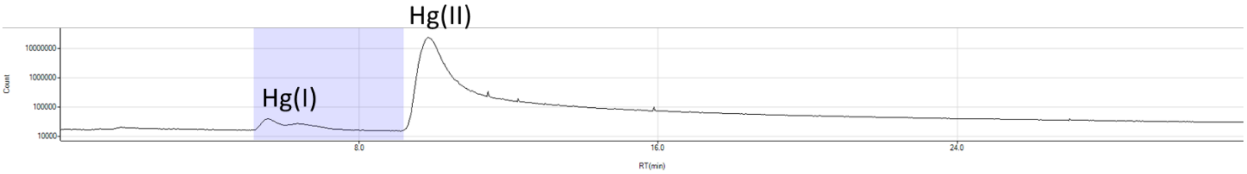

Figure B-29. *Chromatogram of sample 27A from the Pastita River (RP trees – 3). Run 6.*

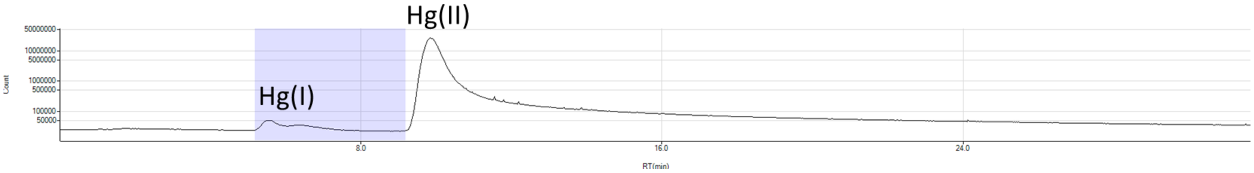

Figure B-30. *Chromatogram of sample 27B from the Pastita River (RP trees – 3). Run 6.*

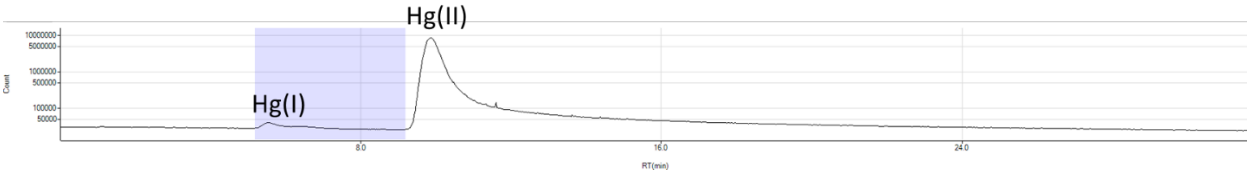

Figure B-31. *Chromatogram of sample 28C from the Pastita River (RP trees – 4). Run 6.*

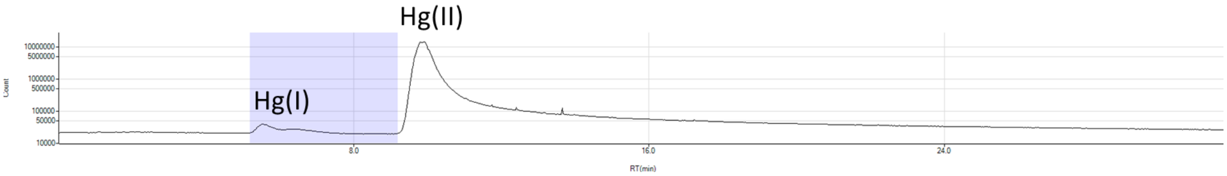

Figure B-32. *Chromatogram of sample 29A from the Pastita River (RP trees – 5). Run 6.*

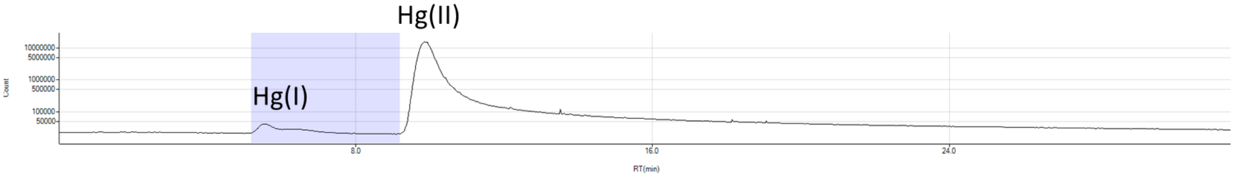

Figure B-33. *Chromatogram of sample 29B from the Pastita River (RP trees – 5). Run 6.*